NASA CR-66493

CORNELL AERONAUTICAL LABORATORY, INC.
BUFFALO, NEW YORK 14221

PROJECT SLOPE
A STUDY OF LUNAR ORBITER PHOTOGRAPHIC EVALUATION TECHNIQUES, IMPLEMENTATION AND ACCURACY

Prepared By:

R.E. Kinzly

and

M.J. Mazurowski

CAL REPORT NO. VS-2182-D-3
PHASE II FINAL REPORT
CONTRACT NO. NAS1-5800

1 APRIL 1967

PREPARED FOR:

NATIONAL AERONAUTICS AND SPACE ADMINISTRATION
LANGLEY RESEARCH CENTER, LANGLEY STATION
HAMPTON, VIRGINIA 23365

Distribution of this report is provided in the interest of information exchange. Responsibility for the contents resides in the authors or organization that prepared it.

PRECEDING PAGE BLANK NOT FILMED.

ABSTRACT

The second phase of a continuing Study of Lunar Orbiter Photographic Evaluation (Project SLOPE) was conducted for the primary purpose of implementing measurement techniques for the image quality parameters selected in the first phase of the effort and for evaluating their accuracy. Extensive use is made of computer-simulated imagery and actual imagery obtained from the preflight readout of the Goldstone test film in the latter task. The quality parameters are related to the objectives of the Lunar Orbiter photographic system through the use of specified system performance criteria. The effects of the attainable accuracy for the quality parameter measurements on the criteria determination are also evaluated.

Several secondary studies which are reported include brief investigations of the feasibility of improved quality parameter estimation techniques.

It was found that by making a reasonable number of measurements on the GRE film utilizing the targets specified in the first phase effort, the expected error of the estimates of the system performance criteria is about 10%. The limitation is primarily imposed by the accuracy of the measurement techniques for the noise level quality parameter. The computer programs developed during the first phase effort have been revised to facilitate anticipated large volumes of data and to take advantage of new computational forms developed during the second phase effort.

PRECEDING PAGE BLANK NOT FILMED.

FOREWORD

This report is the result of studies during the second phase of a continuing contract from NASA Langley Research Center; Contract No. NAS1-5800 monitored by Mr. T. Hansen.

The authors are grateful to a number of co-workers at Cornell Aeronautical Laboratory for their contributions during the second phase of effort. Particular acknowledgement is given to P. G. Roetling, E. A. Trabka and T. M. Holladay for their technical consultations, and to T. Gallagher for his part in the data acquisition processes.

TABLE OF CONTENTS

Section		Page
	ABSTRACT	iii
	FOREWORD	v
1.	INTRODUCTION	1
2.	DESCRIPTION OF QUALITY PARAMETERS	5
3.	MEASUREMENT OF QUALITY PARAMETERS	9
	3.1 Targets in the GRE Image Employed in Measuring the Quality Parameters	9
	3.2 Data Acquisition Techniques	13
	3.3 Data Reduction Techniques	20
	3.3.1 Conversion of Perforated Tape and Removal of the Scan Line Structure	20
	3.3.2 Evaluation of the Signal Level Quality Parameters	22
	3.3.3 Evaluation of the Total Noise Power	31
	3.3.4 Evaluation of the Scanner-Communications-GRS Modulation Transfer Function	36
	3.3.5 Evaluation of the Camera System Modulation Transfer Function	40
	3.3.6 An Alternative Technique for Evaluation of the Complete System Transfer Function	46
	3.4 Study of the Accuracy of the Measurement Techniques	47
	3.4.1 Evaluation of the Effects of the Nonlinearities of the Ground Reconstruction System (GRS)	47
	3.4.2 Accuracy of the Modulation Transfer Function Measurement Techniques	49
	3.4.3 Accuracy of the Noise Level Measurement Techniques	75
	3.4.4 Accuracy of the Signal Level Measurement Techniques	80
	3.5 Estimation of the Number of Measurements Required to Evaluate Each of the Quality Parameters	87

TABLE OF CONTENTS (Cont.)

Section		Page
4.	RELATION OF THE QUALITY PARAMETERS TO LUNAR ORBITER OBJECTIVES BY USE OF SYSTEM PERFORMANCE CRITERIA	91
	4.1 Description of the System Performance Criteria	91
	4.2 Variation of Criteria with Model Geometry and Off-Nominal Performance	96
	4.3 Effect of Accuracy of Quality Parameter Measurements Upon Criteria	109
	4.4 Applicability of the Criteria to Operational Techniques for Extraction of Topographic Data	113
5.	THE STUDY OF THE FEASIBILITY OF ADVANCED MEASUREMENT CONCEPTS	119
6.	CONCLUSIONS	131
Appendix A	STUDY OF THE EFFECTS OF THE COMBINED GRE NONLINEARITIES	135
Appendix B	MATHEMATICAL MODEL OF THE EXPECTED INTENSITY FUNCTION INSIDE A CRATER LOCATED AT AN OFF-NADIR POSITION	145
Appendix C	DERIVATION OF SYSTEM PERFORMANCE CRITERIA	153
Appendix D	SUPPORTING ANALYSIS FOR NOISE MEASUREMENT TECHNIQUES	163

LIST OF FIGURES

Figure No.		Page
1	Lunar Orbiter Photographic Flow Diagram	6
2	Typical Shadow-to-Sunlight Edge Targets in a Medium Resolution Photograph	10
3	Typical Pre-Exposed Edge Data Array and Associated Targets	11
4	A Microdensitometer Trace across Step 6 of the Step Tablet showing the Scan Line Structure	15
5	Data Acquisition Flow Diagram	16
6	Frequency Response for a Numerical Filter Designed to Remove Scan Line Structure from Density Traces (ν_o = 20 lines/mm, M = 3)	23
7	Traces across Step 6 of the Step Tablet showing Scan Line Structure and made from the Original GRE Film Obtained in the Pre-launch Goldstone Readout of Lunar Orbiter I	24
8	Numerically Filtered Traces with Scan Line Structure Removed	25
9	Flow Diagram of the Procedures used in the Signal Level Analysis Program	26
10	Typical Output from Signal Level Analysis Program	27, 28
11	Flow Diagram for the Procedures used in Processing of Noise Level Data	32
12	Response Curves of the Numerical Filters used in the Noise Level Analysis	33
13	Typical Printed Output from the Noise Level Analysis Program	35
14	Flow Diagram of the Procedures for Evaluation of the Scanner-Communications-GRS MTF	38
15	Typical Printed Output from the Scanner-Communications-GRS MTF Evaluation Program	40

LIST OF FIGURES (Cont.)

Figure No.		Page
16	Flow Diagram of the Procedures used in the Evaluation of the Camera System MTF	41
17	Auxiliary Geometric Parameters Required for Evaluation of the Camera System MTF	43
18	Typical Printed Output from Camera System MTF Evaluation Program	45
19	Measured Modulation Transfer Functions Obtained from Hand Smoothed Simulated Noisy Microdensitometer Traces	52
20	Measured Scanner-Communications-GRS MTF Obtained using Four Different Simulations of a Noisy Step Tablet Edge	54
21	The Effect of Knowledge of Edge Location Upon the Camera System MTF	57
22	The Effect of an Error in the Shadow Length Estimate Upon the Camera System MTF	59
23	The Effect of an Error in the Crater Diameter Estimate Upon the Camera System MTF	60
24	The Effect of an Error in Phase Angle Evaluation Upon the Camera System MTF	62
25	Targets in the Goldstone Format of the Original GRE Film in the Pre-launch Readout (Lunar Orbiter I)	66
26	Measured Response Function Representing the Sharpness of Edges in the Pre-Exposed Step Tablet of the Goldstone Leader (Lunar Orbiter I)	67
27	Measured Fractional Standard Deviation of the Response Function used to Specify Edge Sharpness	68
28	Measured Scanner-Communications-GRS MTF using Edge Traces made from Original GRE Film (Pre-launch Goldstone Readout of Lunar Orbiter I)	70
29	Standard Deviation of the Individual Measurements of Scanner-Communications-GRS MTF shown in Fig. 28	71

LIST OF FIGURES (Cont.)

Figure No.		Page
30	Deviation in MTF Measurements from Repeated Traces Across the Edge of a Single Step	74
31	Measured Relationship Between GRE Density and Goldstone Leader Transmittance (Lunar Orbiter I)	84
32	Measured Hurter-Driffield Response for the Lunar Orbiter I Goldstone Leader	86
33	Specified Test Objects for Evaluating System Performance	92
34	Typical Printed Output from the System Performance Criteria Evaluation Programs	97
35	Variation of Signal-to-Noise Ratio with Phase Angle . . .	99
36	Variation of Error in Slope Measurement with Phase Angle	100
37	Variation of Signal-to-Noise Ratio with Exposure Level (2 meter design cone, 70° phase angle).	102
38	Variation of Error in Slope with Exposure Level (70° phase angle)	103
39	Variation of Signal-to-Noise Ratio with Radiation Exposure (2 meter design cone, 70° phase angle)	104
40	Variation of Error in Slope Measurement with Radiation Exposure (70° phase angle)	105
41	Variation of Signal-to-Noise Ratio with Operational Degradations (2 meter design cone, 70° phase angle)	107
42	Variation of Error in Slope Measurement with Operational Degradations (70° phase angle)	108
43	Variation of Signal-to-Noise Ratio with Cone Size (70° phase angle)	110
44	Variation of Error in Slope Measurement with Target Size (70° phase angle)	111
45	Variation of Error in Slope Measurement with (70° phase angle)	112

LIST OF FIGURES (Cont.)

Figure No.		Page
46	Sketch Illustrating Adaptive Filtering Techniques	122
47	Noise Filtering Employing an Adaptive Filter and a Simulated Edge	124
48	Modulation Transfer Function Measurement from Noisy Simulated Microdensitometer Trace using Space Varying Filter	125
49	Measured Modulation Transfer Function from a Noisy Simulated Microdensitometer Trace using Parameter Estimation Techniques	129
50	Lunar Orbiter Photographic Quality Evaluation Flow Diagram	132
A-1	Simulated Density Traces with and without Scan Lines for a 3.7 Micron GRE Scan Spot	137
A-2	Simulated Density Traces with and without Scan Lines for a 4.7 Micron GRE Scan Spot	138
A-3	Resulting MTF from Density Traces Obtained using a 3.7 Micron GRE Scan Spot.	139
A-4	Resulting MTF from Density Traces Obtained using a 4.7 Micron GRE Scan Spot	140
A-5	Difference Between the Actual (measured) MTF and the MTF for a Linear System	141
A-6	Effect of GRE nonlinearity upon Measured Densities of Uniform Gray Levels	143
B-1	Model and Coordinate Geometry	145
B-2	Geometry for the Local Normal Project into Phase Plane .	147
B-3	Geometry for Evaluating the Camera Zenith Angle	149
D-1	Sketch of Effects of Several Analysis Procedures upon the Power Spectrum	165
D-2	Frequency Response of Microdensitometer (10X Objective, 2.5 μ Diameter Aperture Scan Spot)	173

1. INTRODUCTION

This document is the final report on the second phase of a continuing effort of the Study of Lunar Orbiter Photographic Evaluation (SLOPE) conducted under Contract NAS1-5800. As specified in the contract schedule: "The primary objective of this contract is to determine the method by which there can be made a quantitative measure of those factors which define the quality of black-white monoscopic photographs, to be received from the Lunar Orbiter spacecraft".

The results of the Phase I effort which were previously report [1] included a review of the factors which influence photographic quality and selection of a set of representative parameters. The quality parameters and the objectives of a Lunar Orbiter Mission were related by establishing system performance criteria and the feasibility of obtaining the measurements necessary to evaluate the selected quality parameters from reconstructed imagery was demonstrated.

The primary objective of the second phase of the effort on Project SLOPE was the implementation and evaluation of the accuracy of the data acquisition, reduction, and analysis techniques developed during the first phase effort. Towards this end, computer simulated imagery as well as actual Lunar Orbiter images obtained from the preflight readout of the Goldstone test film were extensively employed to aid in refining the data processing techniques and to determine the accuracy with which the selected quality parameters and system performance criteria could be evaluated. Several secondary studies of the feasibility of applying more sophisticated techniques to the evaluation of the quality parameters were also conducted during the second phase effort.

To establish the quality of a photographic image, parameters must be defined so as to describe the rendition of detail in the image, the reproduction of tonal quality (i. e., gray levels), and the level of noise (i. e., spurious fluctuations in gray level). All of these parameters can be functions of location in the image, and the first and last can be functions of orientation as well.

The measurement of detail rendition is accomplished by use of a test pattern of known shape and usually quite detailed, as for example, bar charts (square waves), sinusoidal patterns, impulses (i. e., points of lines), or step functions (i. e., edges). The problem in evaluating the Lunar Orbiter imagery was to select a "test pattern" on the lunar surface, that is, find some pattern on the moon for which the detail is already known. During the first phase effort it was determined that shadow to sunlight edges interior to a crater are the only feasible targets, and the present approach utilizes these edges. Measures which can be used to describe the detail rendition are, for example, point spread, line spread, acutance, or resolution. In the present case a spatial frequency analysis is made to determine a measure of detail rendition referred to as a modulation transfer function.

The measurement of tonal reproduction and noise level present fewer problems. The tonal reproduction can be measured by use of standard sensitometric procedures so long as a series of controlled uniform exposures are placed on the photographic film placed in the spacecraft. Since this procedure is followed in the Lunar Orbiter, this problem has a straightforward solution, and the corresponding quality parameter is simply a measure of dc signal level response or system gain.

The measurement of noise level, that is, the rms fluctuation of a uniform input signal is quite similar to that for other photographic systems. Special test targets are not required so long as adequate knowledge of general noise sources and signal reproduction is available.

The problem of relating the quality parameters to the detection and measurement of topographic features has been approached by application of statistical communication theory to specific detection or measurement problems. In the case of measuring the slope of the lunar surfaces, the topographic model specified by NASA is a square area of constant slope surrounded by a flat surface. Optimum extraction techniques are assumed, and the probable error in the measurement of the slope angle (or brightness longitude) of the model is evaluated. In the case of detection of obstacles, the specified test feature is a cone of given height and base. The approach

again assumes optimum detection in this case by a matched filter, and the corresponding signal-to-noise ratio is selected to characterize the performance of the system for detecting obstacles.

The next section of this report presents a more detailed description of the quality parameters selected for evaluating the performance of the Lunar Orbiter photographic system. Section 3 reviews the selection of targets in the GRE image which are employed in measuring the quality parameters, describes the procedures for making the measurements, and presents the data reduction procedures utilized to reduce the data to the desired quality parameters. In addition, an evaluation of the accuracy of the techniques employed in obtaining each of the quality parameters is presented and the section is concluded with a determination of the number of measurements of each of the quality parameters necessary to attain reasonable accuracy in their values. The fourth section relates the selected quality parameters to the Lunar Orbiter objectives by utilizing the system performance criteria. The variation of the criteria with model geometry and off-nominal performance, the applicability of the criteria to operational techniques for the extraction of topographic data, and the effect of the accuracy of the quality parameter measurements upon the criteria determination are discussed in detail. The next section of the report describes a brief study of the feasibility of several concepts for advancing the state of the art of image quality parameter measurements. The final section presents conclusions and recommendations.

Several appendices are also included to provide detailed mathematical framework of the results presented in the text.

2. DESCRIPTION OF QUALITY PARAMETERS

Quality parameters are a set of factors that define the level of information content of a photograph*. These factors generally can be divided into three classes; namely, factors which describe signal level, noise level, and signal detail rendition. In the first phase of this investigation[1] parameters were selected from each of these three classes to describe the quality of the reconstructed Lunar Orbiter photographs. Preliminary measurement and data reduction techniques were developed so that each of these quality parameters could be evaluated from the reconstructed GRE film received from a Lunar Orbiter.

The quality parameters chosen to describe signal detail rendition is the frequency response or modulation transfer function (MTF) of the photographic system. In essence, this parameter measures the sharpness of the reconstructed image. Since most of the other quality parameters describing detail rendition (e. g., resolution, Schade's equivalent passband) can be derived from the modulation transfer function, the choice of this parameter seems to be the most logical. In addition, it has become common place in the optical industry to provide MTF data for components such as lenses and films, thus allowing the use of existing data in performance comparison. In the case of the Lunar Orbiter photographic system, a non-linear element of the system, the spacecraft film, requires that two modulation transfer functions be evaluated, one for each linear segment of the system (Fig. 1). These transfer functions are called the camera system modulation transfer function and the scanner-communications-GRS modulation transfer function. The product of these functions represents the effective "modulation transfer function" for the entire imaging system for purposes of system evaluation.

The factors describing signal level must relate the input dc signal level, exposure on the spacecraft film, to the output signal level GRE film density. Essentially this parameter measures the reproduction of tonal

---

* In this study attention is confined to black-white monoscopic photographs.

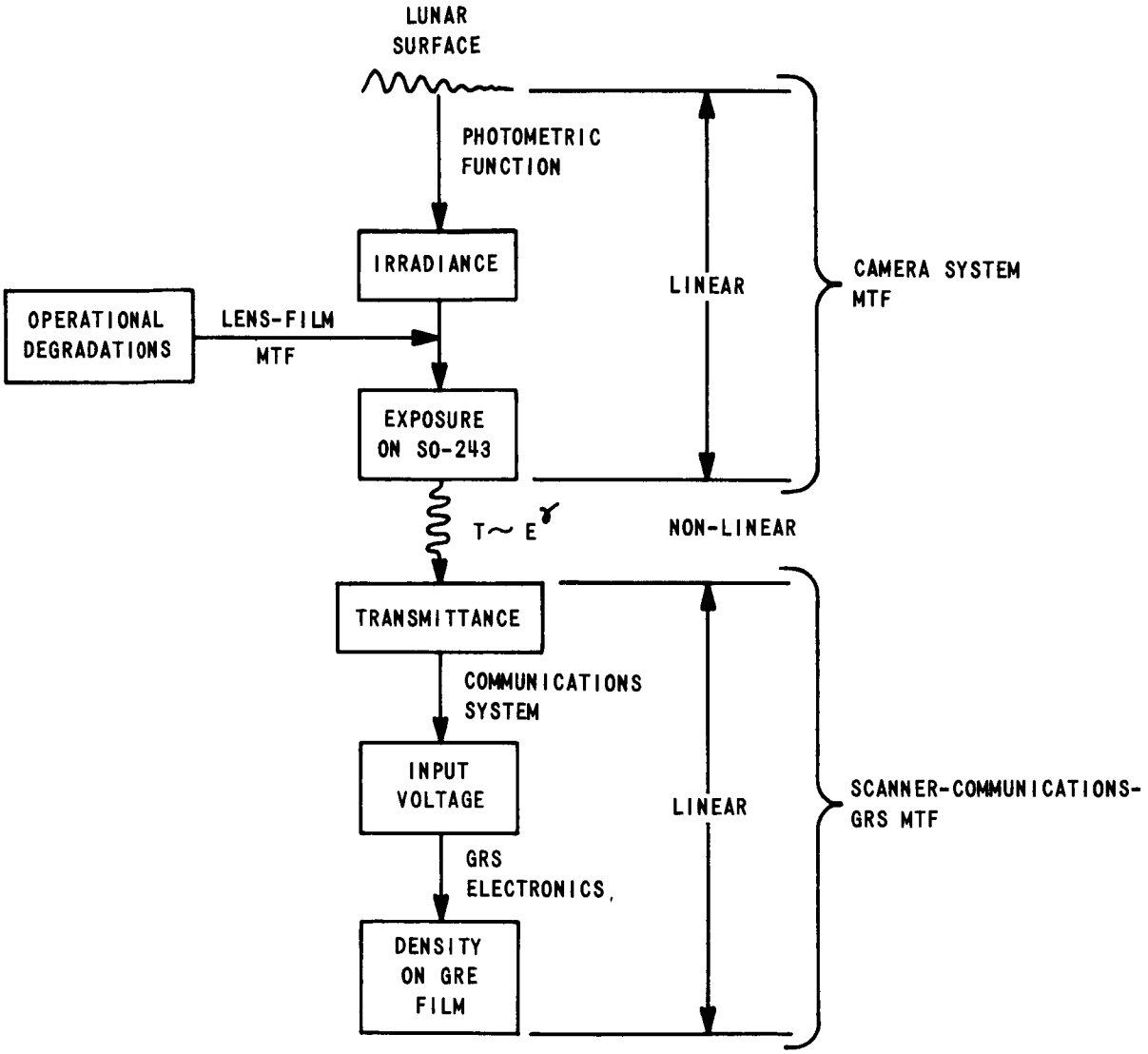

Figure 1 LUNAR ORBITER PHOTOGRAPHIC DATA FLOW DIAGRAM

quality. Because of the non-linear response of the spacecraft film, it is convenient to separate the total response into two functions describing signal level. These are the Hurter-Driffield response curve for the spacecraft film and the linear response characteristic relating the transmittance of the spacecraft film to the recorded GRE density.

A single quantity was chosen to describe the noise level of the system. This quantity is the white noise power density in the GRE image within the spatial frequency band occupied by the signal, namely; ± 20 lines/mm at the GRE film scale. It is evaluated by measuring the total noise power in this band and subsequently dividing by the bandwidth. Since the total noise power is a function of signal level, it must be evaluated near the average density of the GRE image. A more general quantity, namely, the noise power spectrum, could have been chosen as the noise level quality parameter. However, the total noise power is considerably easier to measure and calculations made during the Phase I effort indicated that the assumption of a white noise power spectrum is not unreasonable. Consequently, the white noise power density was chosen as the noise level quality parameter.

3. MEASUREMENT OF QUALITY PARAMETERS

This section describes in detail the techniques required to measure the quality parameters described in the previous section and includes an evaluation of the accuracy of these techniques. The first problem in the measurement of quality parameters is the selection of targets in the GRE image which can be used as sources of data. This was investigated in detail during the Phase I effort and is described briefly in Section 3. 1. It is next necessary to develop methods of actually acquiring the data from the reconstructed imagery. The details of the data acquisition techniques were given brief consideration during the Phase I effort and are discussed at more length in Section 3. 2. Once the data is obtained, reduction techniques are required. Although partially developed during the Phase I effort, the reduction techniques were further refined during the Phase II effort and are discussed in Section 3. 3. One of the primary tasks of the Phase II analysis, reported in Section 3. 4, was to establish a quantitative evaluation of the accuracy of the measurement techniques. The evaluation was performed using both simulated and real data. Based upon the analysis of the accuracy of the measurement techniques, the number of quality measurements needed to assess the Lunar Orbiter photographic system performance with an acceptable precision is established in Section 3. 5.

3. 1 Targets in the GRE Image Employed in Measuring the Quality Parameters. - All the techniques for measuring the modulation transfer function (detail rendition) employ a test object or target whose spatial frequency content is known and can be compared to the resulting frequency content of its image. The target which is chosen must be sufficiently sharp so that it is significantly degraded by the imaging system allowing measurement of the corresponding modulation transfer function. In the case of the Lunar Orbiter imaging system, a non-linear element in the system, the spacecraft film, requires that two modulation transfer functions be evaluated. One transfer function describes the signal detail rendition of the camera system (this system includes the camera lens, the film and any

operational degradations such as image motion, image vibration, and defocus). To evaluate this transfer function, one must select an object which is imaged by the camera lens. Available targets were investigated during the Phase I effort and it was found that the only acceptable target is the shadow-to-sunlight edge interior to a crater. The sharpness of this edge target is dependent upon the length of the penumbral region between complete shadow (umbra) and total sunlight. In selecting a shadow-to-sunlight edge, care must be taken to insure that the penumbral length is less than the expected resolution of the system being evaluated (i. e., one meter for the high resolution camera system and 8 meters for the medium resolution camera system). The penumbral length is dependent upon the crater geometry and the solar zenith angle. Assuming a spherical model for a crater, it has been shown that craters less than 50 resolution elements in diameter with sun elevations less than 30° provide acceptable shadow-to-sunlight edges for the evaluation of either camera system MTF. If possible, selection of craters with diameters in the region of 10 to 20 resolution elements, such as those shown in Fig. 2, are preferred.

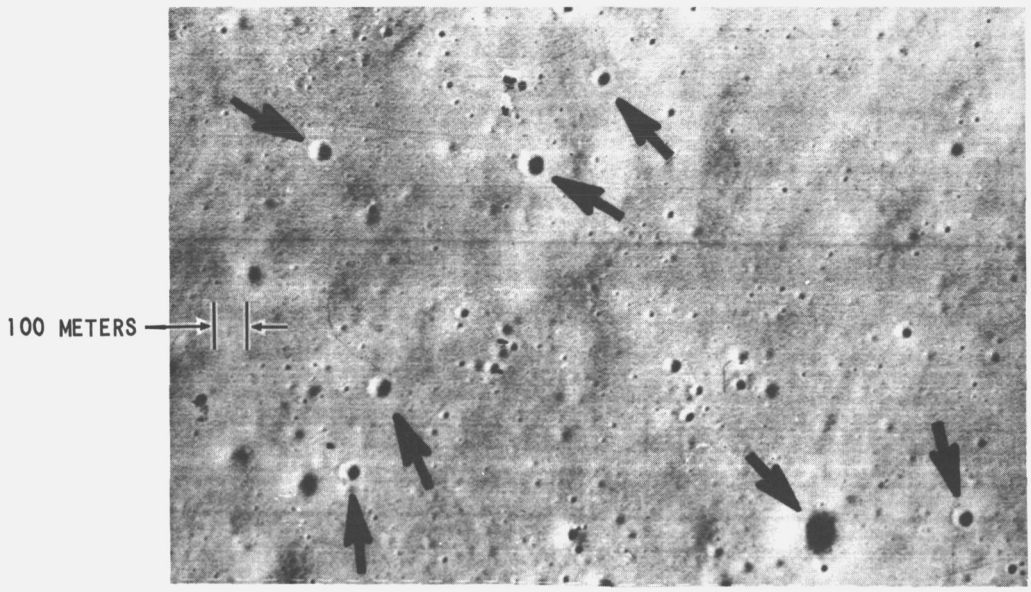

Figure 2 TYPICAL SHADOW-TO-SUNLIGHT EDGE TARGETS IN A MEDIUM RESOLUTION PHOTOGRAPH

The other transfer function describes the signal detail rendition of the combined scanner, communications, and GRE system. To evaluate this transfer function, one must select an object which is not imaged by either camera lens but still transmitted by the electro-optical portion of the imaging system. Fortunately, ample targets are supplied by the pre-exposed edge data array placed on the spacecraft film and shown in Fig. 3. This array consists of high and low contrast bar patterns oriented parallel, perpendicular and at 45° to the length of the spacecraft film with frequencies ranging from 32 to 160 lines/mm and also a step tablet consisting of nine uniform gray scales to provide sensitometric data. The target selected for

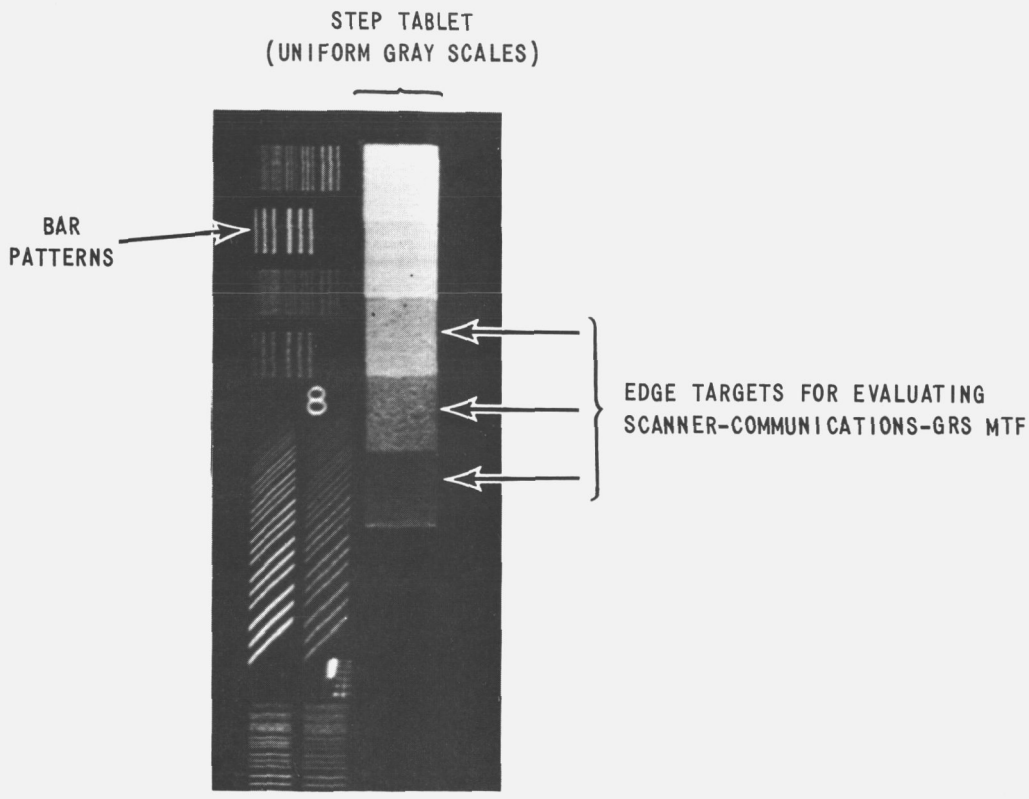

Figure 3 TYPICAL PRE-EXPOSED EDGE DATA ARRAY AND ASSOCIATED TARGETS

evaluation of the scanner-communications-GRS modulation transfer function during the Phase I effort was one of several edges between the intermediate gray levels of the step tablet and the surrounding background. In general, it was found that the edges of Step 5, 6 or 7 may be sufficiently sharp to be useful whereas the edges corresponding to the remaining steps were less sharp, possibly being affected by the response characteristic of the films. The use of these edges limits the evaluation of the modulation transfer function to the mechanical scan direction and requires an auxiliary evaluation of the average sharpness of the test edges as they would appear on the spacecraft film. In the electrical scan direction, no edges are available which are suitable for evaluation of the modulation transfer function and if this data is desired, one must rely upon the bar patterns. There are several reasons why the edge objects were preferred to the bar patterns for evaluation of the modulation transfer function. First, there are no frequencies below 32 lines/mm in the bar patterns. As will be seen later, this region is one of importance in evaluating the quality of the Lunar Orbiter photographs. Secondly, because the bar patterns are not pure sine waves special consideration must be given to their harmonic content when employing them in evaluation of the modulation transfer function. Consequently, the analysis required would be more complicated than that necessary to evaluate the modulation transfer function from the edge targets.

The data required to evaluate the signal level quality parameters is provided by the step tablet in the pre-exposed edge data array. The output signal level is determined by measuring the average density of each of the gray levels in the step tablet. These densities are then related to the known exposure levels used in pre-exposing the edge data array onto the spacecraft film. To separate the corresponding total response for the photographic system into the Hurter-Driffield response curve for the spacecraft film and the linear response characteristic between the transmittance of the spacecraft film and the recorded GRE density, additional data consisting of the expected transmittance values for each step of the step tablet on the spacecraft film must be obtained from other data sources. Additional details of this procedure are given in the following two sections of this report.

The remaining quality parameter, namely, the white noise power density in the GRE image, can also be measured by employing data obtained from the pre-exposed edge data array. A target must be selected to evaluate the total noise power within the spatial frequency bandwidth occupied by the signal. This target must initially have a uniform exposure over its entire area and the exposure level of the target must be near the average exposure level for the lunar scene since the total noise power is dependent upon the signal level. Several possible targets were established during the Phase I effort. These included an area in the lunar scene which appeared to be both uniform and flat or one of the uniform gray scales of the step tablet.

3.2 Data Acquisition Techniques. - Once the targets have been selected, the next procedure in the measurement of the quality parameters is one of data acquisition. On the surface, this appears to be a straightforward problem. However, it is complicated by the fact that the photographic data is transmitted and reconstructed by a scanning or semi-discrete process. In addition some supporting data must be obtained from a bimat processed sample of spacecraft film for use in the data reduction techniques described in the next section. The details of the data acquisition procedures are described in this section.

Most of the required data are obtained by scanning the reconstructed GRE film with a microdensitometer. The selection of a microdensitometer aperture is influenced by the amount of degradation which it will introduce into the resulting density trace and by the presence of the scan line structure in the reconstructed image. In the Phase I final report[1], for example, it was recommended that the trace of an edge selected in the pre-exposed data array used to evaluate the scanner-communications-GRS modulation transfer function be made with "a scanning slit which is narrow with respect to the edge width (i. e., a slit with of less than 20 microns)". This recommendation was made to insure that the degradation introduced into the resulting edge trace by the scanning aperture is sufficiently small so that correction of the edge trace for the finite size of the aperture is not required. During the first part of the Phase II study, test data was acquired by scanning such

edge targets with the slit aperture 25 microns wide. Since the spacing between the scan lines is about 24 microns at the GRE film scale, this aperture was chosen to conveniently remove the scan line structure from the resulting density trace. It was subsequently decided that this procedure was not adequate for several reasons. First, the degradation introduced into the edge trace by scanning with an aperture 25 microns wide is significant over the ± 15 line/mm band occupied by the signal at the GRE film scale. The response of this aperture is below 0.9 at frequencies above 10 lines/mm. In addition, the microdensitometer averages or convolves the scanning aperture with the transmittance (rather than the density) of the GRE film. It can be shown that the combined scanner-communications-GRE systems may be treated as a linear system (amenable to modulation transfer function analysis) when relating the transmittance distribution of the spacecraft film to the reconstructed density distribution of the GRE film*. In acquiring data, therefore, operations should not be employed which act in a non-linear fashion upon the density of the GRE film. Since the microdensitometer aperture integrates the transmittance of the GRE film, and density and transmittance are non-linearly related, viz.

$$D = -\log_{10} T \tag{1}$$

the width of the scanning aperture should be less than the distance between appreciable density fluctuations produced by signal variation on the GRE film. Fig. 4 shows a microdensitometer trace made across the edge of Step 6 in the step tablet. The microdensitometer aperture used in obtaining this trace was 1.25 microns wide at the GRE film scale. To insure that large density fluctuations do not occur across the scanning aperture, at

---

* The analysis presented in the Phase I final report which established the validity of assuming a linear system depended upon the fact that the adjacent scan lines on the GRE film did not overlap to an appreciable extent. The effect of increasing overlap between scan lines upon the linearity of the combined scanner-communications-GRE system was re-examined in the Phase II effort and is discussed in Section 3.3 and Appendix A.

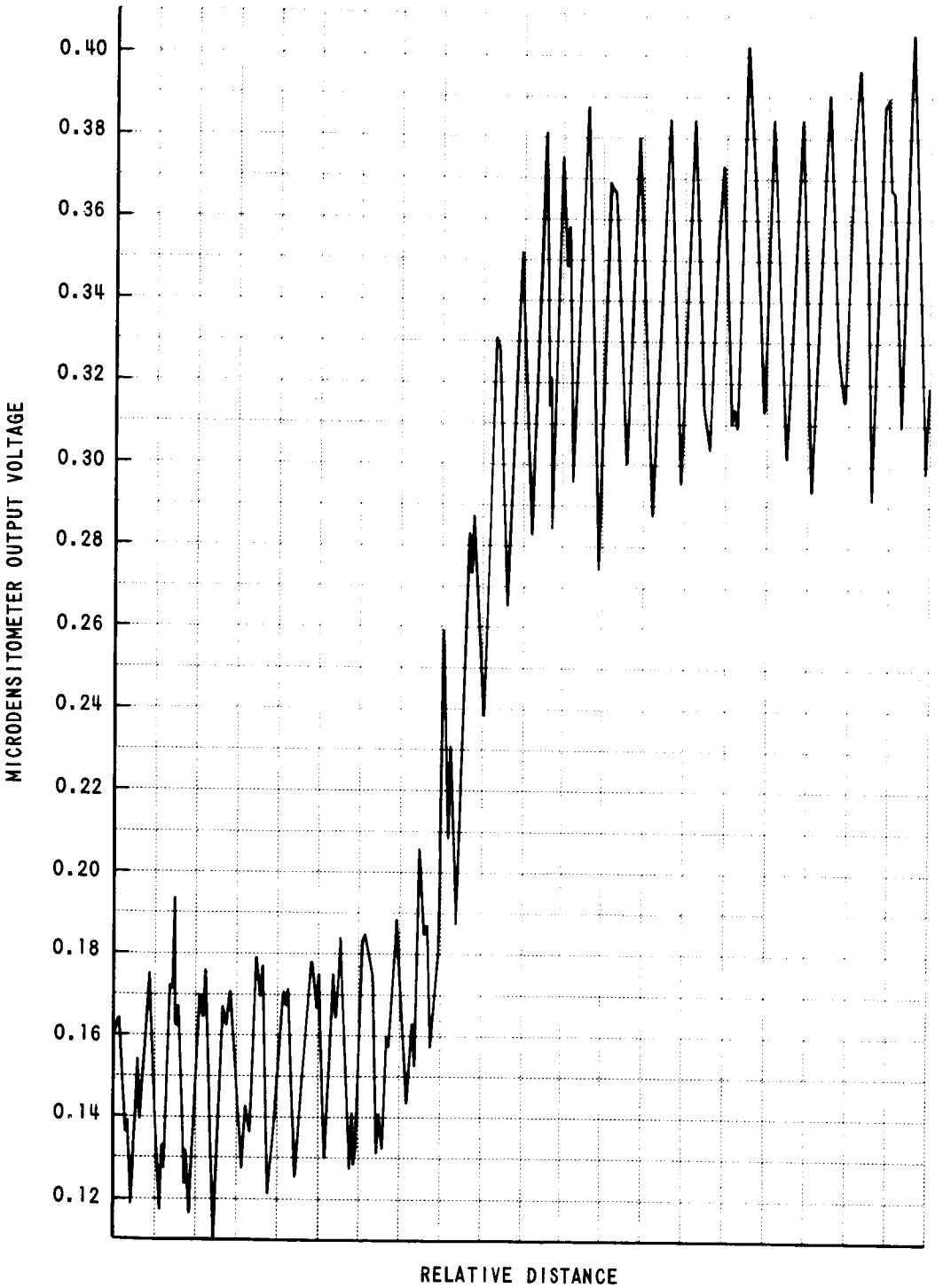

Figure 4 A MICRODENSITOMETER TRACE ACROSS STEP 6 OF THE STEP TABLET SHOWING THE SCAN LINE STRUCTURE

any instant of time, the width of the aperture in the mechanical scan direction should be less than 1/10 of the scan line spacing which is about 24 microns on the GRE film. Therefore, all of the microdensitometer apertures used in obtaining data from the GRE film should have a width of 3 microns or less. In this case, an alternative technique for removal of the "coherent noise" or scan line structure from the density traces must be implemented. This is discussed in more detail in the next section.

Once an appropriate microdensitometer scanning aperture is selected, the output data must be obtained in a form which can be used in the data reduction techniques. This requires that the data be in digital form to facilitate the numerical processing described in the next section. The present procedure employed at CAL is shown in the flow diagram given in Fig. 5. The voltage output of the microdensitometer which is proportional to the integrated intensity within the scanning aperture is employed as an input to an analog-to-digital converter which samples the voltage at a fixed

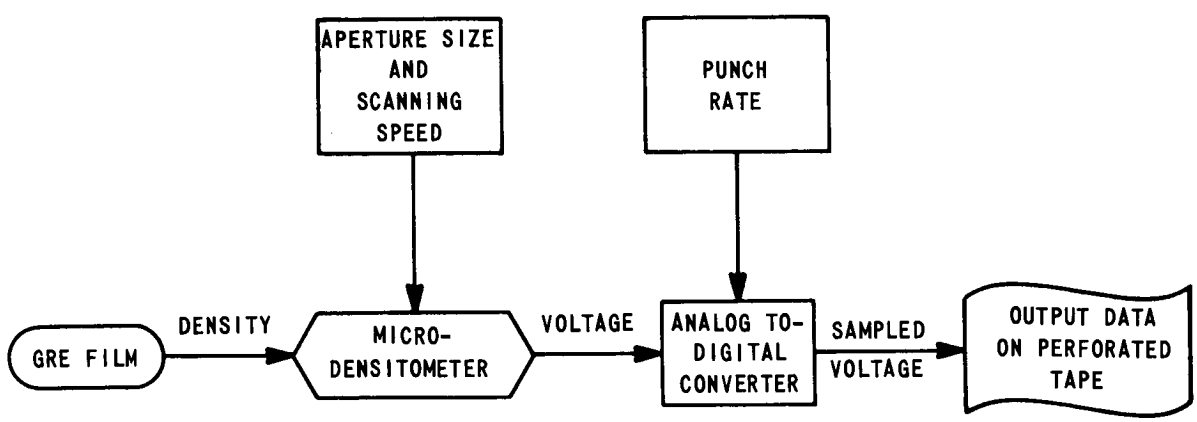

Figure 5 DATA ACQUISITION FLOW DIAGRAM

rate and subsequently punches the sampled voltage signal onto perforated tape. The combination of the punch rate of the analog-to-digital converter and the scanning speed employed in the microdensitometer determines the sampling interval between points in the output data. A sampling rate must be sufficiently large so that the corresponding folding frequency will be large enough to reproduce adequately the scan line structure in the GRE image. About 12 samples per scan line is preferred and can be achieved with the CAL system by employing a scan rate of 1.2 mm/minute and a punch rate of 10.2 punches per second. These or equivalent combinations of scan speed and punch rate should be employed when scanning the GRE film. Naturally, a large punch rate is desirable in order to minimize the time required in obtaining the desired data.

Based upon the targets selected as sources of data in evaluating the quality parameters, the following measurements should be made on the GRE film. Microdensitometer scans are made across each individual gray scale of the step tablet in the mechanical scan direction (that is, perpendicular to the scan lines). A convenient aperture for making these scans is a slit 1.25 microns wide and 95 microns long. This aperture satisfies the requirement established earlier for reproduction of the scan lines (i.e., a width less than 3 microns) and has a response above 0.99 at frequencies below 15 lines/mm. By employing this aperture, the degrading effect upon the signal can be completely ignored. Similarly, the edges between the gray scales and surrounding background which are selected for evaluation of the scanner-communications-GRS modulation transfer function can be scanned using the same slit. In fact, the edge trace shown previously in Fig. 4 was obtained using this technique. When scanning the shadow-to-sunlight edge interior to a crater for the purpose of evaluating the camera system modulation transfer function some additional care must be exercised in choosing the scanning aperture. Various size slits may be required to insure that the length of the slit is less than 1/20 of the diameter of the crater image on the GRE film. This requirement is imposed to avoid the problem of the curvature of the shadow-to-sunlight edge across the crater. The edge is scanned in the sun plane which is inclined slightly to the scan

line structure. The effective width of the scanning slit, that is, the width of the slit in the mechanical scan direction, is slightly greater than its actual width. Since the inclination is expected to be about 12°, it is still acceptable to require that the actual width of the scanning slit be 3 microns or less. For crater diameters of 10 to 20 resolution elements*, a scanning aperture whose length is 50 to 100 microns is acceptable.

To evaluate the noise level quality parameter, that is, the total noise power in the GRE image, a uniform area in the lunar scene or the pre-exposed edge data array is scanned with a circular microdensitometer aperture. In selecting the appropriate aperture the only restriction is that the aperture must be small enough (less than 3 microns) to sample adequately the scan line structure in the GRE image. As indicated in Appendix D, an improved measurement procedure would employ a narrow slit aperture rather than a circular aperture in evaluating the noise level quality parameter. This procedure was not implemented in this study, however, due to the limited time available.

Table 1 presents a summary of appropriate microdensitometer apertures for scanning the targets selected to evaluate the various quality parameters. The table also includes some additional information such as the number of points in an average microdensitometer trace and the sampling interval (that is, the interval between points).

In addition to the data obtained from the reconstructed GRE film, some supplementary data must be obtained from a bimat processed sample of spacecraft film originating from the end of the roll which is loaded into the spacecraft. The data required includes the values of transmittance for each of the gray levels in the step tablet of the pre-exposed edge data array and a measure of the sharpness of the edge between a gray level and its surrounding background for those edges which would be used in evaluating the scanner-communications-GRS modulation transfer function. To obtain these data, microdensitometer scans must be made on the bimat

---

* One resolution element is approximately 96 microns on the GRE film.

Table 1

APPROPRIATE PARAMETERS FOR DATA ACQUISITION*

QUALITY PARAMETER	TARGET	MICRODENSITOMETER		SAMPLING INTERVAL**	NO. OF POINTS	RESTRICTIONS
		OPTICS	APERTURE**			
CAMERA SYSTEM MTF	SHADOW-TO-SUNLIGHT EDGE INTERIOR TO A CRATER	10X OBJECTIVE 10X EYEPIECE	SLIT $3\mu \times 25\mu$	1.965μ	~750	APERTURE SATISFACTORY FOR CRATER DIAMETERS BETWEEN 5 AND 20 RESOLUTION ELEMENTS; SCANNING IN THE SUN DIRECTION
SCANNER-COMMUNICATIONS-GRS MTF	EDGES BETWEEN BACKGROUND AND SELECTED GRAY LEVELS IN THE PRE-EXPOSED DATA ARRAY	10X OBJECTIVE 20X EYEPIECE	SLIT $1.25\mu \times 95\mu$		~750	SCANNING PERPENDICULAR TO THE SCAN LINES
SIGNAL LEVEL QUALITY PARAMETERS	UNIFORM GRAY LEVELS IN THE PRE-EXPOSED DATA ARRAY	10X OBJECTIVE 20X EYEPIECE	SLIT $1.25\mu \times 95\mu$		~350	
TOTAL NOISE POWER	UNIFORM GRAY LEVELS IN THE PRE-EXPOSED DATA ARRAY OR UNIFORM AREAS IN THE LUNAR SCENE	10X OBJECTIVE 20X EYEPIECE	CIRCULAR 2.5μ DIAMETER		~3500	

*SOME OF THE VALUES SHOWN WERE CHOSEN AS A CONVENIENCE FOR EXISTING CAL HARDWARE.

**DIMENSIONS ON THE GRE FILM.

processed film sample. These scans include density traces of each of the gray levels in the step tablet and edge traces across the potential edge targets of the step tablet. Because the scanning involves a sample of spacecraft film rather than reconstructed GRE film, the problem arising from the scan line structure is eliminated. It is both convenient and adequate, however, to obtain the supplementary data by employing the same microdensitometer aperture and sampling interval that is used when scanning the corresponding target on the reconstructed GRE film despite the difference in scale between the film.

Because of the nature of the measurement techniques, data must be obtained from more than one target when evaluating any one of the quality parameters or obtaining the supplementary data. The number of measurements required to evaluate the quality parameters with sufficient accuracy is discussed in more detail in Section 3.5. However, it should be noted here that the data acquisition techniques described in this section may be applied to more than one target of each type. The data obtained from the procedures outlined in this section are employed in the reduction techniques described in the next section to evaluate the selected quality parameters.

3.3 Data Reduction Techniques. - The discussion in this section of the reduction techniques first considers those elements which are common to all the data reduction procedures and then is subdivided into sections which describe the evaluation of an individual quality parameter. The computer programs which were developed during Phase I and Phase II to evaluate the quality parameters are described briefly, however, details such as Fortran listings are not included in this report.

3.3.1 Conversion of Perforated Tape and Removal of the Scan Line Structure: The procedures discussed in this section are common to all the data analyses. The initial process in reducing the data is to convert the perforated tape into punched IBM cards which are an acceptable form of input to the data reduction computer programs. At CAL, the hardware and software to achieve this task were in existence prior to the undertaking

of Project SLOPE and therefore will not be described in detail in this report. The system consists of a perforated tape reader which is integrated on-line to the computer (IBM 7044). An appropriate computer program reads the data from the perforated tape, checks for illegal punches or characters on the tape, and subsequently places the data on punched cards indicating any errors it has found in the perforated tape. The punched cards must then be corrected by hand for any errors discovered and appropriate control cards inserted as required for the data reduction computer programs.

The next procedure which is common to all of the data reduction techniques is the removal of the scan-line structure or "coherent noise". As a result of the analysis of the linearity of the combined scanner-communications-GRE systems reported in the Phase I final report[1], a method for removing the scan-line structure was suggested. The procedure involves filtering the density trace with a low-pass filter whose frequency response has a sharp cutoff at 20 lines/mm (i. e., half the scan line frequency at the GRE film scale). This can be achieved by convolving the sampled density trace with a sinc function in a digital computer. If the convolving function is not truncated, the frequency response of the filter is a rectangular function with a cutoff depending upon the zero spacings of the sinc function. Practically, the sinc function must be truncated after the first few cycles. This procedure introduces undesirable oscillation in the frequency response of the filter which can be eliminated by convolving the edge trace with a function which is the product of two sinc functions, namely*

$$W(x) = \begin{cases} \dfrac{\sin(\pi \nu_0 x)}{\pi \nu_0 x} \cdot \dfrac{\sin(\pi \nu_0 x/m)}{\pi \nu_0 x/m} & |x| \le \dfrac{m}{\nu_0} \\ 0 & |x| > \dfrac{m}{\nu_0} \end{cases} \qquad (2)$$

where ν_0 is half the scan line frequency or equal to 20 lines/mm at the GRE film scale. The normalization condition

---

* The undesirable oscillation is frequently referred to as Gibb's phenomenon and the technique employed for reducing this effect is the use of Lanczo's σ -factors (see Reference 2).

$$\sum_{n=-N}^{N} W(x_n) = 1 \tag{3}$$

determines the weights used in the convolution. The corresponding frequency response for the filter described by expressions (2) and (3) is shown in Fig. 6 for ν_0 equal to 20 lines/mm and $m = 3$. A sharper cutoff can be obtained by retaining additional cycles of the sinc function (i. e., $m > 3$). The practical upper limit to the value of m is dictated by the fact that some data is lost in the convolution process. Specifically, the amount of useful data is reduced by $2m$ scan lines. Fig. 8 shows the filtered edge traces which originally contained scan lines as indicated in Fig. 7. The filter with $m = 3$ was used and indicates that this filter is satisfactory.

3.3.2 Evaluation of the Signal Level Quality Parameters: The signal level quality parameters consist of the Hurter-Driffield response curve for the spacecraft film and the linear response characteristic between transmittance of the spacecraft film and the recorded GRE density. It will be recalled that the data required to evaluate these quality parameters consists of microdensitometer scans across each of the nine gray levels in the step tablet of the pre-exposed data array. A flow diagram for the numerical analysis used to process this data is shown in Fig. 9. A typical printed output from the associated computer program is reproduced in Fig. 10. The first step is to remove the scan lines from the trace of a gray level in the step tablet. After the scan lines have been removed, the average microdensitometer voltage for this gray level is computed and then converted to density by employing the appropriate microdensitometer calibration. This process is repeated until all the gray levels of the step tablets which have been scanned are processed. The individual measurements of density for each gray level are then averaged and the corresponding standard deviation computed. If any of the individual density measurements are more than two standard deviations away from the average, these data are eliminated and an adjusted average and standard deviation computed using the remaining values for that gray level. A typical output of this step is shown in part (b) of Fig. 10.

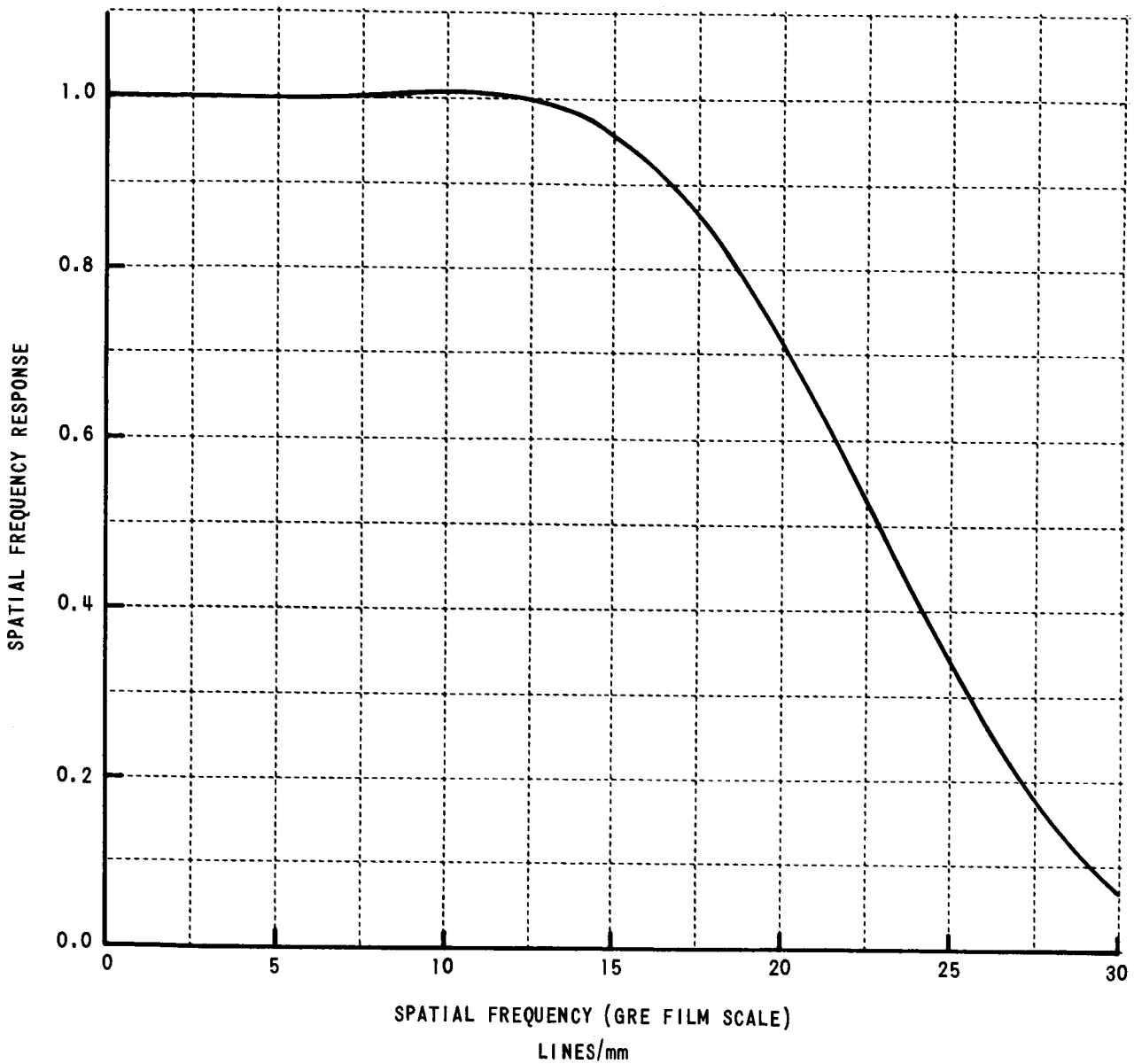

Figure 6 FREQUENCY RESPONSE FOR A NUMERICAL FILTER DESIGNED TO REMOVE SCAN LINE STRUCTURE FROM DENSITY TRACES (ν = 20 LINES/mm, m = 3)

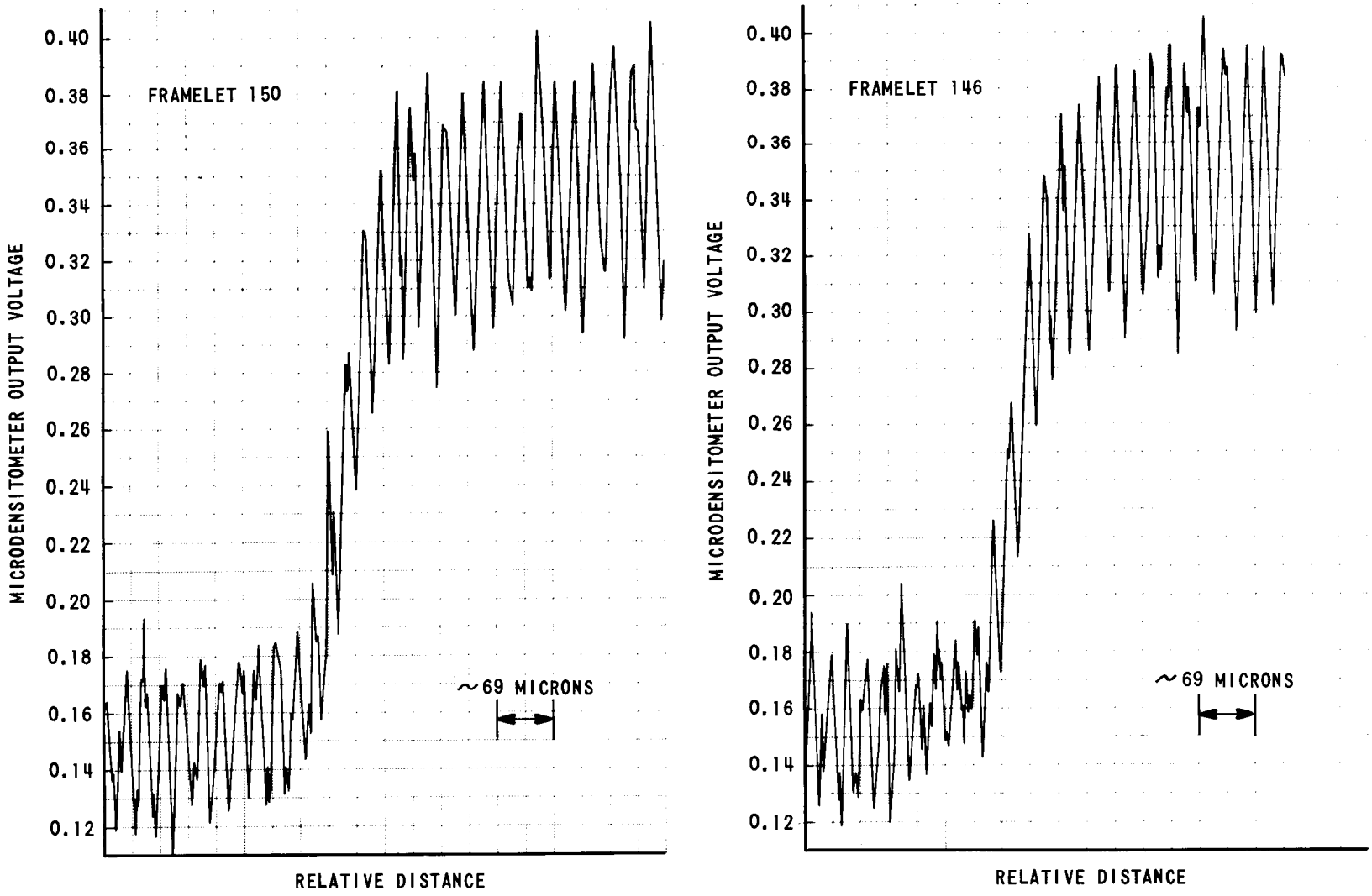

Figure 7 TRACES ACROSS STEP 6 OF THE STEP TABLET SHOWING SCAN LINE STRUCTURE AND MADE FROM ORIGINAL GRE FILM OBTAINED IN THE PRE-LAUNCH GOLDSTONE READOUT OF LUNAR ORBITER I

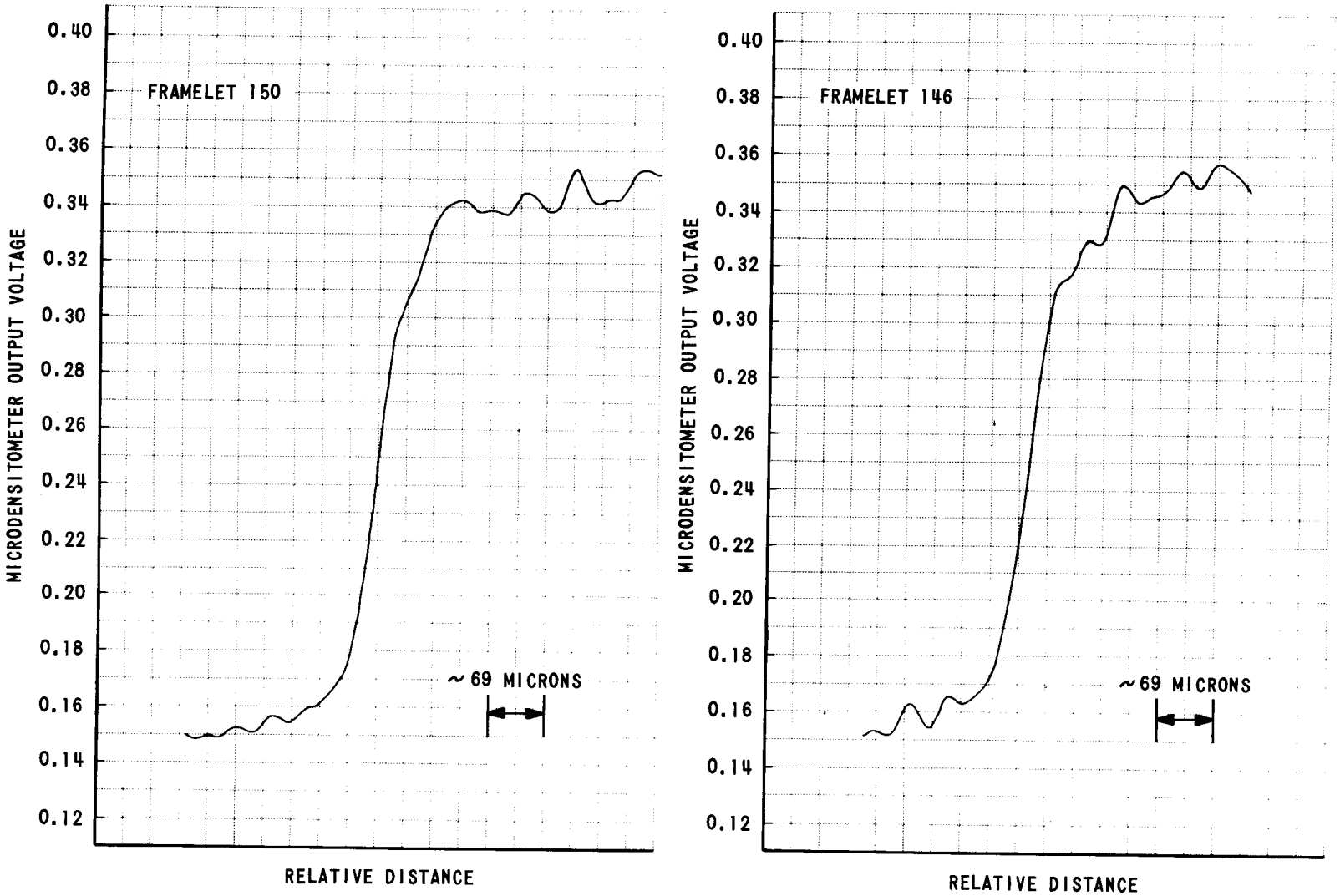

Figure 8 NUMERICALLY FILTERED TRACES WITH SCAN LINE STRUCTURE REMOVED

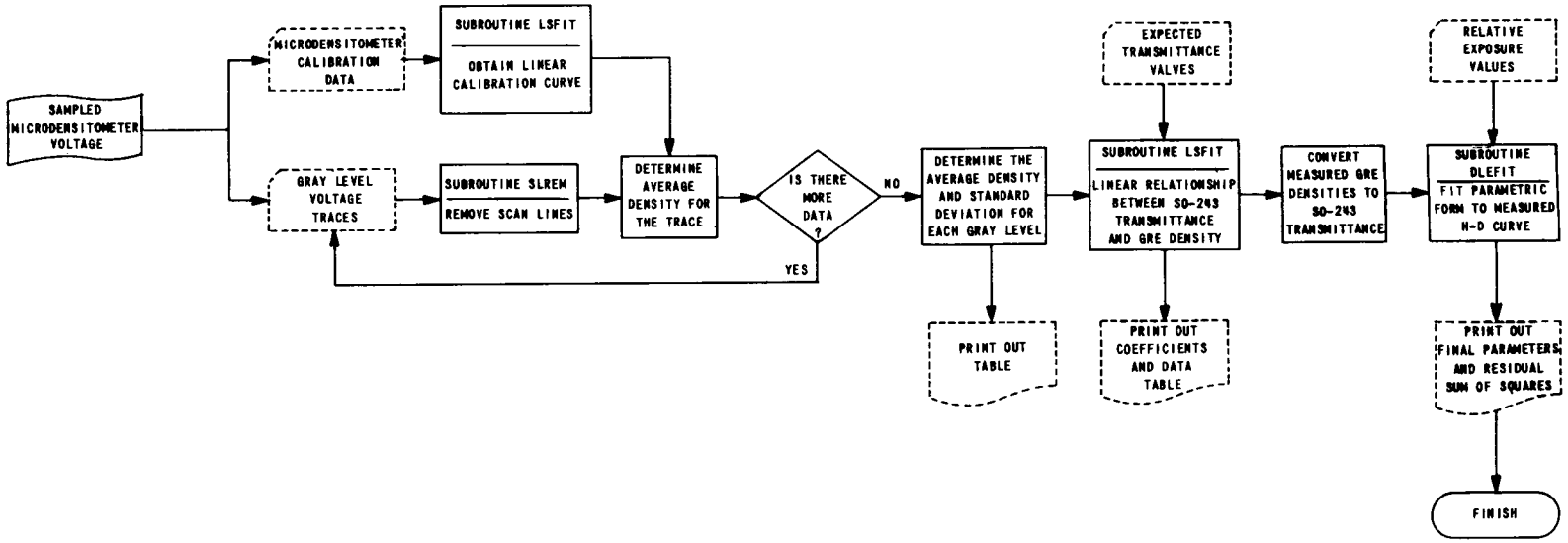

Figure 9 FLOW DIAGRAM OF THE PROCEDURES USED IN THE SIGNAL LEVEL ANALYSIS

***** MICRODENSITOMETER CALIBRATION *****

CALIBRATION EQUATION IS DENSITY = A + B*VOLTS

WHERE A= -0.045345 B= 6.016403 VMIN= 0.007537

THE CALIBRATION DATA IS

LEVEL	DENSITY	AVE. VOLT	COMP. DENS
1	0.	0.007556	0.000112
2	0.6200	0.122833	0.693669
3	1.5100	0.258750	1.511399
4	1.5100	0.260200	1.520122
5	1.8300	0.306000	1.795674
6	1.0600	0.184143	1.062532
7	2.2200	0.378333	2.230860
8	2.6000	0.440625	2.605632

(a) PAGE 1 - MICRODENSITIOMETER CALIBRATION

LUNAR ORBITER SIGNAL LEVEL ANALYSIS GRE999

STEP NUMBER	1		2		3		4		5		6		7		8		9
FRAMELET/GRE	DENSITY																
146	2.214	146	2.327	146	1.964	146	1.525	146	1.182	146	0.857	146	0.763	146	0.733	146	0.742
146	2.258	154	2.242	154	1.981	154	1.670	154	1.075	154	0.765	154	0.694	154	0.672	154	0.695
154	2.221	147	2.220	147	1.929	147	1.638	147	1.183	147	0.862	147	0.760	147	0.724	147	0.744
147	2.339	148	2.284	148	2.038	148	1.632	148	1.232	148	0.871	148	0.741	148	0.711	148	0.749
148	2.358	149	2.254	149	2.026	149	1.689	149	1.171	149	0.865	149	0.750	149	0.728	149	0.706
149	2.291	0	0.	0	0.	0	0.	0	0.	0	0.	0	0.	0	0.	0	0.
AVERAGE	2.280		2.269		1.988		1.631		1.169		0.844		0.742		0.713		0.727
STD. DEV.	0.060		0.039		0.045		0.063		0.058		0.045		0.028		0.025		0.024
ADJ. AVERAGE	2.280		2.269		1.988		1.631		1.169		0.844		0.742		0.713		0.727
ADJ. STD. DEV.	0.060		0.039		0.045		0.063		0.058		0.045		0.028		0.025		0.024

(THE POINTS PRECEDED BY AN ASTERISK DIFFERED FROM THE AVERAGES BY MORE THAN TWO STANDARD DEVIATIONS.
THEY WERE DELETED AND THE ADJUSTED AVERAGES AND DEVIATIONS WERE COMPUTED.)

(b) PAGE 2 - GRE DENSITY MEASUREMENTS

Figure 10 TYPICAL PRINTED OUTPUT FROM SIGNAL LEVEL ANALYSIS PROGRAM

CALIBRATION EQUATION IS SO-243 TRANSMITTANCE = C + D*GRE DENSITY

WHERE C= -0.226330 D= 0.367807 DMIN= 0.615351

THE CALIBRATION DATA IS

STEP NO	TRANS	DENSITY	COMP. TRANS
2	0.6160	2.269384	0.608365
3	0.5130	1.987544	0.504703
4	0.3650	1.630872	0.373516
5	0.2040	1.168681	0.203519
6	0.0955	0.844033	0.084111
7	0.0525	0.741769	0.046497
8	0.0288	0.713468	0.036088

(c) PAGE 3 - GRE DENSITY VS. SPACECRAFT FILM TRANSMITTANCE REGRESSION

NON-LINEAR PARAMETRIC ESTIMATION OF HURTER-DRIFFIELD RESPONSE CURVE

TERMINATED BECAUSE RESIDUALS CHANGED BY LESS THAN 0.01 PERCENT

NUMBER OF ITERATIONS= 11

INITIAL RESIDUAL= 0.63072535E-01 FINAL RESIDUAL= 0.13873741E-03

PARAMETER NO	INITIAL VALUE	FINAL VALUE
1	0.38730000E 00	0.38618703E 00
2	0.14142000E 01	0.11617717E 01
3	0.26400000E 01	0.40310611E 01
4	0.	-0.33021694E 00
5	0.38460000E 00	0.45534081E 00

THE PARAMETRIC FORM IS D=B1**2+B2**2*(ERF(B3*LOG(B4**2+B5**2*E)))

(d) PAGE 4 - HURTER-DRIFFIELD RESPONSE OF SPACECRAFT FILM

Figure 10 TYPICAL PRINTED OUTPUT FROM SIGNAL LEVEL ANALYSIS PROGRAM

Since the photographic system was designed to have a linear relationship between spacecraft film transmittance and recorded GRE density, the measured values of GRE density for each of the gray levels in the step tablet are combined with the expected transmittance values of the corresponding levels on the spacecraft film and a linear regression analysis is performed. The expected values of transmittance are obtained by scanning a section of bimat processed spacecraft film obtained from one end of the roll of flight film loaded into the spacecraft. Part (c) of Fig. 10 shows a representative printed output resulting from the regression.

Several factors can produce a nonlinear relationship between the measured GRE densities and the expected transmittance values. These include time dependent variations of the signal level performance such as non-uniform processing of the spacecraft film, changes in the gain of the scanner with time or format position, and fluctuations in the gain of the GRE system. Since the GRE density corresponding to any one of the gray levels in the step tablet is determined by making measurements from that level on several framelets selected more or less at random on the spacecraft film, the portion of these variations which are of a random nature should not affect the average density measured for the gray level, but rather produce a larger standard deviation in the individual measurements. Systematic variations, on the other hand, should produce a non-linear relationship among the data. Another probable source of systematic variation, in addition to those described above, is the possible additional exposure which the spacecraft film may receive from radiation sources before the film is processed. This exposure is added to the exposure of the pre-exposed edge data array and therefore the values of transmittance for each of the gray levels on the spacecraft film are less than those measured from the bimat processed samples of SO-243 film. Therefore, in a mission where a significant amount of radiation exposure is indicated by the detectors located in the spacecraft, expected values of transmittance should be appropriately adjusted by including the additional radiation exposure which the film received. Such a correction may vary from frame to frame depending upon the total radiation dosage received by the frame before development.

Once the best linear relationship between GRE density and spacecraft film transmittance has been obtained, this relationship is used to compute the value of transmittance corresponding to the average GRE density measured for each of the gray levels in the step tablet. The transmittance values can then be directly converted to the corresponding density on the spacecraft film. These values of density and the known relative exposure for each of the gray levels of the step tablet are the data required to determine the Hurter-Driffield response curve for the spacecraft film. The data is fitted by the parametric form

$$D = b_1^2 + b_2^2 \, erf\left\{ b_3 \log_{10} (b_4^2 + b_5^2 E) \right\} , \tag{4}$$

where

$$erf(x) = \frac{1}{\sqrt{2\pi}} \int_{-\infty}^{x} e^{-\frac{t^2}{2}} dt ,$$

as a convenience in using the response curve in succeeding evaluation procedures. The fitting technique employs nonlinear parametric estimation and requires an initial estimate of the 5 parameters deonted by b_1, b_2, b_3, b_4 and b_5 in expression (4) *. It is desirable to have these estimates reasonably close to those which provide the best fit to the data and a procedure for obtaining the required initial estimates was developed. Since the erf function is confined to values between zero and one, it can be seen from Eq. (4) that

$$b_1 = \sqrt{D_{MIN}} \tag{5}$$

and

$$b_2 = \sqrt{D_{MAX} - D_{MIN}} \tag{6}$$

or that an estimate of b_1 and b_2 can be obtained by estimating the entire range of densities included by the response curve. Further, letting

---

* The squares of b_1, b_2, b_4 and b_5 are employed in the parametric form to satisfy the physical constraint of non-negative density and exposure.

D_i and E_i represent the density and the relative exposure of the ith level of the step tablet and since the initial estimate of $b_4 = 0.0$ is reasonable, an estimate of b_3 and b_5 can be obtained by employing the exposure and corresponding density for two separated gray levels of the step tablet in the following expressions obtained from Eq. (4):

$$b_5 = 10 \frac{K_j \log E_i - K_i \log E_j}{2(K_i - K_j)} \tag{7}$$

where $K_i = \mathrm{arcerf}\left\{(D_i - b_1^2)/b_2^2\right\}$, arcerf representing the inverse of the erf function, and

$$b_3 = \frac{K_i}{2 \log b_5 + \log E_i} = \frac{K_j}{2 \log b_5 + \log E_j} \tag{8}$$

This procedure will be used in Section 3.4 to provide initial estimates for fitting the measured Hurter-Driffield response curve of the processed Goldstone format used in the prelaunch readout test of Lunar Orbiter I.

3.3.3 Evaluation of the Total Noise Power: The quality which describes the noise level is the total noise power in the GRE image in the band occupied by the signal (i.e., $|\nu_x|$, $|\nu_y| \leq 20$ lines/mm). The primary objective of the data reduction technique shown in Fig. 11 is to measure this total noise power with a secondary objective being to acquire any information about the shape of the noise power spectrum. The total noise power can be simply determined by computing the variance of the noise density trace. The input data to the computer program which evaluates the total noise power is a density trace containing approximately 3,000 points with a sampling interval of 1.965 microns. This sampling interval was chosen to sample the scan line structure in the GRE image. The initial processing of the data involves removal of this structure. It should be noted, therefore, that the total noise power will not contain a component from the "coherent noise". In addition to obtaining the total noise power, the data is further analyzed by high pass filtering with a series of five filters shown in Fig. 12. From the figure it can be seen that the frequency

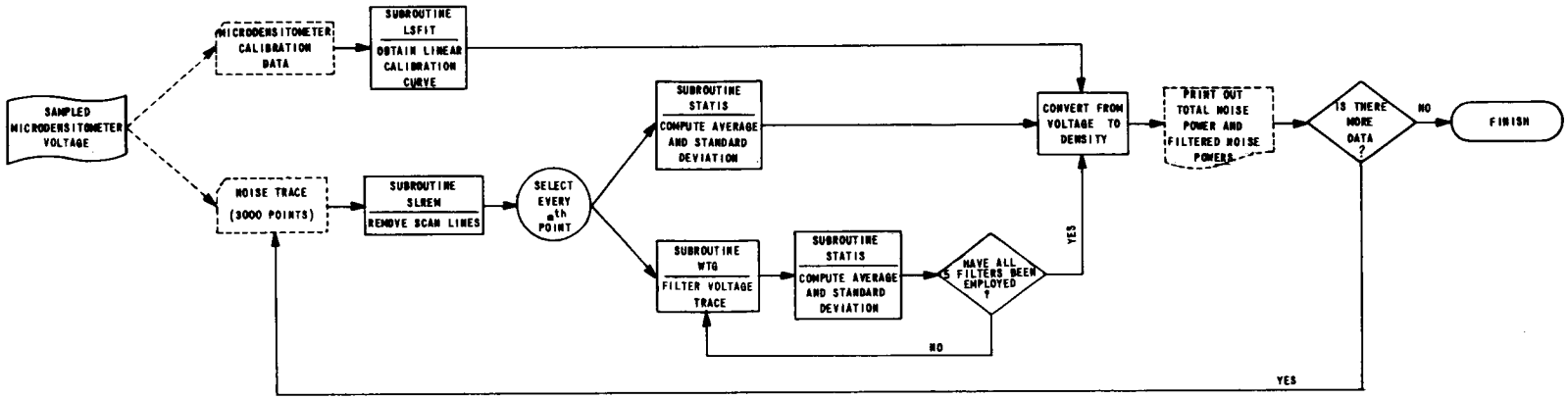

Figure 11 FLOW DIAGRAM OF THE PROCEDURES USED IN PROCESSING NOISE LEVEL DATA

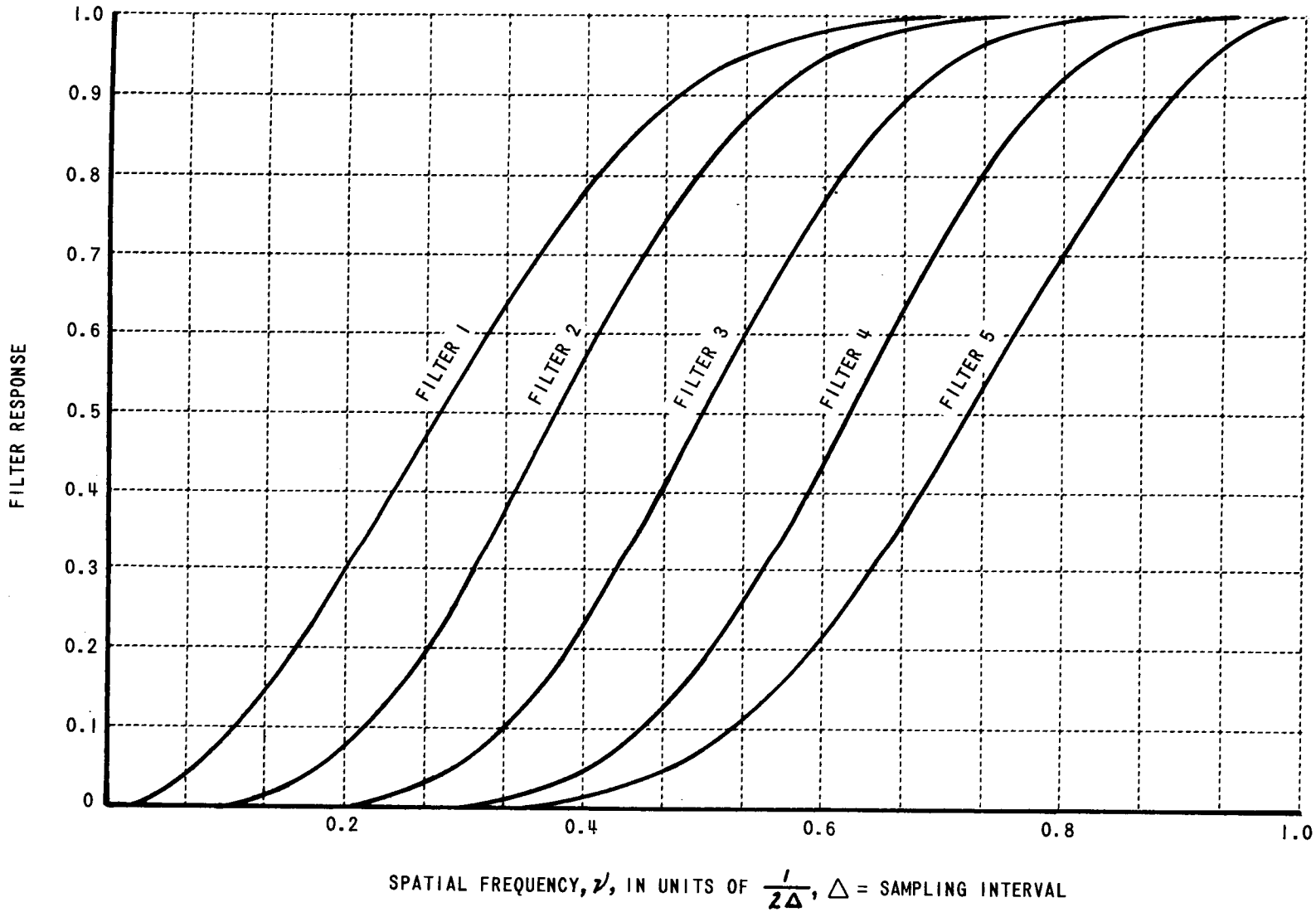

Figure 12 RESPONSE CURVES OF NUMERICAL FILTERS USED IN NOISE LEVEL ANALYSIS

response of the five filters depends upon the sampling interval between the data points. For these filters to operate in the region from 0 to 20 lines/mm, the sampling interval between data points must be increased above the 2 micron interval at which the input data was supplied. To do this, the data is resampled every 10 points* yielding a sampling interval of about 19.6 microns or approximately 1 sample every scan line. The variance of the resampled trace is computed and converted to square density using the appropriate microdensitometer calibration, thereby evaluating the total noise power. The resampled trace is then filtered by each of the series of five filters and the variance of the filtered trace is computed to evaluate the total noise power in the band passed by the filter.

A typical example of the printed output of the computer program used in the analysis is reproduced in Fig. 13. At the sampling interval chosen, the folding frequency is in the neighborhood of 25 lines/mm. In this case, the fraction of the total noise power passed by filters no. 4 and 5 is in a bandwidth between 15 lines/mm and the folding frequency. Due to the frequency response of the scanner-communications link, the only element of the system which can contribute power in this bandwidth in the mechanical scan direction is the granularity of the reconstruction film. Since it is desired to restrict the measurement of total noise power to the signal band, it is necessary to remove the contribution beyond 20 lines/mm due to the grain of the reconstruction film. This is done by using the fraction of the total noise power passed by filter no. 5 to compute the amount of the measured total noise power which is due to the grain of the reconstruction film. The filter factors, shown in Table 2, required for this analysis are derived in Appendix D and represent the ratio of the noise power passed by the corresponding high pass filter to the total noise power assuming that a white noise spectrum is analyzed by the existing techniques. These factors can also be used to obtain some information about the shape of the noise spectrum by comparing the ratio of the measured noise powers to

---

* The resampling rate is adjustable to yield a sampling interval which is a multiple of the initial interval.

FRAMELET NO. 146 SAMPLE AREA GRE GOLDST SCAN DIRECTION MECHANICAL
(THERE WERE -0 POINTS BELOW VMIN AND 2 POINTS OUTSIDE 3.00 SIGMA)

	MEAN DENSITY	SIGMA (DENSITY)	POINTS
UNFILTERED	0.907078	0.0532003	300
FILTER NO. 1	-0.000991	0.0316765	290
FILTER NO. 2	0.001105	0.0271453	290
FILTER NO. 3	-0.000102	0.0210990	290
FILTER NO. 4	0.001661	0.0156160	290
FILTER NO. 5	-0.000923	0.0112711	290

Figure 13 TYPICAL PRINTED OUTPUT FROM THE NOISE LEVEL ANALYSIS PROGRAM

Table 2
NOISE ANALYSIS FILTER FACTORS

FILTER NUMBER	FILTERED NOISE POWER / TOTAL NOISE POWER
1	0.503
2	0.386
3	0.242
4	0.127
5	0.0635

the corresponding filter factor presented in the table. For example, if the measured ratio is smaller than the factor presented in the table, this indicates that the noise power spectrum is "red" or that the noise is correlated.

It is also shown in Appendix D that it is reasonable to assume that approximately 25% of the estimated total noise power for the reconstructing film is within the signal band. Therefore, the correction to the total noise power is made by simply removing 75% of 3/4 of the estimated power contributed by the grain of the reconstructed film. These procedures will be illustrated in Section 3.4.3 where the noise level quality parameter is evaluated from the GRE film obtained in the prelaunch readout of the Goldstone format for Lunar Orbiter I.

3.3.4 Evaluation of the Scanner-Communications-GRS Modulation Transfer Function: The microdensitometer traces made across the edge test targets selected for evaluation of the scanner-communications-GRS MTF contain noise as well as the desired signal. As noted previously, all

of the traces will contain the scan line structure or so called "coherent noise". This noise is removed as described in Section 3. 3. 1. The incoherent noise, however, must also be removed from the trace before the data can be used to evaluate the transfer function. Unfortunately, simple numerical filtering techniques, such as low pass filtering of the data, are not very useful in this case because a large portion of the incoherent noise is contained in the same band as the signal. Low pass filtering to remove the noise degrades the signal or edge, which adversely affects the measured modulation transfer function. The most direct way of "filtering" the noise is to use an "educated observer" to hand smooth the edge trace. An "educated observer" is simply one who has an approximate knowledge about the edge shape and the noise level expected from the system to aid in his judgement of the smooth trace. When analyzing the Lunar Orbiter photographs, this technique is employed to remove the incoherent noise from all of the edge traces which are used to evaluate transfer functions. These data preparation techniques are indicated in the flow diagram of the procedures for the evaluation of the scanner-communication-GRS MTF shown in Fig. 14(a). The edge trace data is numerically filtered to remove the scan line structure and plotted by the computer so that the manual operation of hand smoothing may be performed. The smooth edge trace must then be converted back to digital form for additional numerical processing used to evaluate the transfer function. This is achieved by reading the ordinate of the edge trace at equally spaced intervals on an instrument called a tele-reader which converts the ordinate distance to scaled voltages and punches these on IBM cards. The data is then ready for the main processing program which evaluates the scanner-communications-GRS MTF. The procedures used in this program are included in part (b) of Fig. 14.

In order to evaluate the scanner-communications-GRS MTF, the sharpness or spatial frequency content of the original test object must be known. A measure of this sharpness is obtained by scanning several corresponding edge targets in the bimat processed sample of flight film. For convenience in analysis, the departure of these edge traces from a perfectly sharp edge can be represented by a linear degrading process

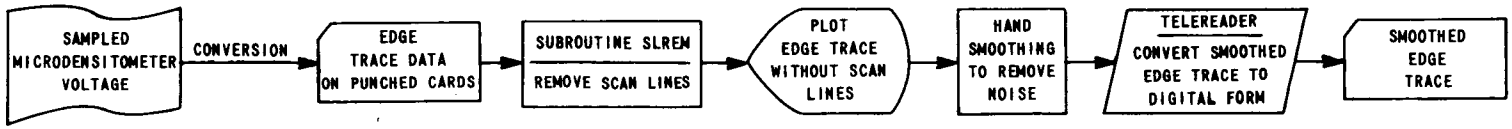

(a) DATA PREPARATION OPERATIONS

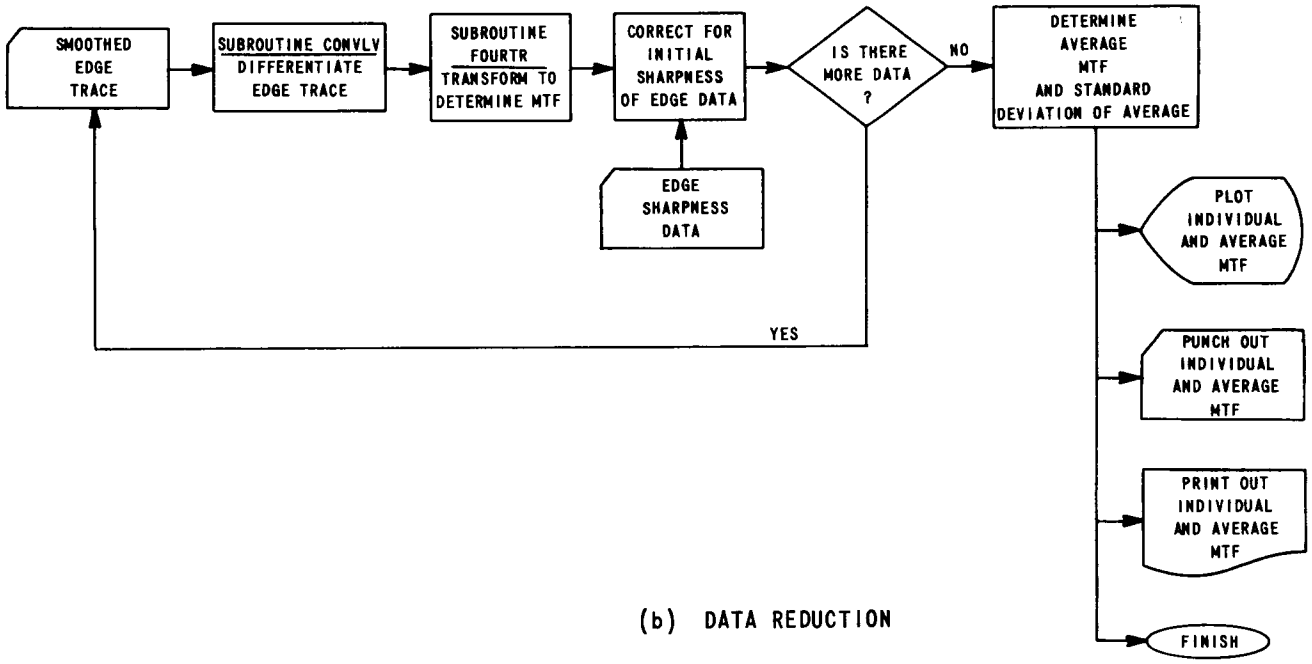

(b) DATA REDUCTION

Figure 14 FLOW DIAGRAM OF THE PROCEDURES FOR EVALUATION OF THE SCANNER-COMMUNICATIONS-GRS MTF

specified by a frequency response function. To determine this function, the edge traces are converted to transmittance and then differentiated and Fourier transformed. The resulting function represents the response of a linear system which would generate the test object from a perfectly sharp edge. For convenience in determining the scanner-communications-GRS MTF, this transfer function, which represents the sharpness of the original test object, is fitted by the parametric form

$$\tau(\nu) = b_0 e^{-b_1|\nu|} + (1-b_0) e^{-b_2 \nu^2} \tag{9}$$

by employing a nonlinear parametric estimation techniques.

To evaluate the scanner-communications-GRS MTF, the smooth edge trace measured from the GRE film is differentiated and Fourier transformed. The resulting transfer function includes the combined effects of the initial edge sharpness and the degradation introduced by the scanner, communications, and GRE systems. When this transfer function is corrected for the finite sharpness of the original test object by employing the parametric form in expression (9), the scanner-communications-GRS modulation transfer function is determined. The modulation transfer function is evaluated at frequency intervals determined by the total length of the edge trace. In normal circumstances, the edge trace will contain approximately 300 points and the spacing between the points will be about 1 micron at the spacecraft film scale. Therefore, the interval between points of the modulation transfer function is approximately 3 lines/mm.

Because of the variability of any single edge trace, it is customary to evaluate the modulation transfer function by employing more than one test target. In this circumstance, the measured quality parameter is the average value of the individual measurements of the scanner-communications-GRS MTF and, as indicated in the flow diagram shown in Fig. 14, the reduction technique includes an evaluation of the standard deviation of the average MTF as an indication of the variability of the individual measurements. The output of the analysis includes both tabulated and plotted values of the individual measurements and their average value. A typical example of the printed output is reproduced in Fig. 15.

GOLDSTONE LEADER STEP 6 SHARPNESS

FRAMELET NO. 239 STEP NO. 6

FREQ	MTF	FREQ	MTF
0.	1.0000	66.18	0.2986
4.73	0.9829	70.91	0.2868
9.45	0.9342	75.64	0.2787
14.18	0.8615	80.37	0.2726
18.91	0.7751	85.09	0.2658
23.64	0.6856	89.82	0.2557
28.36	0.6019	94.55	0.2405
33.09	0.5296	99.28	0.2200
37.82	0.4707	104.00	0.1953
42.55	0.4247	108.73	0.1690
47.27	0.3887	113.46	0.1438
52.00	0.3597	118.19	0.1223
56.73	0.3354	122.91	0.1055
61.46	0.3149	127.64	0.0932

Figure 15 TYPICAL PRINTED OUTPUT FROM THE SCANNER-COMMUNICATIONS-GRS MTF EVALUATION PROGRAM

3.3.5 Evaluation of the Camera System Modulation Transfer Function: The procedures for evaluating the camera system modulation transfer function are identical for both the high resolution system and the medium resolution system. As shown in the flow diagram presented in Fig. 16(a), the initial data preparation steps involving the removal of the scan line structure and hand smoothing the incoherent noise, which were described in the previous section, are also applied to the edge trace obtained by scanning the shadow-to-sunlight edge interior to a crater.

The procedure for obtaining the camera system MTF assumes that the spatial frequency content of the undegraded test object is known. This is determined by computing the exposure distribution corresponding to a perfect image. In the Phase I final report, this exposure distribution was shown to depend upon the crater diameter, the shadow length, and the solar zenith angle. The shape of the exposure distribution corresponding to the undegraded or ideal edge is zero in complete shadow (umbra), increases

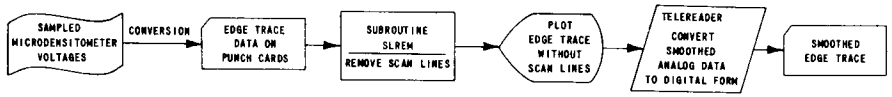

(a) DATA PREPARATION OPERATIONS

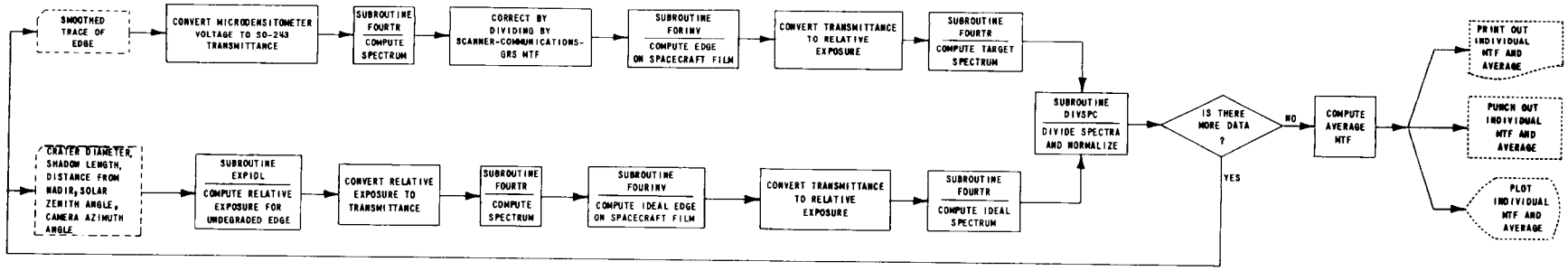

(b) DATA REDUCTION

Figure 16 FLOW DIAGRAM OF THE PROCEDURES USED IN THE EVALUATION OF CAMERA SYSTEM MTF

through the penumbral region and has a shape determined by the curvature of the crater floor in the complete sunlight region. The increase in intensity through the penumbral region is controlled by the shape of the solar disc and the curvature of the crater floor. In the analysis, the effect due to the curvature of the crater floor is neglected, however, the shape of the solar disc is included. The shape of the exposure distribution in the region of total sunlight can be shown to be approximately linear over a small region of the trace.

The model assumed to derive the ideal exposure distributions during the Phase I effort and in the current data reduction program is a spherical crater. Certain auxiliary geometric data are necessary to evaluate the ideal exposure distribution. These data include the crater diameter and the shadow length, both of which can be measured directly from the reconstructed GRE film and the solar zenith angle at the center of the crater. In the Phase I Final Report[1], the derivation of the ideal distribution was confined to craters located at or near the nadir in the photograph. During the Phase II effort, it was found that targets may have to be selected at a considerable distance from the nadir and, consequently, the ideal exposure distribution was generalized to include targets located at other format positions. This is reported in Appendix B. As a result of the generalization, additional auxiliary data are required to evaluate the ideal exposure distribution for the edge. These data include the distance of the center of the crater from the nadir, the aximuth angle to the spacecraft (camera) measured from the direction away from the sun, the spacecraft altitude, and the spacecraft radius. A sketch showing some of these auxiliary geometric parameters is shown in Fig. 17.

Before the spectrum of the ideal exposure distribution can be compared to the spectrum of the shadow-to-sunlight edge obtained from the GRE film, the measured edge trace is converted from GRE density to SO-243 transmittance as indicated in Fig. 16. This edge trace is then Fourier transformed so that it may be corrected for the degradation introduced by the combined effect of the scanner, communication, and GRE systems using the transfer function measured in the manner described in the previous

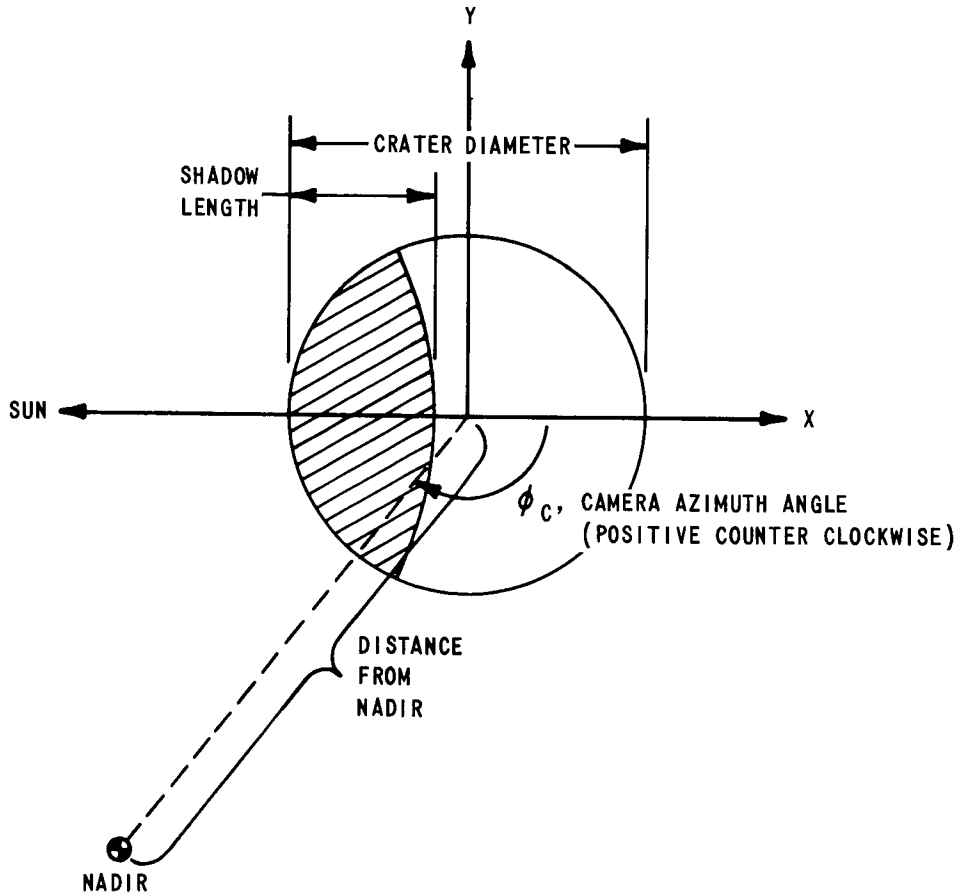

Figure 17 SOME AUXILLARY GEOMETRIC PARAMETERS REQUIRED FOR EVALUATION OF THE CAMERA SYSTEM MTF AS THEY APPEAR ON THE GRE FILM

section. Once the spectrum has been corrected for this degradation, the inverse Fourier transform is taken to compute the edge distribution in transmittance as it existed on the spacecraft film. In computing the inverse transform, one caution must be observed. Since the edge transmittance distribution varies between two unequal transmittance levels, the Fourier series representation of the edge used in the analysis represents a repetitive object with discontinuities at both ends of the edge trace. When such discontinuities exist, direct Fourier inversion methods yield oscillations in the output customarily known as "Gibb's phenomena". These

oscillations were discussed earlier in Section 3. 3. 1 during the discussion of the technique for removal of the scan line structure. To reduce the magnitude of the oscillations, the spectrum must be smoothly decreased to zero at the folding frequency. This is accomplished by use of a sinc function often referred to as Lanczos' σ-factors. The first zero of the sinc function is set equal to the folding frequency of the spectrum. This corresponds to convolving the edge trace with a narrow rectangular pulse whose width is twice the sampling interval and should leave the edge trace essentially unaltered. However, in order to minimize any effect that this technique could introduce into the measured value of the camera system modulation transfer function, the ideal exposure distribution is converted to a transmittance distribution by employing the measured Hurter-Driffield response curve for the spacecraft film and subsequently undergoes identical computational operations as the measured edge trace except for the correction of the degradation introduced by the combined scanner, communications, and GRE systems. To determine the camera system modulation transfer function, both the ideal transmittance trace and the measured transmittance trace are converted to relative exposures by employing the measured Hurter-Driffield response curve for the spacecraft film. The two exposure distributions are then Fourier transformed once more to determine the respective spectra and the spectrum determined from the measured trace is divided by the spectrum originating from the ideal trace to determine the degradation introduced by the camera system.

A typical printed output from the computer program is reproduced in Fig. 18. In addition to the camera system MTF, some additional information is determined in the data reduction process. This information includes the phase angle at the center of the crater, the angle between the phase plane and the sun plane, the penumbral length, the diameter-to-depth ratio of the crater, and the brightness longitude for a flat surface located at the crater*.

---

* The brightness longitude is a term which designates the angle between the projection of the local surface normal into the phase plane and the camera direction. The phase plane is defined by the direction of the incident sunlight and the direction of the emitted sunlight collected by the camera.

LUNAR ORBITER CAMERA SYSTEM TRANSFER FUNCTION ANALYSIS

SAMPLE - SIMULATED DATA FOR 50 METER CRATER
FRAMELET NO. 1 CRATER NO. 1
PHASE ANGLE 70.00 DEGREES
PHASE PLANE/SUN PLANE ANGLE -0. DEGREES
CRATER DIAMETER 50.0 METERS
PENUMBRA LENGTH 0.746 METERS
DIAMETER TO DEPTH RATIO 6.21
BRIGHTNESS LONGITUDE FOR FLAT SURFACE -0. DEGREES

FREQ	MTF	FREQ	MTF
0.	1.0000	65.94	0.1757
3.47	0.9163	69.41	0.1893
6.94	0.7669	72.88	0.1725
10.41	0.4978	76.35	0.2364
13.88	0.4786	79.82	0.2648
17.35	0.3481	83.29	0.4807
20.82	0.3491	86.76	0.3538
24.29	0.2931	90.23	0.1809
27.76	0.3088	93.70	0.0735
31.23	0.2739	97.17	0.0472
34.70	0.2859	100.64	0.0728
38.18	0.2641	104.11	0.0597
41.65	0.2809	107.59	0.0733
45.12	0.2614	111.06	0.0645
48.59	0.2705	114.53	0.0656
52.06	0.2483	118.00	0.0675
55.53	0.2563	121.47	0.0499
59.00	0.2246	124.94	0.0477
62.47	0.2186	128.41	0.0210

Figure 18 TYPICAL PRINTED OUTPUT FROM CAMERA SYSTEM MTF EVALUATION PROGRAM

3.3.6 An Alternative Technique for Evaluation of the Complete System Transfer Function: It will be recalled that because the spacecraft film is a nonlinear element of a photographic system, the modulation transfer function of the photographic system had to be evaluated in two parts; the camera system modulation transfer function and the scanner-communications-GRS modulation transfer function. The effective modulation transfer function for system evaluation is the product of these individual transfer functions. If low contrast test targets were available on the lunar surface, the nonlinearity of the spacecraft film could be ignored and an alternative procedure for evaluation of the modulation transfer function of the entire photographic system could be employed. The available target, namely, the shadow-to-sunlight edge interior to a crater is high contrast in nature so that the alternative analysis which neglects the nonlinearity of the spacecraft film introduces an error into the measurement of the total system modulation transfer function. However, under circumstances where the techniques described in the previous sections cannot be employed to evaluate the modulation transfer functions individually*, this technique may be employed as a reasonable approximation and will be described further. The evaluation procedure still employs an edge trace across the shadow-to-sunlight edge interior to a crater. In this case, however, the crater diameter must be chosen in the region of 5 to 10 resolution elements to insure that the penumbral length is much less than the resolution of the system and can be neglected. The resulting edge trace obtained by scanning the selected target is then treated in a manner similar to the analysis presented in the Section 3.3.4. The scan line structure and the incoherent noise are removed from the edge trace; it is differentiated and Fourier transformed to determine the modulation transfer function for the entire system. There is no correction for the finite sharpness of the initial test object since the sharpness is primarily determined by the penumbral length and targets are selected so that it is negligible.

---

* Such as extreme exposures of the spacecraft film or lack of sufficient sharpness of the edge data target.

3.4 Study of the Accuracy of the Measurement Techniques. - One of the primary tasks of the Phase II effort is to establish the accuracy of the measurement techniques described in the previous sections. The first problem considered under this task is the effect of the assumption that the reconstruction is a linear process when actually it is composed of two compensating nonlinear effects. In addition, an error analysis of the measurement techniques are presented for each of the quality parameters. For some of the measurement errors, the analysis employs Taylor series expansions to linearize the analytical expressions and treats the error in the quality parameter as a perturbation on the actual but unknown value of the parameter. In other cases, the error produced in the quality parameter is evaluated explicitly for the expected range of the measurement errors. In addition, both simulated data and data obtained from the reconstructed GRE film of the pre-launch readout of the Goldstone format (Lunar Orbiter I) are employed to demonstrate the accuracy of the measurement techniques. The simulated data has the advantage that the computed results can be compared to controls provided by the known inputs to the simulation whereas the data obtained from the original GRE film is typical of that which will be obtained under actual analysis conditions.

3.4.1 Evaluation of the Effects of the Nonlinearities of the Ground Reconstruction System (GRS): The subject considered in this section is an additional study of the assumption of linearity in the Lunar Orbiter imaging system, since this may influence the accuracy of the measurement techniques. In the Phase I Final Report[1], it was shown that a linear analysis could be applied to relate the spacecraft film transmittance to the GRE film density. Although the system was designed to have a linear relationship between the output voltage of the scanner in the spacecraft and the recorded GRE film density, this was done by employing two compensating nonlinear operations in the reconstruction process. The input voltage at the GRE is related in a nonlinear manner to the exposure on the GRE film, which is in turn, nonlinearly related to the GRE film density. Since the film integrates the exposure it receives, a linear

analysis is not correct unless it can be shown that the combined effect of the two nonlinearities can be neglected when measuring the quality parameters. Initially to establish the linearity of the system, it was assumed that the spread of the reconstructing scan spot was small in the electrical scan direction and that the spot was not wobbled excessively in the mechanical scan direction so that the adjacent scan lines would retain their identity (i. e., not blur together). An additional study was undertaken to assess the effect on the measurement techniques of increasing the size of the GRE scan spot. The details of the analysis are presented in Appendix A. The investigation employs simulation of microdensitometer traces of the various targets selected to evaluate the quality parameters. The traces were simulated for two systems. In one system, the recorded GRE density is directly in proportion to the sum of the individual voltages at each point in the reconstructed photograph (linear system). In the second simulation, which represents the actual Lunar Orbiter imaging system, the reconstructed densities depended upon the total exposure received at a point in the format. It was assumed that the reconstructing spot had an approximately Gaussian shape and a variable width. The simulation, performed on a digital computer, synthesized microdensitometer traces of an edge target and various gray levels for several different widths of the GRE scan spot. The simulated edge traces were processed by the data reduction techniques described in Section 3. 3. 4 to evaluate the modulation transfer function employed in the simulation. The measured modulation transfer functions for the two simulated systems were compared with each other as a function of the scan spot size varying from 3. 7 microns to 6. 6 microns at the spacecraft film scale. It was found that the variation between the transfer function of the actual system (i. e., that which would be measured) and the transfer function of the linear system are not significantly different. The difference between the two transfer functions did increase as the scan spot became broader, but remains less than 0. 05 for the largest spot size. Such a deviation would produce a variation in the measures of system performance described later in this report which would be less than 1%.

The simulated gray levels were used to determine the effect of the combined nonlinearities upon the measurement of the signal level quality parameters. With the established signal level data reduction techniques, it was found that the combined nonlinearities introduce slight effects into the measured relationship between SO-243 transmittance and GRE density and negligible effects into the Hurter-Driffield response curve. The gain of the communications system (i. e., the rate of change of GRE density with respect to SO-243 transmittance) is less than that observed for a point by point calibration of the system. This effect is not a source of error because the measured relationship correctly relates SO-243 transmittance and the measured values of GRE density when the data acquisition and scan line removal techniques described in this report are employed. It is concluded that the combined effects of the nonlinearities of the GRE system produced essentially no effect upon the measurement of the signal level quality parameters or the noise level quality parameters.

3.4.2 Accuracy of the Modulation Transfer Function Measurement Techniques: Numerical techniques were previously employed to simulate the end-to-end Lunar Orbiter imaging system and are described in the Phase I Final Report. The associated computer program was used to synthesize shadow-to-sunlight crater edges for the purpose of evaluating the accuracy of some of the measurement techniques. For convenience, attention was confined to the high resolution photographic system and microdensitometer traces for the edge target originating from a crater 50 meters in diameter (i. e., 50 resolution elements), having a diameter to depth ratio of 6.2 were constructed for a phase angle of 70°. Simulation techniques were also employed to construct microdensitometer traces representative of those that will be obtained when scanning across the edge of one of the gray levels in the step tablet of the pre-exposed data array. These simulated edge traces were employed to investigate the following problems: (1) The effect of hand smoothing techniques upon the variability of the resulting modulation transfer function, and (2) the convergence of the average of several measurements of modulation transfer

function made from traces across different edges to the true modulation transfer function to demonstrate the validity of employing statistical techniques in estimating a transfer function.

To demonstrate the accuracy of the computational operations employed in the data reduction techniques outlined in Sections 3. 3. 4 and 3. 3. 5, the noiseless simulations of the shadow-to-sunlight edge and the step tablet edge were also constructed. These were employed in the data reduction procedures along with the auxiliary parameters used initially in their synthesis and the resulting modulation transfer functions agreed with that used in simulation. This indicates that the accuracy with which the modulation transfer function can be measured is not limited by the computational operations, but is influenced by other sources such as noise contamination and data acquisition procedures.

Before investigating the accuracy of the modulation transfer function measurement techniques in more detail, it should be noted that a constraint upon the modulation transfer function will influence the behaviour of the standard deviation (or error) in any one measurement of transfer function. Since the response or modulation transfer function is constrained to be unity at zero spatial frequency and decrease to zero at high spatial frequencies, it is evident that the standard deviation in any one measurement must vanish at these limits. It is reasonable to expect therefore, that the standard deviation of an individual measurement of response would increase from zero at the low spatial frequencies peaking somewhere in the mid-spatial frequency region and subsequently decrease toward zero again at higher spatial frequencies. The spatial frequency where the deviation will peak depends upon how rapidly the true response function being evaluated decreases to zero. The more rapid the decrease of the response function with spatial frequency, the lower the location of the peak in the standard deviation. Because of this behaviour the approach taken to specify the error in an individual measurement of modulation transfer function is to employ a linear relationship which increases with spatial frequency and bounds the observed standard deviation. It is expected that this procedure will tend to overestimate the standard deviation at both the low and high spatial frequencies and, therefore, represents a conservative bound in evaluating the accuracy.

The microdensitometer scans made across both of the edge test targets used in evaluating the modulation transfer functions contain noise as well as the required signal. This noise must be removed from the edge trace before the data can be used to evaluate the transfer function. The method for removing the noise is to hand smooth the edge traces. It is reasonable to inquire about the effect of the hand smoothing technique upon the variability of the resulting modulation transfer function. The resulting smooth edge trace is the subjective opinion of the observer and variations between observers are to be expected. Consequently, a study was undertaken where the same set of simulated edge traces, one trace simulating the edge of a gray level in the pre-exposed edge data array and the other edge trace simulating the shadow-to-sunlight crater edge were smoothed by five different observers. Fig. 19(a) shows the average value and associated $\pm \sigma$ error bars of the individual measurements of the scanner-communication-GRS modulation transfer function. It is seen that edge was enhanced so that the measured transfer function is considerably above the true value. In fact, all of the five of the individual measurements of modulation transfer function were above the true value indicating that this was a systematic error and is not characteristic of the hand smoothing technique. This error is introduced by the particular noise sample used in synthesizing this case. When the gradient across the edge is relatively smooth, the observer has no criteria for judging the amount of noise in this region and, therefore, has a tendency to leave this portion of the edge trace unaltered, consequently introducing a systematic error into the measurement of the modulation transfer function. On the other hand, it is to be expected that the hand smoothing of several edge traces obtained using different noise samples would yield individual results whose average converged to the true modulation transfer function.

The same observers also smoothed the simulated shadow-to-sunlight edge. The average camera system modulation transfer function determined from the individual measurements derived from the smooth edge traces is presented in part (b) of Fig. 19. Since the data reduction procedure employs the measured scanner-communications-GRS transfer function to

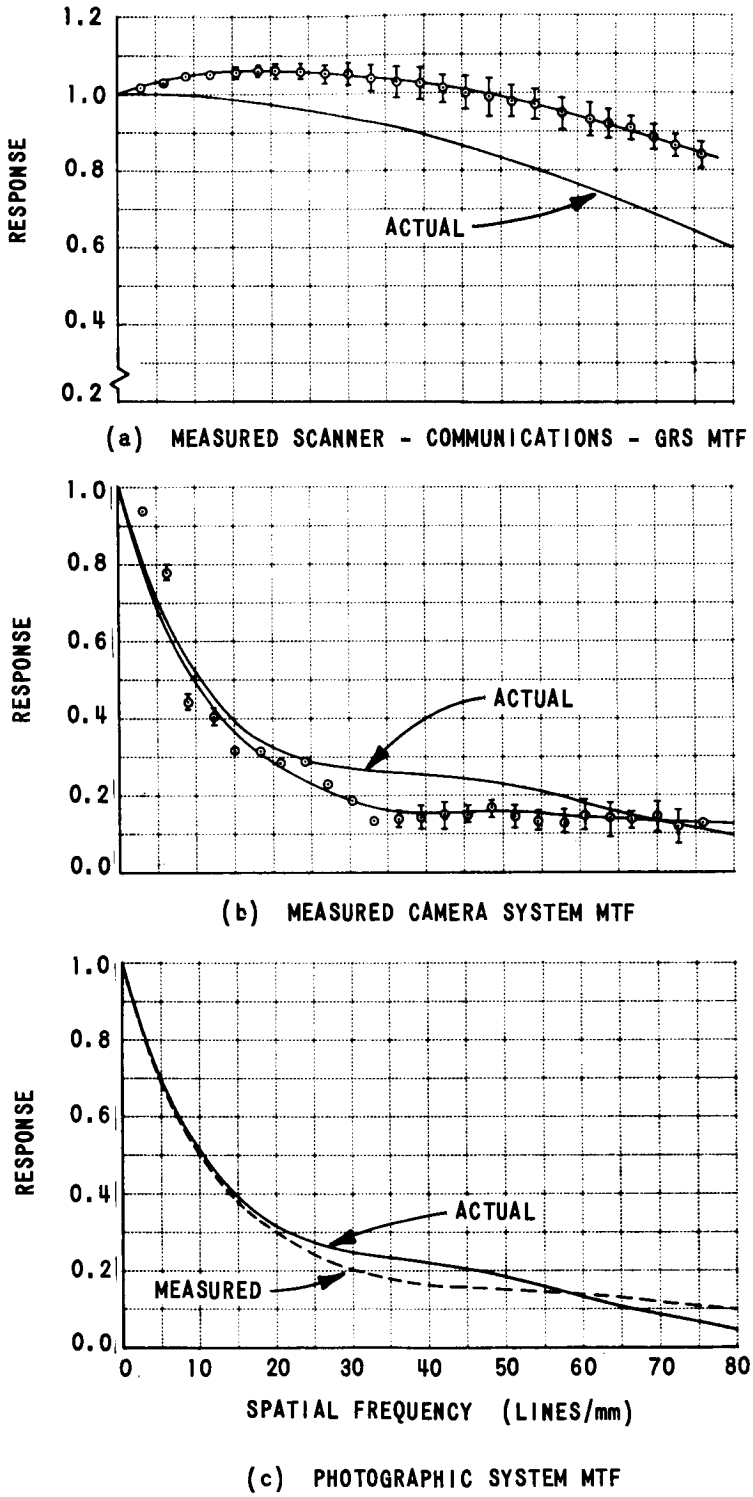

Figure 19 MEASURED MODULATION TRANSFER FUNCTIONS OBTAINED FROM HAND SMOOTHED SIMULATED NOISY MICRODENSITOMETER TRACES

correct the shadow-to-sunlight crater edge, the effect of over estimation of this transfer function is also seen in the measured camera system modulation transfer function. In the region where the scanner-communications-GRS modulation transfer function is overestimated, the camera system modulation transfer function is underestimated. The fact that these effects are always in opposite directions is fortunate since they tend to compensate for each other when the complete photographic system modulation transfer function shown in part (c) of the figure is determined by multiplying the individual results. The reader is reminded that the results shown in the figure indicate the variability of the hand smoothing technique and comparison of the measured values of MTF to the true values of MTF do not necessarily indicate how well the modulation transfer functions can be measured when several measurements having different noise samples are averaged.

An investigation employing simulated data was performed to demonstrate the convergence of the average of several measurements of modulation transfer function made from traces across different edges to the true modulation transfer function. In this case, the simulated data consisted of several representative traces of the edge of a gray level in the pre-exposed data array. These traces were synthesized using the nominal scanner-communications-GRS modulation transfer function and independent additive noise samples having spectral properties equivalent to those reported in the Phase I Final Report[1]. Under actual analysis conditions, several edge traces will be employed in evaluating a transfer function. It is reasonable to expect that the noise component will be different from edge trace to edge trace and, therefore, that the average value of the modulation transfer function determined from each of the individual measurements would tend to converge to the true value of the modulation transfer function (unknown in this case) as the number of edge traces employed increases. To verify this conclusion, the simulated edge traces having different additive noise samples were hand smoothed by a single observer. The resulting average modulation transfer function from four simulated edge traces is shown in Fig. 20. Compared to the results in Fig. 19(a), the average value is considerably closer to the true value

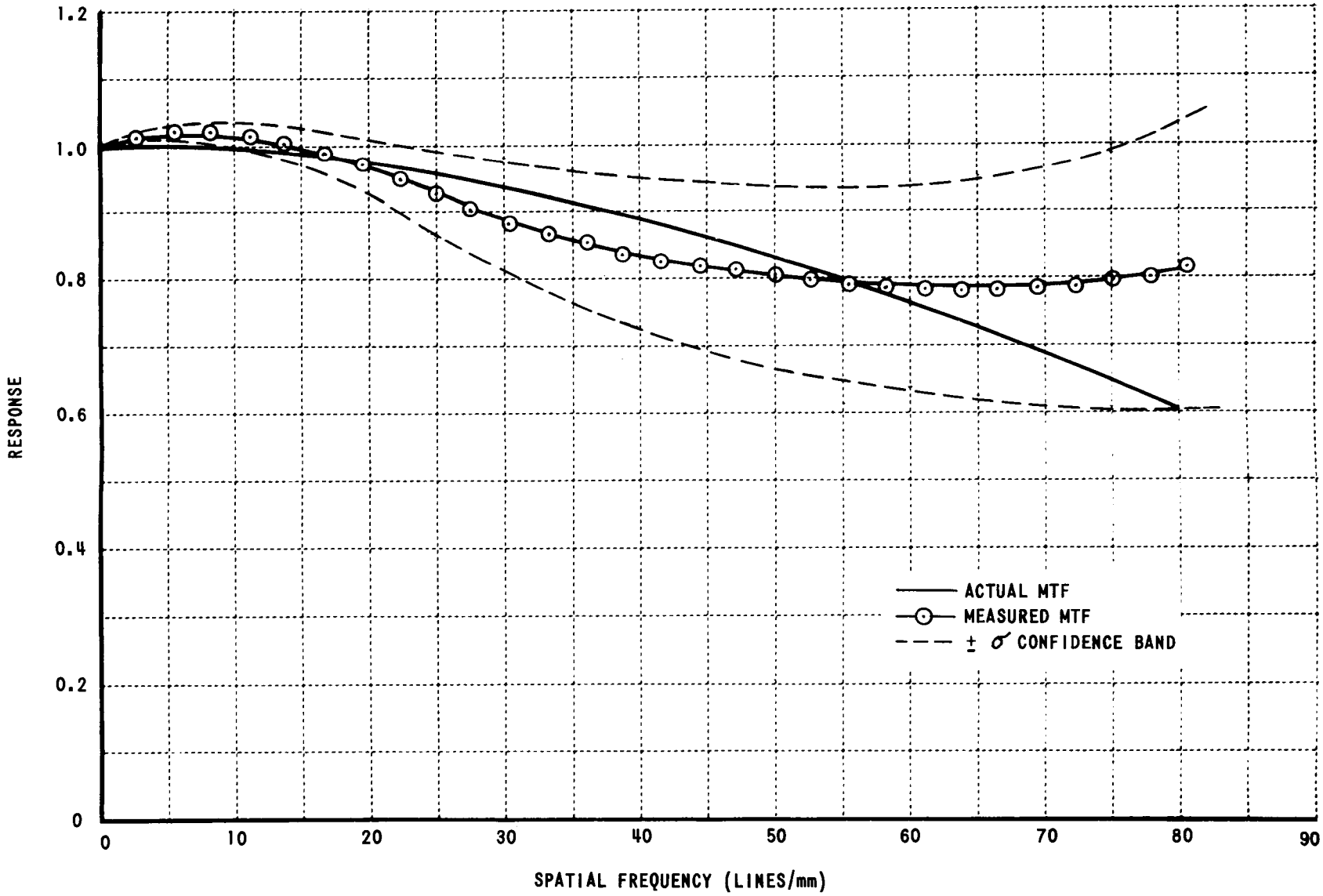

Figure 20 MEASURED SCANNER-COMMUNICATIONS-GRS MTF OBTAINED USING FOUR DIFFERENT SIMULATIONS OF A NOISY STEP TABLET EDGE

of the modulation transfer function. Therefore, it is reasonable to expect that the average of successively more individual measurements of modulation transfer function from additional edge traces would converge to the true value of the transfer function. In addition, the comparison indicates that the contribution to the error due to the contamination of the signal with noise is greater than the variability of the hand smoothing technique. The results verify that the random variability produced by the combined effects of the noise characteristics and hand smoothing can be minimized by using averaging techniques. The number of samples employed in an analysis depends upon the confidence desired in the measured transfer function and will be discussed in more detail in a later section.

In addition to the microdensitometer traces made across the edge targets, the evaluation of both modulation transfer functions requires some auxiliary data. In the evaluation of the camera system modulation transfer function, an ideal exposure distribution must be computed so that its spectrum can be compared to the spectrum of the actual exposure. This computation requires the measurement of several auxiliary geometric parameters. The accuracy with which these parameters can be measured will influence the resulting value of the measured camera system modulation transfer function. In studying this problem, it is sufficient to consider the effect of the measured value of crater diameter, shadow length, edge location, and phase angle upon the resulting measured value of the camera system modulation transfer function*. These parameters can conveniently be measured from the GRE film or obtained from orbital data. However, they cannot be measured exactly and therefore the ideal image or its spectrum cannot be determined without error. This error will introduce

---

* The auxiliary geometric parameters described in Section 3. 3. 5 also included some additional parameters such as the distance of the center of the crater from the nadir, the azimuth angle of the camera system, the spacecraft altitude and the spacecraft's radius. These parameters, however, are used to determine the phase angle and consequently their influence upon the measured value of the modulation transfer function can be described by investigating the influence of the phase angle alone.

a corresponding error in the measured MTF for the camera system. The effects of the inaccuracies in the measured values of these parameters are discussed below. An approximate bound in the fractional error of the measured MTF is determined individually for each parameter by dividing the spectrum of the true ideal exposure by that obtained with one of the parameters containing an error. In each case, an estimate of a reasonable error to be expected is given and combined to establish a bound for the error in the camera system MTF due to the variation of the auxiliary geometric parameters. The analysis employs the shadow-to-sunlight edge of a 50 meter diameter crater having a diameter-to-depth ratio of 6.2 at a phase angle of 70°.

When a trace is made using a microdensitometer, a finite length record or sampled interval is obtained and used in the data reduction program. To do this, the location of the measured edge (i. e., the location of the umbral to penumbral interface or the penumbra to sunlight interface) must be determined. The location of the ideal edge can then be adjusted accordingly, or equivalently the location of the sampled interval changed, so that the spectra of the ideal edge exposure and the degraded edge exposure differ by the true modulation transfer function of the camera system. If the edge location is not known exactly, the true MTF cannot be determined. Fig. 21 shows the fractional error which is included in the measured MTF for various amounts of error in the estimate of the location of the edge within the sampled interval. Note that the error has a small oscillation about an average error which is about 1% per micron of uncertainty of the location of the edge*. The length of the data record determines the rate of the oscillations which occur at equally spaced intervals. Filters for estimating edge location (i. e., estimation of "arrival time" of a signal) could be employed on the measured, degraded image. In the present case, however, the exposure change between the umbra (complete shadow) and sunlight portion of the image is large and extends over a distance equal to the penumbra length, which is less than the nominal resolution element of the camera system. Therefore, the location of the edge should be

* At the spacecraft film scale.

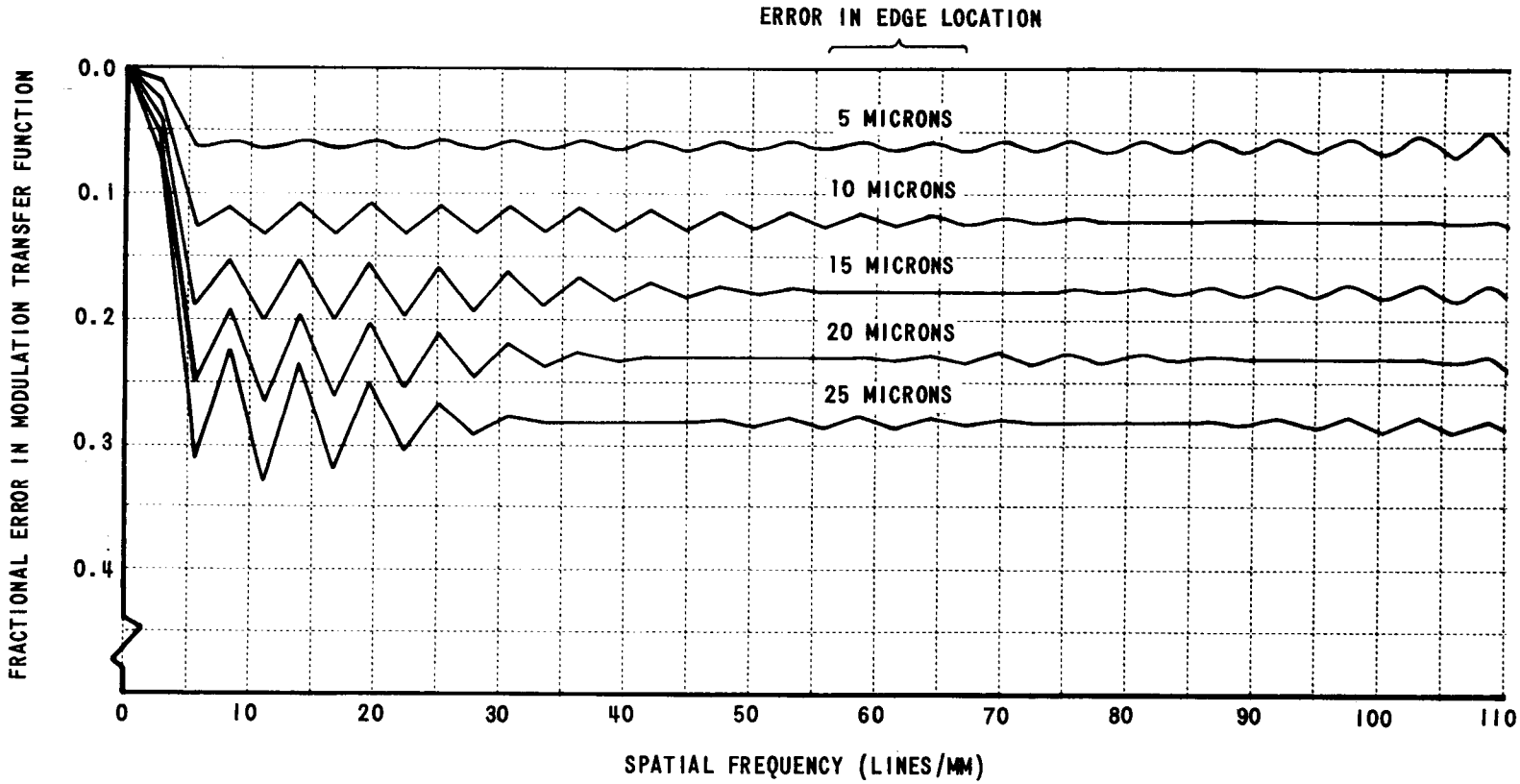

Figure 21 THE EFFECT OF KNOWLEDGE OF EDGE LOCATION UPON THE CAMERA SYSTEM MTF

estimable within a standard deviation of less than one-half a resolution element or about five microns on the SO-243 film plane. The corresponding fractional error in the measured transfer function is 0. 06.

The measurement of the shadow length is made directly from the reconstructed GRE film image. Particularly important is the determination of the length of the penumbral region. This region contains the majority of high spatial frequency information in the image and the measured modulation transfer function reflects any inaccuracy in the determination of the penumbral intensity distribution. An incorrect measurement of shadow length produces an error in the determination of the penumbral lenght as well as altering the exposure distribution in the "sunlight portion" of the image. The fractional error introduced into the measured transfer function for various values of the error in the measurement of shadow length (expressed in meters on the lunar surface) is shown in Fig. 22. Note from the figure that the error at a fixed spatial frequency is approximately linearly proportioned to the magnitude of the error in the shadow length measurement. A reasonable standard deviation to expect in the measurement of shadow length is one-half a resolution element or a half-meter for the high resolution system. From the figure, it can be seen to correspond to a fractional error in the measured modulation transfer function less than 0. 03 for frequencies less than 70 lines/mm.

The effects produced by an error in the measurement of the crater diameters are similar to those discussed above. This is seen in Fig. 23 where the fractional error introduced into the measured MTF is shown for various amounts of error in the measurement of crater diameter. It is seen that the error in the MTF is linearly proportional to the error in the diameter measurement and that an error of half a resolution element produces a fractional error in the MTF measurement less than 0. 03 for frequencies less than 70 lines/mm.

The phase angle is measured from an analysis of the orbital data rather than from measurements on the reconstructed photograph. The accuracy of the determined value of the phase angle will influence the measured value of the MTF. The results obtained by employing the same

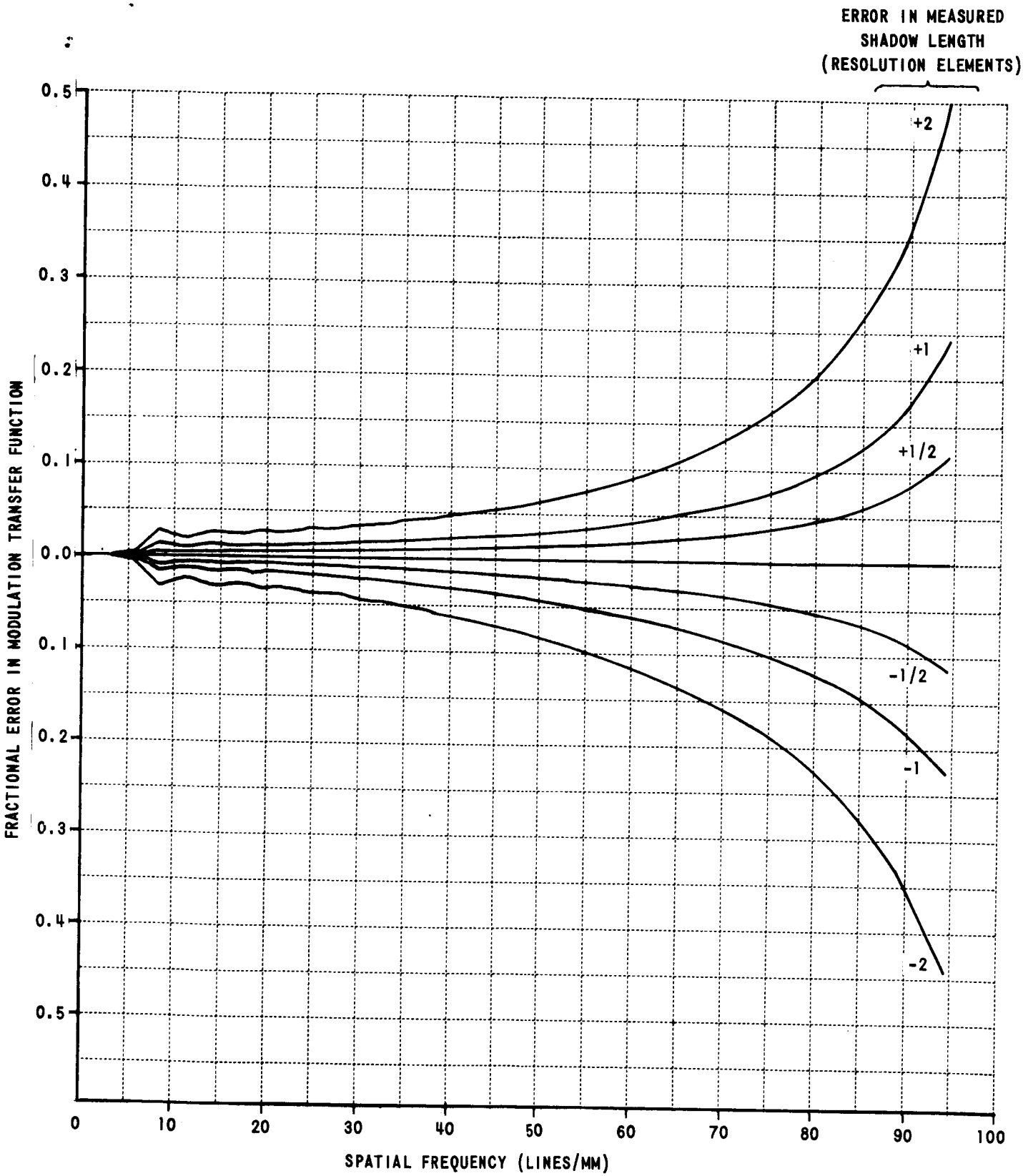

Figure 22 THE EFFECT OF AN ERROR IN THE SHADOW LENGTH ESTIMATE UPON CAMERA SYSTEM MTF

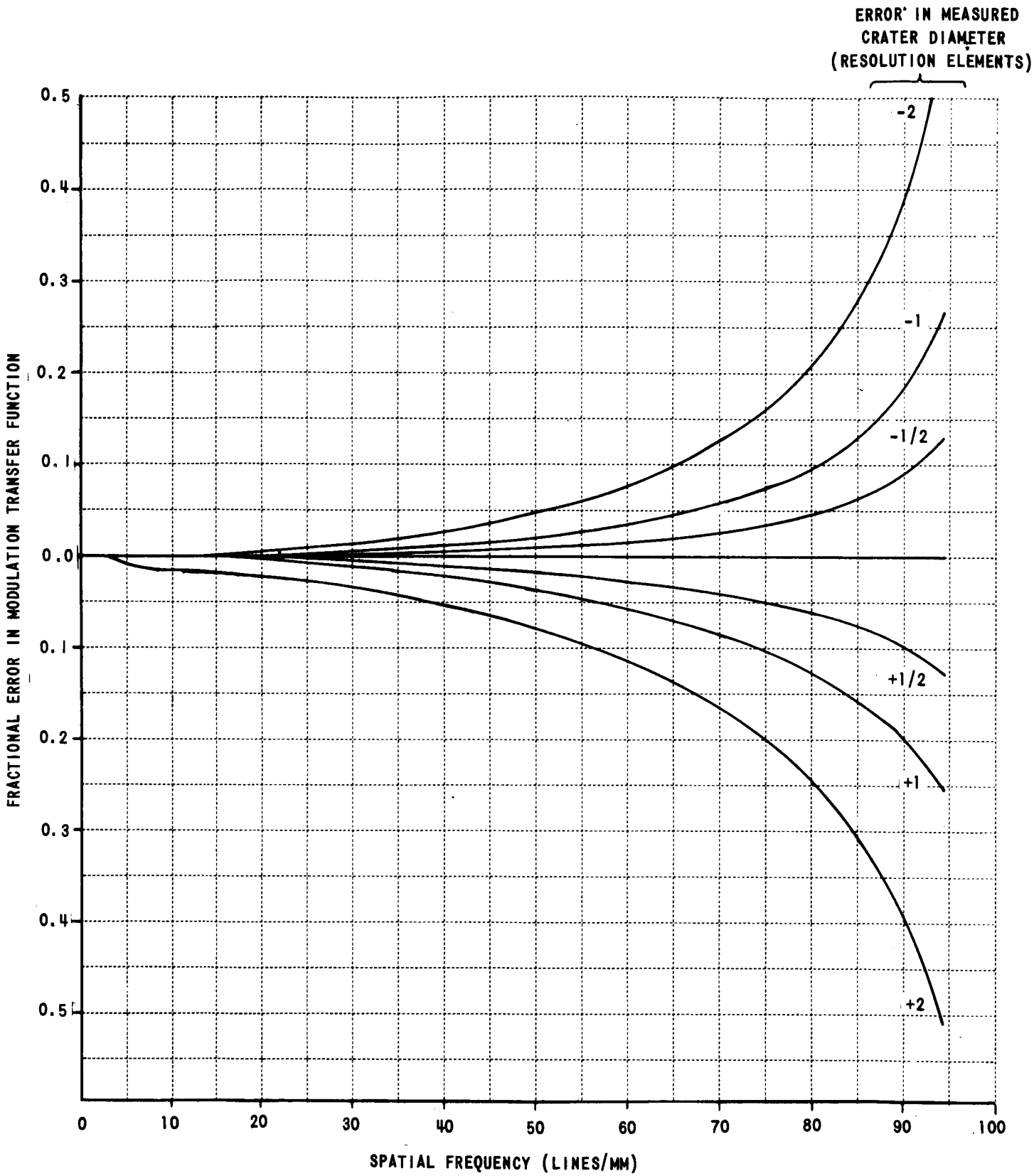

Figure 23 THE EFFECT OF AN ERROR IN THE CRATER DIAMETER ESTIMATE UPON CAMERA SYSTEM MTF

analysis techniques used above are shown in Fig. 24. An error of 0.2 degrees in the phase angle will produce a fractional error of 0.02 in the measured MTF at frequencies less than 70 lines/mm.

Each of the errors discussed in the previous paragraphs can contribute to the total error in the measured MTF. If all the errors are independent, the total error (fractional standard deviation) in the measured MTF is given by the rms value of the individual errors. Because of measurement procedures, two of the errors, namely those produced by the errors in the shadow length and diameter measurements, are correlated. This occurs because both measurements will use the same point on the rim or edge of the crater as a reference. Due to this condition, and the fact that the same amounts of error in both of these parameters will produce errors in opposite directions in the measured MTF, their correlation coefficient is -1/2. Therefore, the error (fractional standard deviation) in the MTF produced by the combined effects of errors in measurement of shadow length and crater diameter is given by

$$\beta_T = \sqrt{\beta_1^2 + \beta_2^2 - \beta_1 \beta_2} \tag{10}$$

where β_1 and β_2 are the fractional standard deviations introduced by each factor alone. These were previously determined to have equal values of 0.03. Thus, the resulting fractional standard deviation in the MTF contributed by the combined error is 0.03. Taking the rms value of this error and the errors produced by the error in edge location and phase angle, all of which are independent, the total fractional standard deviation in each measured MTF is estimated to be less than 0.07 due to the variability of the geometric parameters. This error must be combined with the error introduced by the data acquisition procedures (microdensitometry, hand smoothing, noise characteristics, etc.) to evaluate the accuracy of the complete measurement technique. These latter errors should be approximately equivalent in measuring either transfer function and therefore are only evaluated for the measurement of the scanner-communications-GRS modulation transfer function.

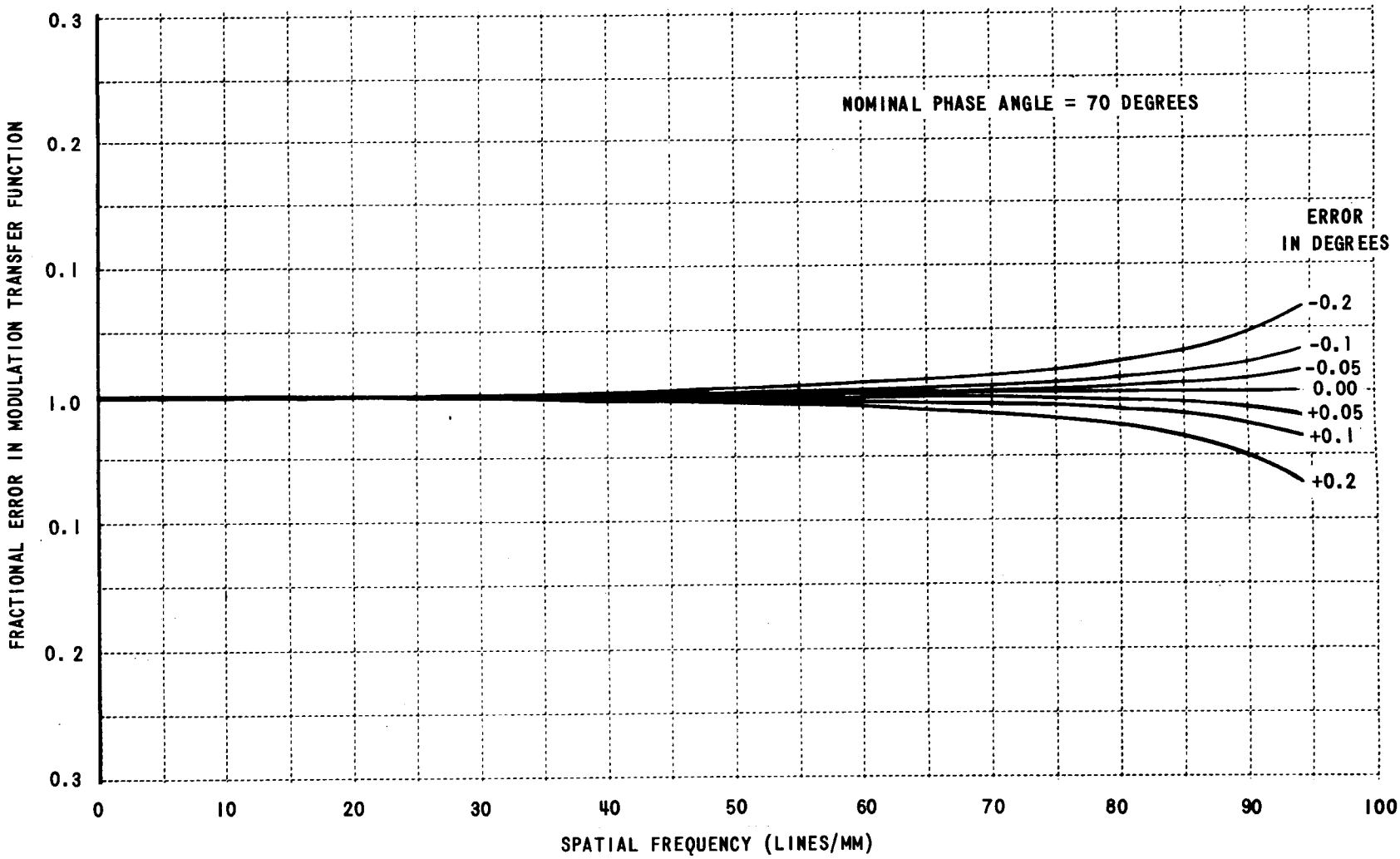

Figure 24 THE EFFECT OF AN ERROR IN PHASE ANGLE EVALUATION UPON CAMERA SYSTEM MTF

The measurement of the scanner-communications-GRS modulation transfer function also requires some auxiliary data. The original edge on the spacecraft film must be sharp enough to be degraded by the frequency response of the combined-scanner-communications-GRE system. It cannot, however, be assumed that this edge is perfectly sharp. The accuracy to which the sharpness of the original edge on the spacecraft film is known will, therefore, influence the measured value of the scanner-communications-GRS modulation transfer function. To obtain the correction factor representing the unsharpness of the original edge, it is assumed that the test object is a degraded step function, that is, an edge between two constant levels, and that the degradation of the edge can be expressed in the form of a corresponding frequency response or modulation transfer function.

The entire measurement technique for the scanner-communications-GRS modulation is amenable to analysis. If the following notation is employed, $\tau_{SCR}(\nu)$, the scanner-communications-GRS transfer function, $\tau_c(\nu)$, the response function representing the average edge sharpness and $\tau_m(\nu)$, the measured response function obtained from the GRE film edge trace, the basic procedure described in Section 3. 3. 4 can be represented mathematically as

$$\tau_{SCR}(\nu) = \frac{\tau_m(\nu)}{\tau_c(\nu)} \tag{11}$$

Employing a rule for propagation of errors based upon a Taylor series expansion[3], the standard deviation in the measured value of the scanner-communications-GRS MTF is given by

$$\delta_{\tau_{SCR}}(\nu) = \sqrt{\frac{\delta^2_{\tau_m}(\nu)}{\tau_c^2(\nu)} + \left(\frac{\tau_{SCR}(\nu)}{\tau_c(\nu)}\right)\frac{\delta^2_{\tau_c}(\nu)}{N_c}} \tag{12}$$

where the symbol δ with an appropriate subscript represents the standard deviation of the corresponding transfer function and N_c is the number of individual response measurements employed to evaluate $\tau_c(\nu)$. From expression (12), it is evident that the accuracy attained in the measured scanner-communications-GRS MTF is better (i. e., $\delta_{\tau_{SCR}}(\nu)$ smaller) if $\tau_{SCR}(\nu) << \tau_c(\nu) \leq 1$ or that the edge target must be sharp compared

to the degradation to be measured. It is easily shown, in fact, that $s_{\tau_{SCR}}(\nu)$ is minimized by having $\tau_c(\nu) = 1$ or a perfect edge test object and that in lieu of such a test object the sharpest edge target available should be selected.

Expression (12) may be simplified by noting that it is reasonable to expect equal standard deviations, that is

$$s_{\tau_m}(\nu) \approx s_{\tau_c}(\nu) = s(\nu) \tag{13}$$

since both response functions are measured by similar techniques*. With this condition $s_{\tau_{SCR}}(\nu)$ becomes

$$s_{\tau_{SCR}} = \frac{s(\nu)}{\tau_c(\nu)} \sqrt{1 + \frac{\tau^2_{SCR}(\nu)}{N_c}} \tag{14}$$

Since $\frac{\tau^2_{SCR}(\nu)}{N_c} \leq \frac{1}{N_c}$ by expanding the radical it is seen that

$$1 \leq \sqrt{1 + \frac{\tau^2_{SCR}(\nu)}{N_c}} < 1.05 \tag{15}$$

if at least 10 edge samples ($N_c > 10$) are used to evaluate the sharpness response function. Therefore, the accuracy in the measured scanner-communications is given by

$$s_{\tau_{SCR}}(\nu) \approx \frac{s(\nu)}{\tau_c(\nu)} \tag{16}$$

and depends primarily upon the accuracy of the data acquisition techniques (i. e., microdensitometry, hand smoothing, noise characteristics, etc.) and the sharpness of the original edge target when a reasonable number of edge samples are employed in evaluating the sharpness response function, $\tau_c(\nu)$. It also should be noted that the standard deviation given in expression (16) may be evaluated directly from the deviations observed in the individual measurements of the transfer function.

---

* This assumption is verified by the measurements made employing the Goldstone readout GRE film of Lunar Orbiter I and reported later in this section.

Measurements of the scanner-communications-GRS MTF were made using the Goldstone readout GRE film obtained from Lunar Orbiter I shown in Fig. 25. The purpose of the measurements is to demonstrate the conclusions of the previous analysis and to establish reasonable values for the deviations.

Measurements of the response function representing the average edge sharpness were made from a sample of bimat processed Goldstone leader for the edge of Steps 5, 6 and 7 on four framelets using a slit 1.25 microns wide. The solid curves shown in Fig. 26 represent the average response function for each edge target. Since a higher response indicates a sharper edge, it may be concluded that measurements of the scanner-communications-GRS modulation transfer function made from the corresponding reconstructed GRE film should have the least deviation or error when the edge of step 5 is employed and the greatest error when the edge of step 7 is employed.

The fractional standard deviation, $\delta_{\tau_c}(\nu) / \tau_c(\nu)$, to be expected in a typical measurement of the response function corresponding to the average sharpness of the edge target such as those shown in the figure can be estimated from the microdensitometer scans made across the edge of the gray levels in the step tablet on bimat processed samples of SO-243 film by computing the standard deviation of the individual measurements as a function of spatial frequency and dividing by the average response function. The results, presented in Fig. 27, indicate that the fractional standard deviation is approximately linearly proportional to spatial frequency and may be slightly dependent upon the edge sharpness. The data from the Lunar Orbiter I flight film sample was included because it was obtained from 10 to 12 individual measurements, whereas the data from the Goldstone leader employed only four individual measurements and the increased number of measurements is preferred from the standpoint of accuracy when evaluating the fractional standard deviation. The fractional standard deviation for a single measurement of the response function is approximately $0.003\,\nu$ and as the number of measurements is increased, the fractional standard deviation of the average response function decreases by the square root of the number of measurements.

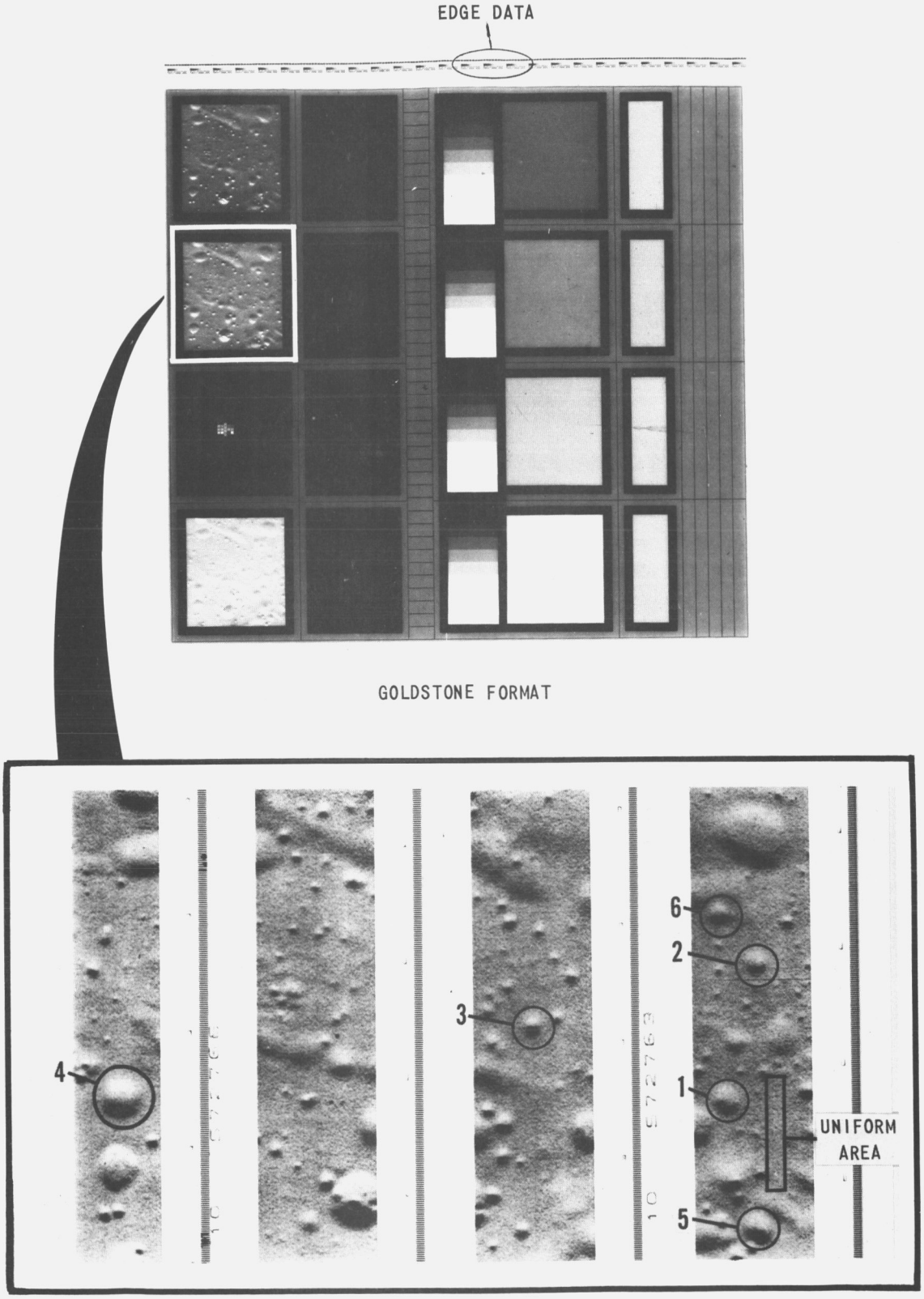

Figure 25 TARGETS IN THE GOLDSTONE FORMAT OF THE ORIGINAL GRE FILM FROM THE PRE-LAUNCH READOUT (LUNAR ORBITER I)

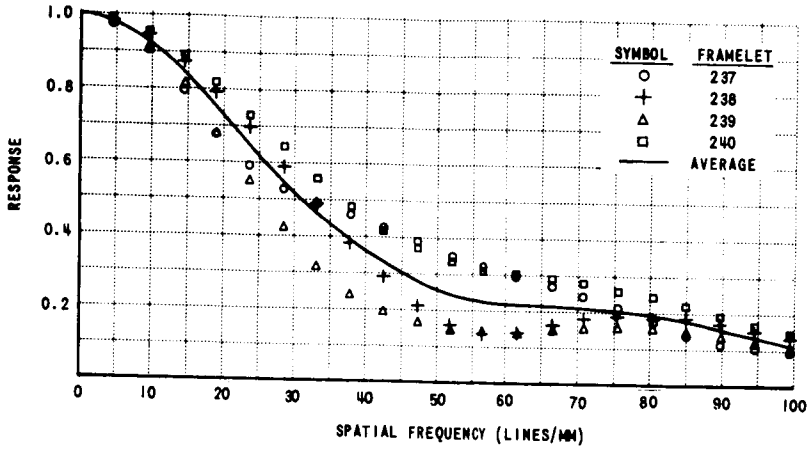

(a) STEP NO. 7

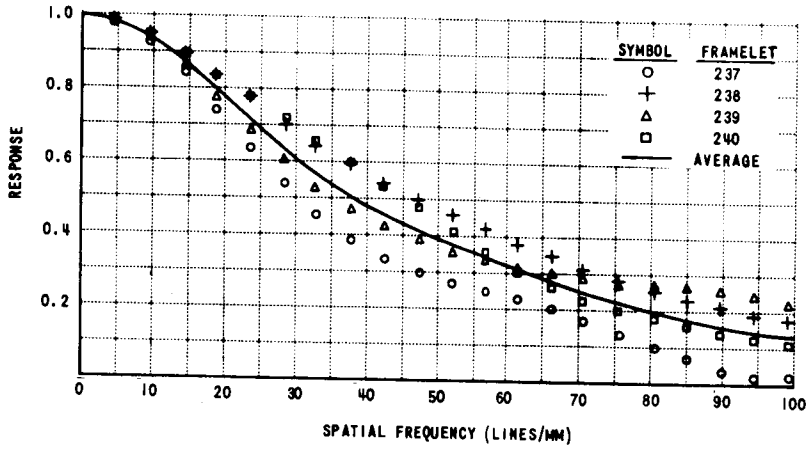

(b) STEP NO. 6

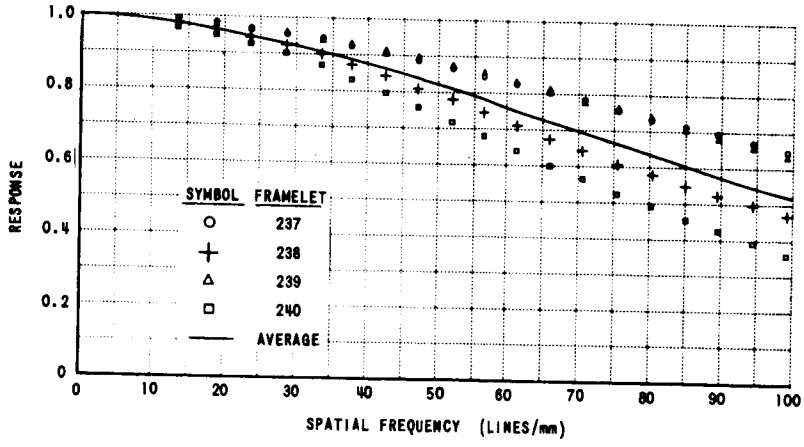

(c) STEP NO. 5

Figure 26 RESPONSE FUNCTION REPRESENTING THE SHARPNESS OF EDGES IN THE PRE-EXPOSED STEP TABLET OF THE GOLDSTONE LEADER (LUNAR ORBITER I)

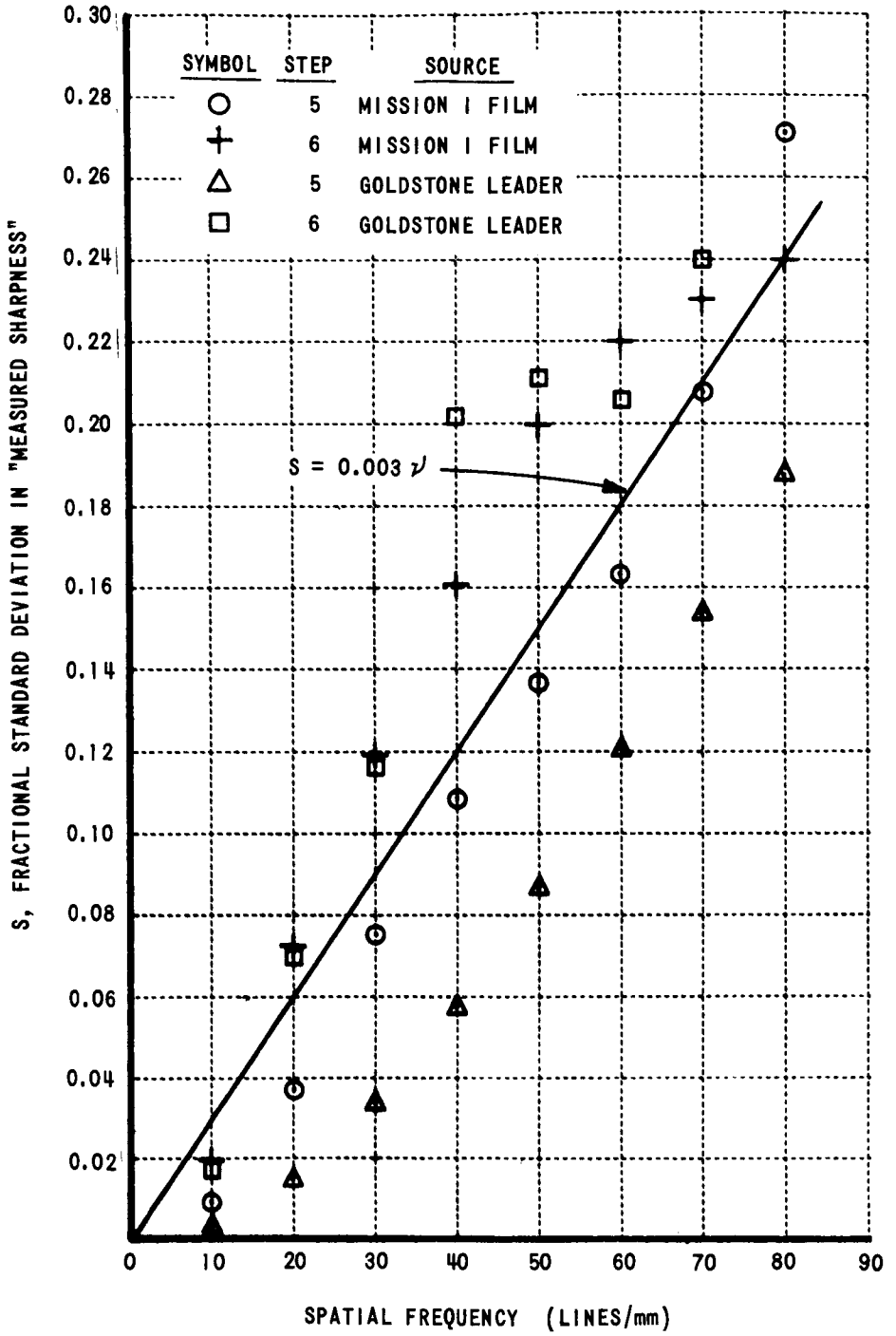

Figure 27 MEASURED FRACTIONAL STANDARD DEVIATION OF THE RESPONSE FUNCTION USED TO SPECIFY EDGE SHARPNESS

The edges of steps 5, 6 and 7 were scanned on the reconstructed GRE film obtained from the prelaunch Goldstone readout in order to evaluate the scanner-communications-GRS modulation transfer function. These edge traces were combined with the measurements of edge sharpness reported above and employed in the data reduction program described in Section 3.3.4 to evaluate the transfer function. The results of these measurements are presented in Fig. 28. The nominal transfer function is shown in (a) as a convenience for comparison. It is evident from the figure that step 5 (the sharpest test object) produced the most reasonable results, whereas the measurements which employed the edge of step 7 (the least sharp of the test objects) produced results which appeared to oscillate around unity. It should be noted that in the range from 0 to 15 lines/mm all of the results are in agreement. The standard deviation of the individual measurements of transfer function for each of the edge targets is shown in Fig. 29*. The standard deviations have approximately linear dependence on spatial frequency and also exhibit the inverse correlation between the magnitude of the deviation and the sharpness of the initial test object hypothesized earlier. It would be expected, therefore, that the measured value of the transfer function would be more reliable when obtained from measurements from the edge of step 5 as opposed to the edge of step 6 or 7. The results shown indicate this behavior. The reader may be disturbed by the fact that the measured responses obtained from the edge targets of steps 6 and 7 appear to be significantly different from that obtained from step 5. That is, if the results are superimposed, the two sigma error bars (double those shown) would not overlap in the region above 30 lines/mm. There is an explanation for this fact. We note that the errors shown in the figure are equivalent to the value obtained by evaluating Eq. (16). The reader is reminded that this expression for error in the measured transfer function was derived using the first order approximation of a Taylor series

---

* By comparing the results presented in Fig. 27 to those of Fig. 29, it can be shown that $\mathcal{S}_{\tau_m}(\nu) \simeq \mathcal{S}_c(\nu)$ as assumed earlier [expression (13)].

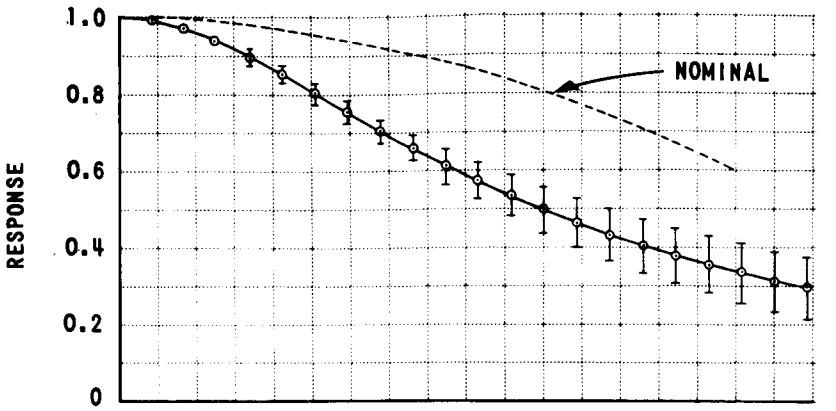

(a) MEASUREMENTS USING EDGE OF STEP 5

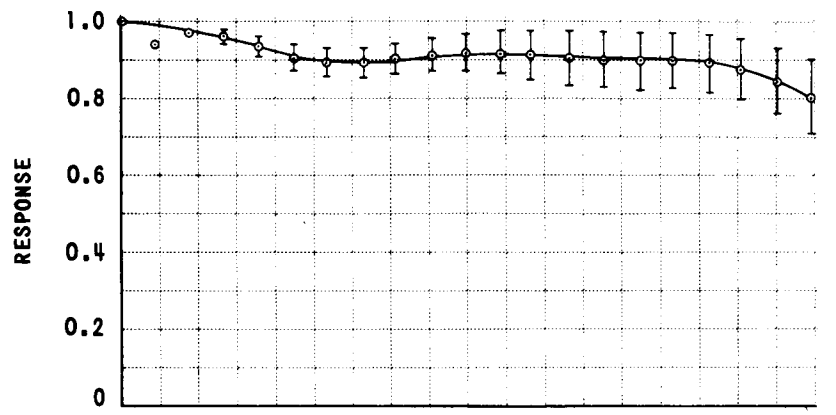

(b) MEASUREMENTS USING EDGE OF STEP 6

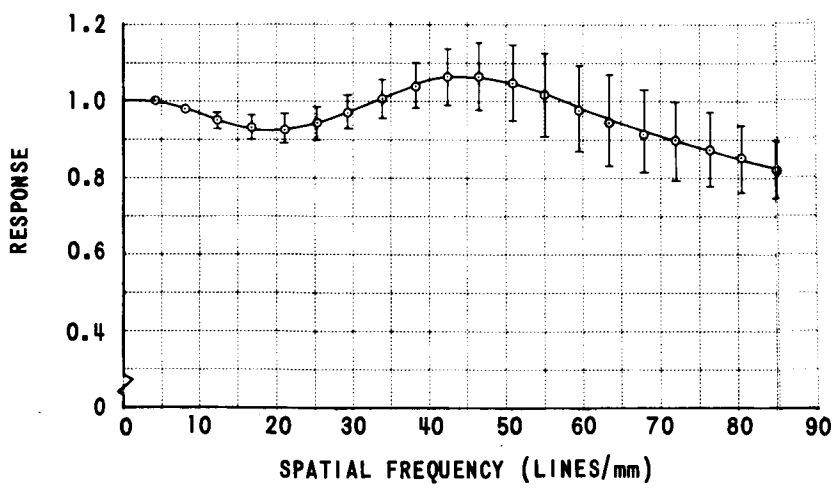

(c) MEASUREMENTS USING EDGE OF STEP 7

Figure 28 MEASURED SCANNER-COMMUNICATIONS-GRS MTF USING EDGE TRACES MADE FROM ORIGINAL GRE FILM OBTAINED (PRE-LAUNCH GOLDSTONE READOUT OF LUNAR ORBITER I)

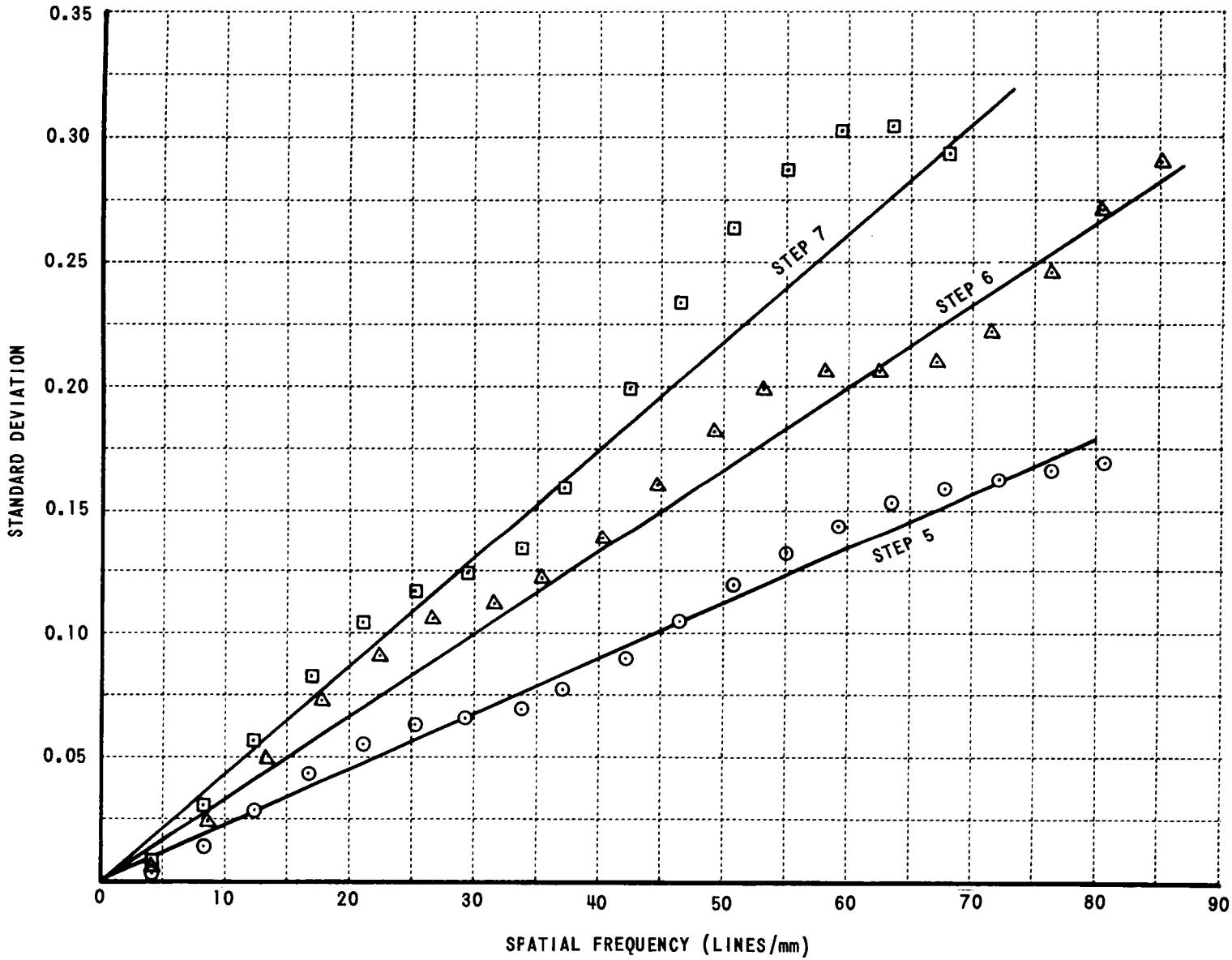

Figure 29 STANDARD DEVIATION OF THE INDIVIDUAL MEASUREMENTS OF SCANNER-COMMUNICATIONS-GRS MTF SHOWN IN FIGURE 28

expansion for the propagation of errors. For this approximation to be valid, the measurement errors must be small compared to the quantity being measured. When this is not true, expression (16) underestimates the actual error. To estimate the transfer function, the measure response, $\tau_m(\nu)$, is divided by the sharpness response function $\tau_c(\nu)$. Since both of these functions are measured using similar techniques they have similar errors or deviations. At spatial frequencies where the magnitude of either function is comparable to the measurement error, the first order approximation is not valid and the error predicted by Eq. (16) is too small. It is easily shown that the magnitude of the measured response is less than the magnitude of the sharpness response at any fixed spatial frequency consequently the magnitude of $\tau_m(\nu)$ will approach the measurement error at a lower spatial frequency than $\tau_c(\nu)$. Near the spatial frequency where this occurs the error of the measurement can be expected to increase rapidly above the value predicted by Eq. (16) and indicated by the error bars in Fig. 28. In an intuitive approach to this problem during the Phase I effort, a threshold was selected for the response function describing the edge sharpness and only at the spatial frequencies where the response function exceeded this threshold could the evaluation of the transfer function be considered reliable. The motivation for this approach is based upon the fact that the combined effect of the sharpness response function and the modulation transfer function must not reduce the signal power to a point where it is comparable or less than the noise power at any given spatial frequency. In terms of the current formulation, this means that the magnitude of $\tau_c(\nu)$ must be greater than the standard deviation of the measurement procedure. The threshold was initially chosen to be the 30% point. Table 3 shows the spatial frequency in lines/mm at several points of the sharpness response functions shown previously in Fig. 26. If the 30% threshold is reasonable, then the measured values of the transfer function obtained from measurements of the edges of step 5 and step 6 should not vary significantly at spatial frequencies below 60 lines/mm and the comparison between the transfer functions from the edges of step 5 and step 7 should not vary significantly below spatial frequencies below 45 lines/mm/ However, this is not the case indicating that this threshold

Table 3

SPATIAL FREQUENCIES OF SOME RESPONSE POINTS OF EDGE SHARPNESS (GOLDSTONE LEADER)

STEP NO.	RESPONSE		
	30%	50%	70%
	SPATIAL FREQUENCY (LINES/mm)		
5	-	102	69
6	62	38	24
7	45	31	22

may be too low. To investigate this problem further, repeated measurements of the transfer function were made from microdensitometer traces across the edge of step 6 in a single framelet of the Goldstone readout GRE film. The standard deviation of the individual measurements as a function of spatial frequency is shown in Fig. 30. The arrows in the figure are located at the spatial frequencies corresponding to the response indicated next to each arrow. From the figure, it is seen that at responses below 50%, the standard deviation shows a rapid increase with spatial frequency. It is reasonable to assume that this increase in variability reflects the inability of the measurement technique to extract the signal accurately from the noise. If the magnitude of $\tau_c(\nu)$ for the edge of step 6 shown in Fig. 26(b) is compared to twice the standard deviation of the repeated measurements, we find that they are equal approximately at the 30% point* and therefore this threshold is indeed too low. If we increase the threshold to the 50% point of the sharpness response function, the observed results presented in Fig. 28 are reasonable. From the values presented in Table 3 the transfer function determined from the three edge targets should not be significantly different for spatial frequencies below 30 lines/mm which indeed is the case. It is concluded, therefore, that the accuracy of

* The magnitude of the measured response, $\tau_m(\nu)$, will be less than the two standard deviation level in this region.

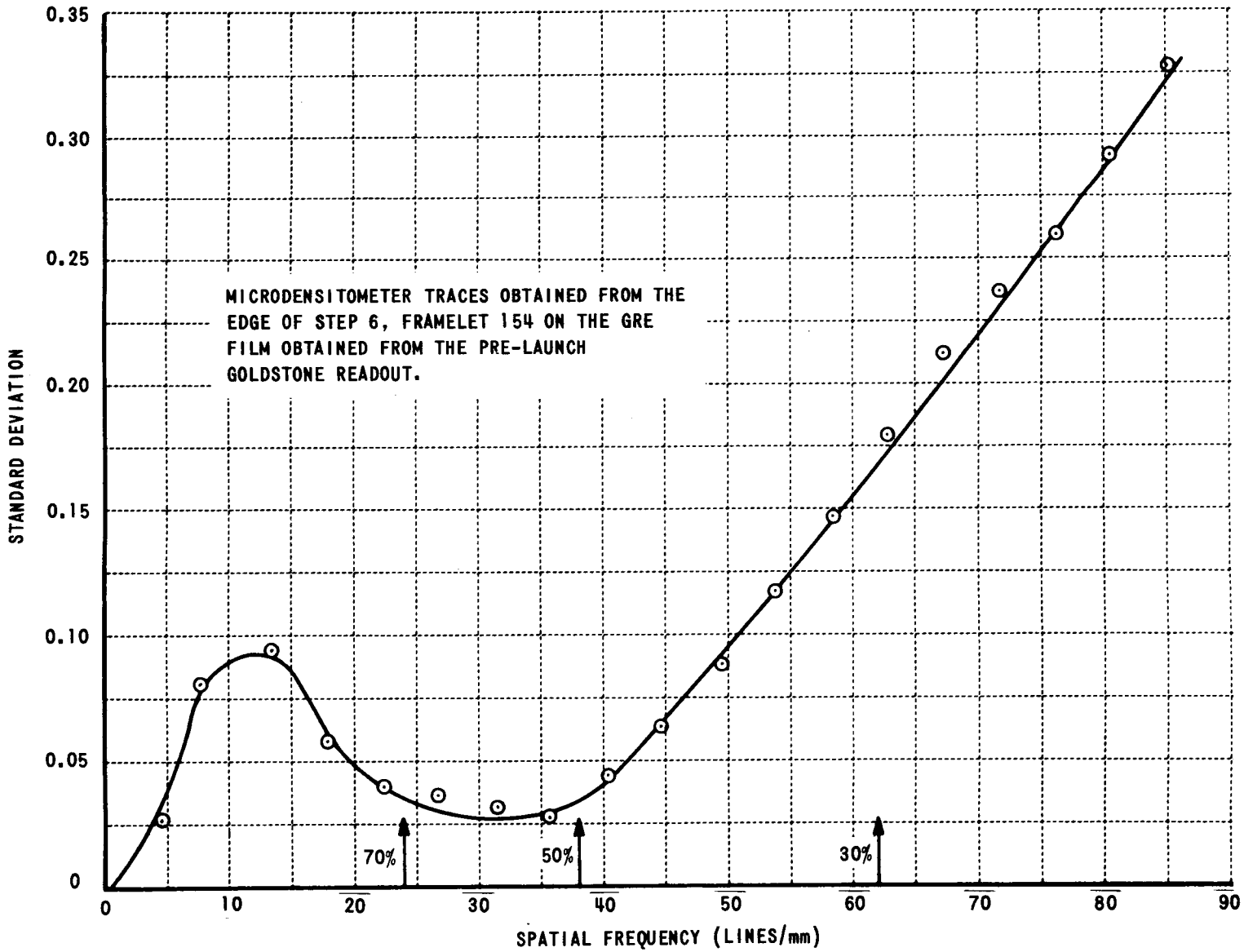

Figure 30 DEVIATION IN MTF MEASUREMENTS FROM REPEATED TRACES ACROSS THE EDGE OF A SINGLE STEP

the measurement techniques used to evaluate the scanner-communications-GRS modulation transfer function is adequately determined by Eq. (16) at spatial frequencies below that corresponding to the 50% point of the response function.

It was decided that the evaluation of the camera system modulation transfer function from data supplied by the GRE film of the pre-launch Goldstone readout was not possible for several reasons. First, the method employed in the construction of the Goldstone leader involved several nonlinear photographic processes between the original negative and the Goldstone leader. The Goldstone leader, therefore, does not appropriately simulate the spacecraft film and the photometric control required to evaluate the ideal exposure distribution required in the measurement of the camera system modulation transfer function is not possible. In addition, three of the six craters shown previously in Fig. 25 were profiled from the model supplied by the Eastman Kodak Company and were found to be unrealistically rounded and shallow with diameter to depth ratios of 8:1 to 10:1.

3.4.3 Accuracy of the Noise Level Measurement Techniques: In contrast to the previous error analyses, the effect of the data acquisition and data reduction techniques upon the accuracy of the measured value for the noise level quality parameters were made separately. To access the effect of the data acquisition techniques, an analysis was made of the repeatability of the measurement of total noise power in which a series of microdensitometer scans were made across a uniform area of a step tablet on 70mm bimat processed SO-243 film. Since this sample did not contain scan lines, because it was not reconstructed GRE film, a 10.2 micron diameter aperture was utilized in making the microdensitometer scans. These scans were made at randomly selected positions in the uniform area and were made by two different microdensitometer operators. The values obtained for the total noise power and for the mean density are shown in Table 4 along with the variance of the two measurements. It can be seen from these results that the accuracy of the data acquisition techniques is such

Table 4
REPEATABILITY OF MEASUREMENTS
OF TOTAL NOISE POWER

SCAN	MEAN DENSITY	NOISE POWER
1	1.36	.044
2	1.36	.042
3	1.36	.044
4	1.37	.047
5	1.37	.042
6	1.38	.040
7	1.38	.039
8	1.38	.042
9	1.38	.043

MEAN NOISE POWER = 0.043
RMS DEVIATION = 0.002
AVERAGE DENSITY = 1.37
RMS DEVIATION = 0.01

that a single scan can be used to estimate the total noise power to within 5%. The noise level quality parameter, however, is not simply the total noise power obtained from a microdensitometer trace but the effective white noise power density over the bandwidth occupied by the signal. The data reduction techniques in Section 3. 3. 3 described the procedure for adjustment of the total noise power to include only that portion within the signal bandwidth. The procedure has a simple mathematical formulation and therefore the accuracy which can be attained in the measurement is amenable to analysis. The following notation will be employed. The total noise power measured by employing the techniques described in earlier sections will be denoted by P_T , the adjusted noise power within the signal bandwidth will be denoted by P_{ADJ} and the measured noise power after filtering by the ith filter denoted by P_i , $i = 1, 2, 3, 4, 5$. The correction of the measured total noise power to arrive at the adjusted noise power is shown in Appendix D to be

$$P_{ADJ} = P_T - 11.8\, P_5 \tag{17}$$

where it is assumed that the noise power passed by filter no. 5 will be used to estimate the white noise power attributed by the reconstructing film. The standard deviation of the adjusted noise power can be written directly as

$$s_{P_{ADJ}} = \sqrt{s^2_{P_T} + (11.8)^2 s^2_{P_5}} \tag{18}$$

where $s^2_{P_T}$ and $s^2_{P_5}$ represent the variance of the measured total noise power and the measured noise power passed by filter no. 5, respectively. From empirical results presented above and in Appendix D, we note that these variances may be written as

$$s_{P_T} = 0.05 P_T$$

and

$$s_{P_5} = 0.23 P_5$$

and the standard deviation of the adjusted noise power becomes

$$s_{P_{ADJ}} = \sqrt{(0.05)^2 P_T^2 + (2.72)^2 P_5^2} \tag{19}$$

Combining expressions (17) and (19) the fractional standard deviation is written as

$$\frac{s_{P_{ADJ}}}{P_{ADJ}} = \frac{\sqrt{(0.05)^2 P_T^2 + (2.72)^2 P_5^2}}{P_T - 11.8 P_5} \tag{20}$$

To continue the analysis, it is convenient to relate the filtered noise power to the total noise power. Let their ratio be denoted by R . Substituting this into Eq. (20) yields

$$\frac{s_{P_{ADJ}}}{P_{ADJ}} = \frac{\sqrt{(0.05)^2 + (2.72R)^2}}{1 - 11.8R} \tag{21}$$

The value of the ratio P_5 / P_T depends upon the shape of the spectrum being analyzed. Since it is expected that the noise is correlated or that its

spectrum is "red", the ratio will have a value which is less than 0.0635 which corresponds to a white noise spectrum (see Table 2, on page 36). By examining expression (21) it can be seen that the smaller of the value of the ratio (i.e., increased correlation of the noise) the more accurate the established technique for measurement of the adjusted noise power. The value of the ratio does, in fact, depend upon the average exposure on the spacecraft film since this influences the shape of the noise spectrum. Underexposure of the film tends to produce a red spectrum and overexposure of the film tends to produce a whiter spectrum. Consequently, it can be concluded that the measurement technique will become less accurate as the average exposure on the spacecraft film is increased. For example, if the average exposure on the spacecraft film is equivalent to that received by step 9 of the step tablet in the pre-exposed edge data array, the value of R , evaluated from the original GRE film of Lunar Orbiter I, is found to be approximately 0.047. Substituting this value into expression (21), the fractional standard deviation in a single measurement of the adjusted noise power is about 30%.

Measurements of the adjusted noise power were also made using the GRE film obtained in the Goldstone readout of Lunar Orbiter I. Microdensitometer scans were made using the data acquisition techniques described previously in Section 3.2 to obtain noise data. The data was obtained from the uniform gray levels corresponding to steps no. 5 and 6 in the pre-exposed edge data array. These steps were scanned in each of four framelets. Table 5 presents the summary of the resulting data including the measured GRE density, the total noise power, and the adjusted noise power for each of the areas sampled. The analysis of the data also provided results which were used to estimate the ratio of the filtered noise power to the total noise power (i.e., R) required to evaluate the fractional standard deviation using expression (21). From these estimates, the expected fractional standard deviation for a single measurement of the adjusted noise power are computed to be 12% at an average exposure equal to that of step 5 and 25% at an average exposure equal to that of step 6. These values compare favorably to the measured standard deviation

Table 5

NOISE LEVEL DATA OBTAINED FROM
GRE FILM OF GOLDSTONE READOUT (LUNAR ORBITER I)

STEP SCANNED	FRAMELET NO.	DENSITY	TOTAL NOISE POWER x 10^4	ADJUSTED POWER X 10^4		FRACTIONAL STANDARD DEVIATION IN A SINGLE MEASUREMENT OF ADJUSTED POWER	
				MEASURED	ESTIMATED*	FROM DATA	ESTIMATED
STEP 5	146	1.15	54.50	38.93			
	147	1.14	54.74	34.99			
	148	1.14	64.77	49.44			
	154	1.07	54.98	39.01			
	AVERAGE	1.11	57.25	40.59 ±3.1	46.0	15%	12%
STEP 6	146	.907	28.30	13.30			
	147	.907	34.00	18.53			
	148	.893	29.31	11.56			
	154	.794	27.24	9.74			
	AVERAGE	.870	29.71	13.28 ±1.9	19.6	28%	25%

*BASED UPON ANALYSIS PRESENTED IN PHASE I FINAL REPORT (REFERENCE 1)

of the data included in Table 5. The average value of the adjusted total noise power also compares favorably to the analytically determined value of noise power determined by the procedures outlined in the Phase I report.

In a "nominally exposed" photograph, that is, one which has an average density of 0.8 on the spacecraft film, the fractional standard deviation for a single measurement of the adjusted noise power of approximately 18% is to be expected.

3.4.4 Accuracy of the Signal Level Measurement Techniques: The signal level quality parameters consist of the Hurter-Driffield response curve for the bimat processed spacecraft film and the linear relationship between the spacecraft film transmittance and the recorded GRE density. The accuracy to which these two functional relationships can be measured depends primarily upon the ability to accurately measure the average density corresponding to each of the gray levels in the step tablet on the GRE film and the transmittance values of each of the levels as they would appear on the spacecraft film. Since the pre-exposed edge data array contains a large amount of sensitometric calibration information, it is reasonable to assume that the measurements of GRE density can be made with acceptable accuracy. The transmittance values for the gray levels on the spacecraft film are measured from a bimat processed sample of flight film taken from the same roll which is loaded into the spacecraft assuming that the processing in the spacecraft is equivalent to that of the sample on the ground.

It is difficult to specify the accuracy of the signal level quality parameter measurements. Although confidence intervals for the measured functions would appear to be a logical choice, they are signal dependent functions which would be difficult to employ in subsequent analysis such as estimation of sample size. In addition, since the same measured density values are used to determine both the linear relationship between GRE density and spacecraft film transmittance and the Hurter-Driffield response curve, the confidence intervals are not independent and their analytical form would be quite complex. Instead, to measure the error of the signal

level measurement techniques it is more convenient to use an estimate of the accuracy to which the densities of the gray levels on the spacecraft film in the step tablet can be predicted. These densities are computed from the expression

$$D_{SC} = -\log_{10} T_{SC} = -\log_{10} (c + d\, D_{GRE}) \tag{22}$$

where c and d are the coefficients of the linear regression representing the relationship between GRE density (D_{GRE}) and spacecraft film transmittance (T_{SC}). Employing a Taylor series expansion to linearize this expression and neglecting the correlation between the GRE density and the regression coefficients, the standard deviation of the predicted value for the spacecraft film density can be written

$$s_{D_{SC}} \simeq \sqrt{\left(\frac{\partial D_{SC}}{\partial c}\right)^2 s_c^2 + \left(\frac{\partial D_{SC}}{\partial d}\right)^2 s_d^2 + \left(\frac{\partial D_{SC}}{\partial D_{GRE}}\right)^2 s_{D_{GRE}}^2} \tag{23}$$

where s_c^2 and s_d^2 are the variance in the intercept and slope estimate obtained in the linear regression and $s_{D_{GRE}}^2$ is the variance in the measurement of GRE density. Obtaining the partial derivatives from expression (22) and substituting

$$s_{D_{SC}} \simeq \frac{0.434}{T_{SC}} \sqrt{s_c^2 + D_{GRE}^2\, s_d^2 + d^2 s_{D_{GRE}}^2} \tag{24}$$

From this expression we note that $s_{D_{SC}}$ depends upon the signal level since it is a function of T_{SC} and D_{GRE} . To evaluate the standard deviation, estimates of s_c^2 , s_d^2 and $s_{D_{GRE}}^2$ are required. These can be obtained from the signal level measurements and estimates are available from the analysis of the GRE film from the pre-launch Goldstone readout of Lunar Orbiter I. Before discussing these measurements, consider the influence of the number of measurements (i. e., number of step tablets sampled) upon the deviation. Both s_c^2 and s_d^2 depend upon the residual error in the linear regression between the measured average GRE densities and spacecraft film transmittance for the nine steps of the step tablet. It is easily shown that this residual, and hence s_c^2 and s_d^2 , are expected to be inversely proportional to the number of step tablets

sampled. Similarly, $\sigma^2_{D_{GRE}}$, the variance of the average density measured for a particular step in the tablet, should decrease in proportion to the number of samples and therefore $\sigma_{D_{SC}}$ should decrease with the square root of the sample size.

In evaluating the quality parameters from the pre-launch Goldstone readout, the transmittances were determined by measuring the density of each of the levels in the step tablet from a sample of the Goldstone leader taken from that employed in the Lunar Orbiter I spacecraft. The densities were evaluated for three framelets, averaged and then converted to transmittance. Table 6 presents the relative log exposure, the measured density

Table 6

GRAY SCALE DATA OBTAINED FROM A SAMPLE OF THE GOLDSONE LEADER

STEP NO.	RELATIVE LOG EXPOSURE*	MEASURED DENSITY	TRANSMITTANCE
1	0.0	0.16	0.692
2	0.13	0.21	0.616
3	0.27	0.29	0.513
4	0.40	0.44	0.363
5	0.56	0.69	0.204
6	0.77	1.02	0.0955
7	0.94	1.28	0.0525
8	1.10	1.54	0.0288
9	1.26	1.72	0.0190

* BASED UPON THE Δ (LOG E) INCREMENTS FOR RETICLE NO. 8 AND SPECIFIED IN L-020495-KU, 6 MAY 1966.

on the Goldstone leader, and the corresponding transmittance for each of the gray levels. These transmittances are combined with the measured GRE density for each of the gray levels to estimate the linear relationship between spacecraft film transmittance and the recorded GRE density.

Measurements of the GRE density were made for each of the gray levels in five framelets from the reconstructed film obtained in the pre-launch readout. The average value of the density for each of the steps is presented in Table 7, along with the standard deviation of the individual measurements.

Table 7

MEASURED GRE DENSITY AND STANDARD DEVIATIONS FROM THE GOLDSTONE READOUT OF LUNAR ORBITER I

STEP NO.	MEASURED GRE DENSITY
1	2.28 ± 0.06
2	2.27 ± 0.04
3	1.99 ± 0.04
4	1.63 ± 0.06
5	1.17 ± 0.06
6	0.84 ± 0.04
7	0.74 ± 0.03
8	0.71 ± 0.02
9	0.73 ± 0.02

The resulting linear relationship between the transmittance of the Goldstone leader and the reconstructed GRE film is shown in Fig. 31. The step number is indicated in the figure. Steps 2 through 8 all exhibited a linear relationship which is somewhat different from the nominal linear relationship also shown in the figure*. The transmittance of step 1 (refer to Table 6) is quite high and its departure from linearity may be attributable to clipping by the scanner electronics. Such a phenomenon would produce

* The constant difference in GRE density between the measured relationship and nominal value could be simply a change in base fog of the recording film.

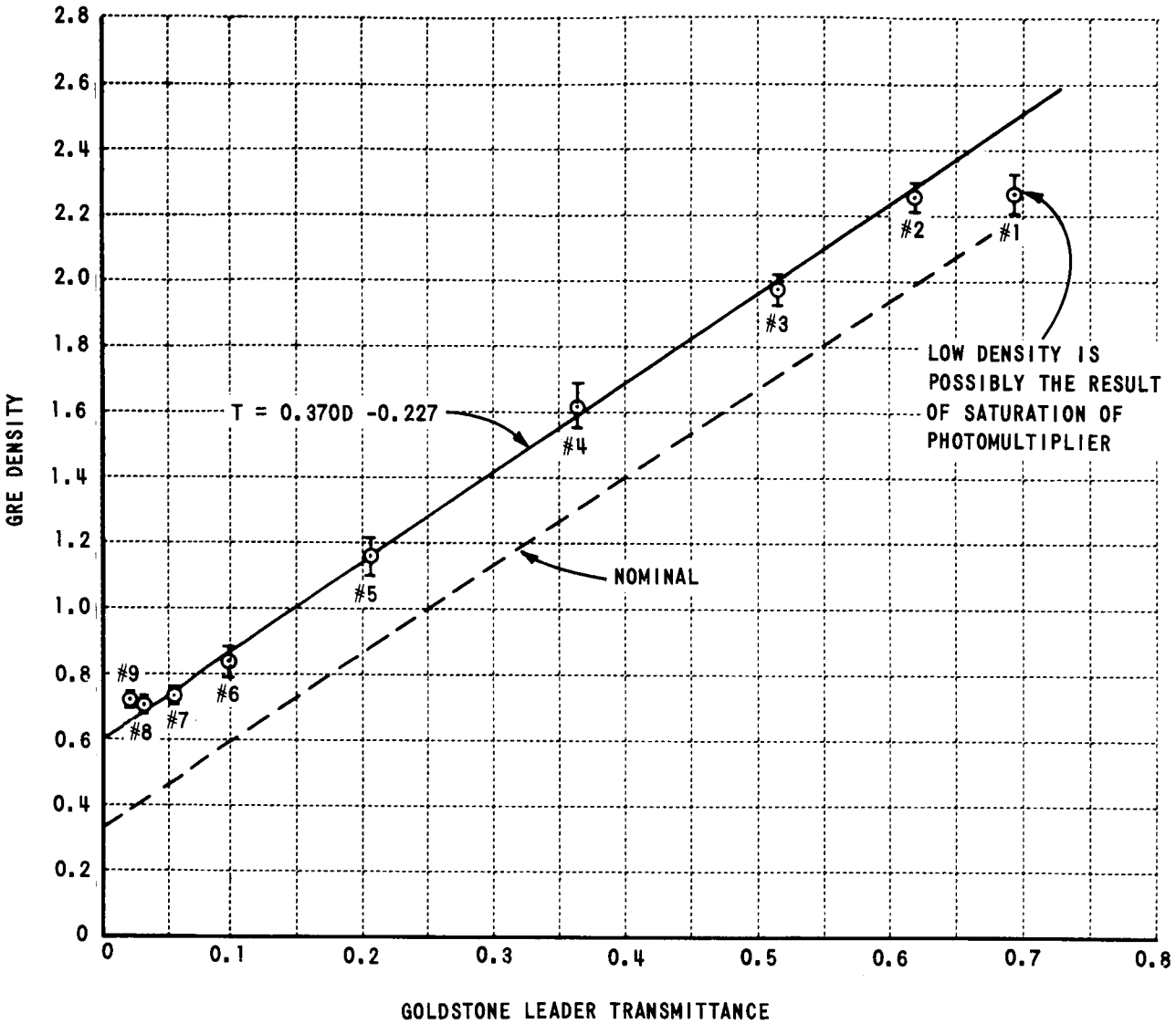

Figure 31 MEASURED RELATIONSHIP BETWEEN GRE DENSITY AND GOLDSTONE LEADER TRANSMITTANCE (LUNAR ORBITER I)

a constant GRE density at high values of transmittance. The departure of step 9 from linearity could be produced by several effects. First, the transmittance of the step simply could be in a region where the response region of the scanner is nonlinear. Secondly, since this step also received the least exposure in the GRE film, it would be more susceptible to flare light in the reconstruction.

Using the experimentally measured relationship between GRE density and the leader transmittance, the Hurter-Driffield response curve for the Goldstone leader was determined by omitting the first and the ninth steps of the step tablet. The resulting curve shown in Fig. 32 compares favorably to the response curve obtained directly from the measurements of the step tablet from the sample of bimat processed Goldstone leader.

From the complete analysis of these data it was found that the fractional standard deviation in the predicted values of spacecraft film density determined by dividing expression (24) by D_{sc} , is approximately constant over the linear region of the Hurter-Driffield response curve (steps 4 through 7, inclusive) and has a value of about 10%. In addition, this deviation was observed to decreased approximately as the square root of the number of samples verifying an earlier prediction.

It should be noted that the measurement of the signal level quality parameters can be considered valid only over the range occupied by the GRE densities of the step tablet. To predict the exposure on the spacecraft film for densities on the GRE film which are above that of step 9 or below that of step 1, requires that the fitted parametric forms be used as estimators. It is well known that the accuracy of such estimators decreases rapidly as one attempts to predict values which lie outside the range of the data.

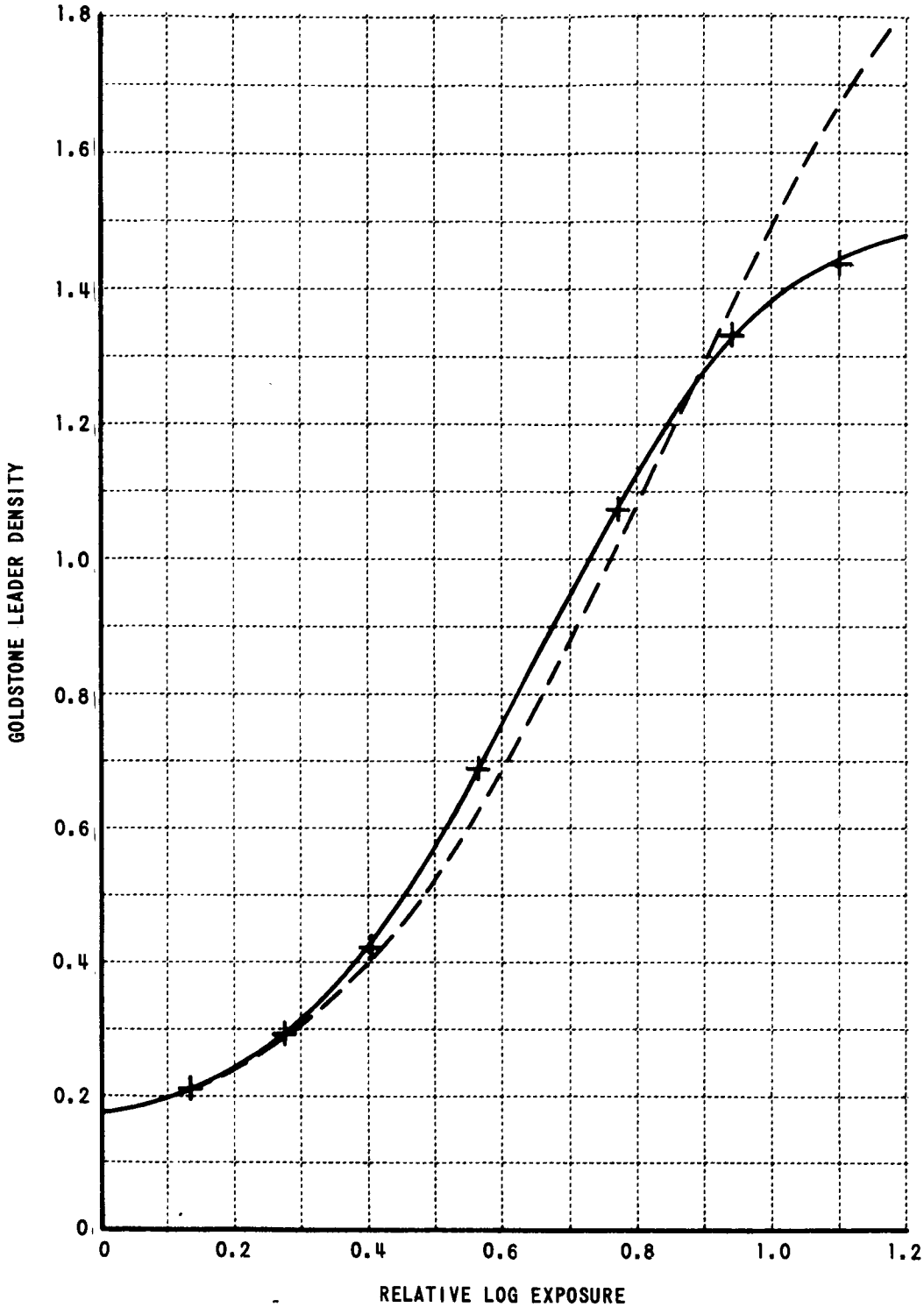

Figure 32 MEASURED HURTER-DRIFFIELD RESPONSE FOR THE LUNAR ORBITER I GOLDSTONE LEADER

3.5 Estimation of the Number of Measurements Required to Evaluate Each of the Quality Parameters. - In the previous sections, error estimators were described for each of the quality parameters. Because of the nature of the measurement techniques and the observed variability between individual measurements, a statistical approach must be employed to evaluate any one quality parameter. Several targets will be selected and the values measured from these targets averaged to estimate the quality parameter. Since, in all cases, the errors were found to decrease as the number of measurements increases, there is a tradeoff between the accuracy attained in the estimated value of the quality parameter and the extent of the measurements.

The measured values of the quality parameters are used to determine quantitative measures of system performance based upon the objectives of the Lunar Orbiter mission. Since errors in any of the quality parameters introduce corresponding errors in the performance criteria, the combined effect of the errors in each quality parameters must be given consideration when estimating the number of measurements to be made (sample size) in evaluating any one quality parameter. Generally, performance criteria are functions of the quality parameters similar in form to the ratio of the combined effects of signal level and signal detail rendition to the noise level of the system. Consequently, in estimating sample size, it is reasonable to measure the accuracy attained in the performance criteria by the rms value of the fractional standard deviations in the individual quality parameter measurements.

In the analysis presented in the previous sections, it was found that the standard deviation of the modulation transfer function measurements could be bounded by a linear function of spatial frequency. For purposes of estimating the number of measurements required to evaluate a transfer function, it is convenient however to compute the fractional standard deviation at a fixed spatial frequency. In evaluating the performance of the Lunar Orbiter system, it is found that accurate measurement of the transfer function is most important for spatial frequencies below 20 lines/mm.

Consequently, in evaluating the number of measurements to be employed in the analysis of modulation transfer function, an upper bound for the fractional standard deviation at 15 lines/mm is employed.

Table 8 presents the fractional standard deviation for an individual measurement of each quality parameter, an estimate of the number of measurements required, resulting fractional standard deviation in the averaging value obtained from these measurements, and a qualitative estimate of the relative contribution to the total error in the measured performance criteria. As indicated from the results presented in the table, the largest error occurs in the measurement of the noise level quality parameter. In an analysis of system performance, the accuracy is limited primarily by the expected error in this quality parameter. As concluded from the analysis presented in Appendix D, the magnitude of this error is primarily due to the effect of a finite sample size and the quasi-spectral analysis employed in estimating total noise power within the bandwidth occupied by the signal. To increase the accuracy in the measurement of system performance, an increase in the amount of data or the number of samples employed to evaluate the noise level quality parameter would be required. In either case, the cost of acquiring and analyzing the additional data needed for a significant improvement in the measurement of system performance would appear to be unjustified.

In addition to the data obtained from the reconstructed GRE film, the measurement technique for evaluating the scanner-communications-GRS modulation transfer function requires an evaluation of the average sharpness of the edge chosen to evaluate this transfer function. The number of measurements which are required to measure the sharpness of the perspective test objects depends upon the influence of the accuracy of this measurement on the scanner-communications-GRS modulation transfer function. In Section 3.4.2, it was concluded that the effect of the accuracy of the measurement of sharpness could be neglected if at least 10 samples were used to evaluate the sharpness response function.

Table 8

RECOMMENDED NUMBER OF MEASUREMENTS

QUALITY PARAMETER		EXPECTED ERROR FOR A SINGLE SAMPLE	RECOMMENDED NUMBER OF SAMPLES	EXPECTED ERROR IN QUALITY PARAMETER	EFFECT UPON ACCURACY OF PERFORMANCE CRITERIA	REMARKS
MODULATION TRANSFER FUNCTION	SCANNER	6%*	10-25	2%*	SECONDARY	ERROR PRIMARILY DUE TO NOISE IN EDGE TARGET
	CAMERA	17%*	10-25	4%*	SECONDARY	ERROR DUE TO NOISE AND ACCURACY OF GEOMETRIC PARAMETERS
SIGNAL LEVEL		10%	10-15	3%	SECONDARY	LIMIT IMPOSED BY ACCURACY OF GRE DENSITY MEASUREMENTS
NOISE LEVEL		12%-30%**	5-10	4%-10% **	PRIMARY	MAJOR CONTRIBUTION TO ERROR DUE TO STSTISTICAL FLUCTUATIONS OF DATA EMPLOYED IN REDUCTION PROCEDURE

*AT A SPATIAL FREQUENCY OF 15 LINES/MM.

**DEPENDS UPON THE AVERAGE EXPOSURE OF THE FRAME

4. RELATION OF THE QUALITY PARAMETERS TO THE LUNAR ORBITER OBJECTIVES BY USE OF SYSTEM PERFORMANCE CRITERIA

Having established and verified the techniques for computing the quality parameters from measurements of specific targets in a reconstructed image on the GRE film, it is desirable to use these measures of quality to determine an index or set of indices which "specify" how well the photographic system performed with respect to the Lunar Orbiter objectives. Such a set of indices, referred to as system performance criteria, are described in this section. The criteria are based upon the objective of establishing the general roughness of the lunar surface in support of the Apollo program. The discussion is divided into four topics. The first topic considered is a description of the topographic models used to establish the criteria and the relationship between the criteria and the measured values of the quality parameters. This is followed by a section showing the variation of the criteria with model geometry and off-nominal operating conditions of the Lunar Orbiter photographic system. To assess the accuracy to which the system performance can be measured by the criteria, the relationship between the error in the measurement of the quality parameters and the accuracy to which the criteria are determined is evaluated in the third section. The final topic considered concerns the applicability of the criteria to assessment of the capability to extract topographic data from the Lunar Orbiter imagery.

4.1 Description of the System Performance Criteria. - To relate the measured values of the quality parameters to system performance, a test object representing a topographic feature on the lunar surface must be selected. Two such test objects or models have been specified by NASA to assess how well the objective of establishing the general roughness of the lunar surface is met by the Lunar Orbiter photographic system. These test objects shown in Fig. 33 are a right circular cone with a vertical axis, and protruding from or recessed into a horizontal surface, and a uniform square area inclined toward or away from the sun surrounded by a horizontal

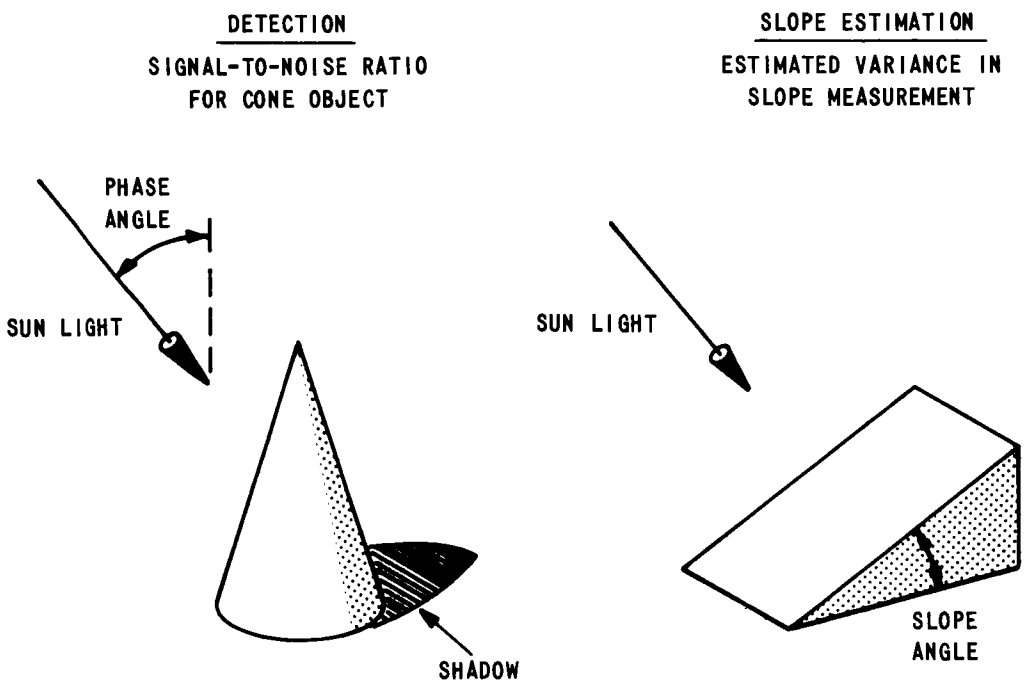

Figure 33 SPECIFIED TEST OBJECTS FOR EVALUATING SYSTEM PERFORMANCE

surface. Using these test objects for models, a set of performance criteria were developed and reported in the Phase I Final Report. The criteria were subsequently revised and the new criteria described below.

During an actual mission, the Lunar Orbiter spacecraft will photograph the lunar surface in the nadir direction for a major portion of the mission. Variations in exposure on the spacecraft film will be produced by the dependence of the reflectance of the lunar surface upon its orientation. The relative reflectance is expressed through the photometric function. One objective of the Lunar Orbiter mission is the detection of small obstructions on the lunar surface. The topographic test object or model specified by NASA for evaluation of system performance for this objective is a conical obstruction of height h and radius r. This object is assumed to protrude from or recess into a horizontal surface located at the nadir position of the photograph*. In the analysis, the phase angle, or equivalently in this case the solar zenith angle, is not restricted to the range where no shadow is cast by the obstacle, as done previously during the Phase I effort. It is still assumed that the object is of low enough contrast so that the photographic response is approximated by the total response determined by multiplying the two measured values of modulation transfer function obtained as the signal detail rendition quality parameters. In practice, however, the test cones may have a sufficiently large height-to-radius ratio compared to the phase angle so that the irradiance distribution produced by the cone is high contrast in nature. This is particularly true when a shadow is cast by the cone. In these circumstances, the approximation of a linear system is inaccurate** but not unreasonably so and is therefore retained on the basis of expediency.

---

* The assumption of vertical photography implies that the nadir point and the principal ground point are reasonably coincident in the photographic image.

** The error made tends to yield slightly higher performance measure than that representative of system performance.

Since the question is one of detection, the visual detection process is simulated for purposes of analysis by a matched filter designed for the specified size and shape of obstacle. This filter is used to make a decision in the optimum manner as to whether an obstacle or only the noisy background is present. The measure of system performance is taken to be the amplitude signal-to-noise ratio for this filter. The relationship between this criterion and the measured quality parameters is derived in Appendix C. Assuming that the noise in the GRE image is approximately white it is found that

$$S/N = \sqrt{Q/N_o} \tag{25}$$

where N_o is the two-dimensional noise power density obtained by dividing the adjusted noise power (that is, the noise level quality parameter) by the bandwidth of the GRE image and Q is called the "quadratic content" and represents the power contained in the difference between the signals with and without the obstruction present. It should be noted that Q will depend upon the frequency response of the system and the signal level. However, because of integration over the signal, the value of Q does not depend uniquely on target shape. As shown in an earlier report[1], the value of Q can be written in terms of the autocorrelation function of the system point spread and the autocorrelation function of the difference between the signals expected from the perfect system with and without a conical obstacle present.

Another objective of a Lunar Orbiter Mission is to obtain topographic information from the density variations observed in the reconstructed photographs. A different topographic feature has been specified by NASA for evaluation of the system performance with regard to photometric topographic profiling. This test object is a two-dimensional uniform square area inclined toward or away from the sun at an angle α from a horizontal surface*. If such a test object did exist on the lunar surface, it would appear in the GRE image to be a degraded square on a uniform background.

---

* The sign convention employed is that positive α represents an inclination away from the sun.

The measure of system performance is chosen to be the accuracy to which the angle α could be measured from the hypothetical image on the GRE film. This measure is related to the quality parameters by employing maximum likelihood techniques of statistical communication theory in Appendix C. The resulting criterion, that is, the minimum standard deviation to be expected from an unbiased estimate of the angle α using all the information available in the photograph, is therefore indicative of limiting performance which may not be achieved in actual data reduction*. The resulting mathematical expression for the standard deviation are similar in structure to those for the signal-to-noise ratio discussed above. In fact, if the "signal" is defined as the derivative with respect to α of the density distribution on the GRE film, then the standard deviation is shown in Appendix C to be the reciprocal of the signal-to-noise ratio of a filter matched to this signal. Assuming that the test object is a square area of length ℓ on a side and inclined at an angle α from a horizontal surface, the error in the measurement of α is shown to be

$$\sigma = \sqrt{\frac{N_0}{\left[\frac{\partial \Delta D(\alpha)}{\partial \alpha}\right]^2 \ell^2 \iint \left|\tau(\nu_x, \nu_y)\right|^2 \operatorname{sinc}^2(\pi \ell \nu_x) \operatorname{sinc}^2(\pi \ell \nu_y)\, d\nu_x d\nu_y}} \tag{26}$$

In this expression, two of the quality parameters, N_0 and $\tau(\nu_x, \nu_y)$ appear directly. The third quality parameter, namely, the total response from the GRE film density to aerial exposure, is included in $\frac{\partial \Delta D(\alpha)}{\partial \alpha}$, the rate of change of density level on the GRE film with respect to α. The influence of the system frequency response upon the standard deviation is seen to depend upon ℓ, the size of the test object through the terms $\operatorname{sinc}^2(\pi \ell \nu_x)$ and $\operatorname{sinc}^2(\pi \ell \nu_y)$. For large ℓ both of these functions decrease rapidly with ν_x and ν_y and only the value of the transfer function at low frequencies $(\nu_x, \nu_y \leq \frac{1}{\ell})$ contributes in the integral to reduce the magnitude of the standard deviation. As ℓ becomes smaller, the transfer function at correspondingly higher frequencies becomes more important as would be expected. The variation of the variance with target size (that is, ℓ) is discussed in the next section.

---

* In developing this criterion it was assumed that the photometric function and relationship between the relative and absolute exposure are accurately known.

Digital computer programs were written to evaluate both of these criteria on the IBM 7044. Typical examples of the printed output from these programs is reproduced in Fig. 34.

4.2 Variation of Criteria with Model Geometry and Off-Nominal Performance: The previous sections have defined a set of quality parameters, measurement techniques, and the mathematical relationships needed to reduce the measured data. The quality parameters have been related to specific Lunar Orbiter tasks through system performance criteria. In this section the variation of the performance criteria, σ and S/N for off-nominal conditions and variation in the geometry in the test targets are considered. The variation of the performance criteria is examined as a function of phase angle, exposure level, radiation exposure, and operational degradations (i. e., image motion, image vibration, and defocus). The data presented in this section were obtained using an IBM 7044 programmed with the solution of the equations described in Appendix C. For convenience, attention was confined to the high resolution photographic system. In the analysis, it is assumed that the exposure on the spacecraft film is such that the density for a flat surface or essentially the average density on the spacecraft film near the nadir is 0. 75 and that the nominal phase angle is 70°. Table 9 summarizes the nominal values for these and other parameters used to evaluate the criteria. The graphs showing the variation of the signal-to-noise ratio were obtained using cones protruding from a horizontal surface with a height of 0. 5 meter and base diameters of 2. 0 and 7. 0 meters. In the following discussion these cones are called the two-meter design cone and seven-meter design cone, respectively. For an evaluation of the error in the slope measurement, a test object seven meters on a side at the lunar surface was chosen. If the medium resolution photographic system were evaluated, the geometrical distances of the test objects would be increased by a factor of 8. The results presented are intended to be a demonstration of the behavior of the criteria and are not intended to reflect on the choice of any of the parameters in the mission or hardware design.

***** SIGNAL TO NOISE RATIO FOR CONE DETECTION *****

MRF NO. 61

RADIUS (IN METERS ON THE LUNAR SURFACE)	HEIGHT	Q	SIGNAL/NOISE
8.00	4.00	0.1043E-05	18.05
12.00	6.00	0.3913E-05	34.96
16.00	8.00	0.9292E-05	53.88
20.00	10.00	0.1740E-04	73.74
24.00	12.00	0.2863E-04	94.58
28.00	14.00	0.4306E-04	115.98

(a) SIGNAL-TO-NOISE RATIO CRITERION

ERROR IN ESTIMATE OF SLOPE ANGLE

MRF NO. 61

WHITE NOISE POWER DENSITY 0.3201E-08 (IN TRANSMITTANCE)

DLOGE CONSTANTS

C1= 0.07300
C2= 1.71800
C3= 8.90000
C4= 0.73600
C5= 0.50000

DENSITY FOR FLAT SURFACE 1.66000

PHASE ANGLE 60.9 DEGREES

SIZE OF TARGET 0.096 MM

ALPHA (DEGREES)	DTDG	VARIANCE	STANDARD DEVIATION
-15.0	0.1090E-03	0.3654E 02	6.045
-13.0	0.1338E-03	0.2426E 02	4.926
-11.0	0.1651E-03	0.1593E 02	3.991
-9.0	0.2050E-03	0.1033E 02	3.214
-7.0	0.2564E-03	0.6604E 01	2.570
-5.0	0.3231E-03	0.4160E 01	2.040
-3.0	0.4104E-03	0.2578E 01	1.606
-1.0	0.5262E-03	0.1568E 01	1.252
1.0	0.6816E-03	0.9346E 00	0.967
3.0	0.8931E-03	0.5443E 00	0.738
5.0	0.1185E-02	0.3089E 00	0.556
7.0	0.1597E-02	0.1703E 00	0.413
9.0	0.2185E-02	0.9094E-01	0.302
11.0	0.3043E-02	0.4689E-01	0.217
13.0	0.4317E-02	0.2330E-01	0.153
15.0	0.6234E-02	0.1117E-01	0.106

INTEGRAL= 0.7372E-02

(b) SLOPE ANGLE ERROR CRITERION

Figure 34 TYPICAL PRINTED OUTPUT FROM THE SYSTEM PERFORMANCE CRITERIA EVALUATION PROGRAMS

Table 9

NOMINAL CONDITIONS USED IN EVALUATING PERFORMANCE CRITERIA

PARAMETER	VALUE	SOURCE
PHOTOMETRIC FUNCTION	QUADRATIC FIT TO "REVISED LUNAR REFLECTIVITY MODEL", JPL TECH. REPT. 32-664	TABLE G-1, REFERENCE (1)
PHASE ANGLE	70°	-
EXPOSURE LEVEL	AVERAGE DENSITY OF 0.75 ON SPACECRAFT FILM	-
HURTER-DRIFFIELD CURVE FOR SPACECRAFT FILM	LOW SPEED LIMIT CURVE	EQUATION (10) WITH $b_1^2 = 0.207$, $b_2^2 = 1.787$, $b_3 = 2.689$, $b_4^2 = 0.077$, $b_5^2 = 0.564$
FREQUENCY RESPONSE OF 24" LENS	NOMINAL	FIGURE G-1, REFERENCE (1)
SCANNER-COMMUNICATIONS-GRS FREQUENCY RESPONSE	NOMINAL	EQUATION G-13 AND FIGURE G-3 OF REFERENCE (1)
TOTAL NOISE POWER WITHIN SIGNAL BANDWIDTH	0.0438 VOLTS^2	APPENDIX D, REFERENCE (1)

Several factors including phase angle, exposure level and radiation exposure can alter the density recorded on the spacecraft film and, therefore, alter the value of the criteria. The variation of signal-to-noise ratio with phase angle is shown in Fig. 35 for both design cones. The effect of phase angle upon the error in slope measurement is shown in Fig. 36 for several values of α (all toward the sun). As would be expected, the signal-to-noise ratio increases with phase angle for both the design cones and the error in estimating slope is, in general, less at higher phase angles.

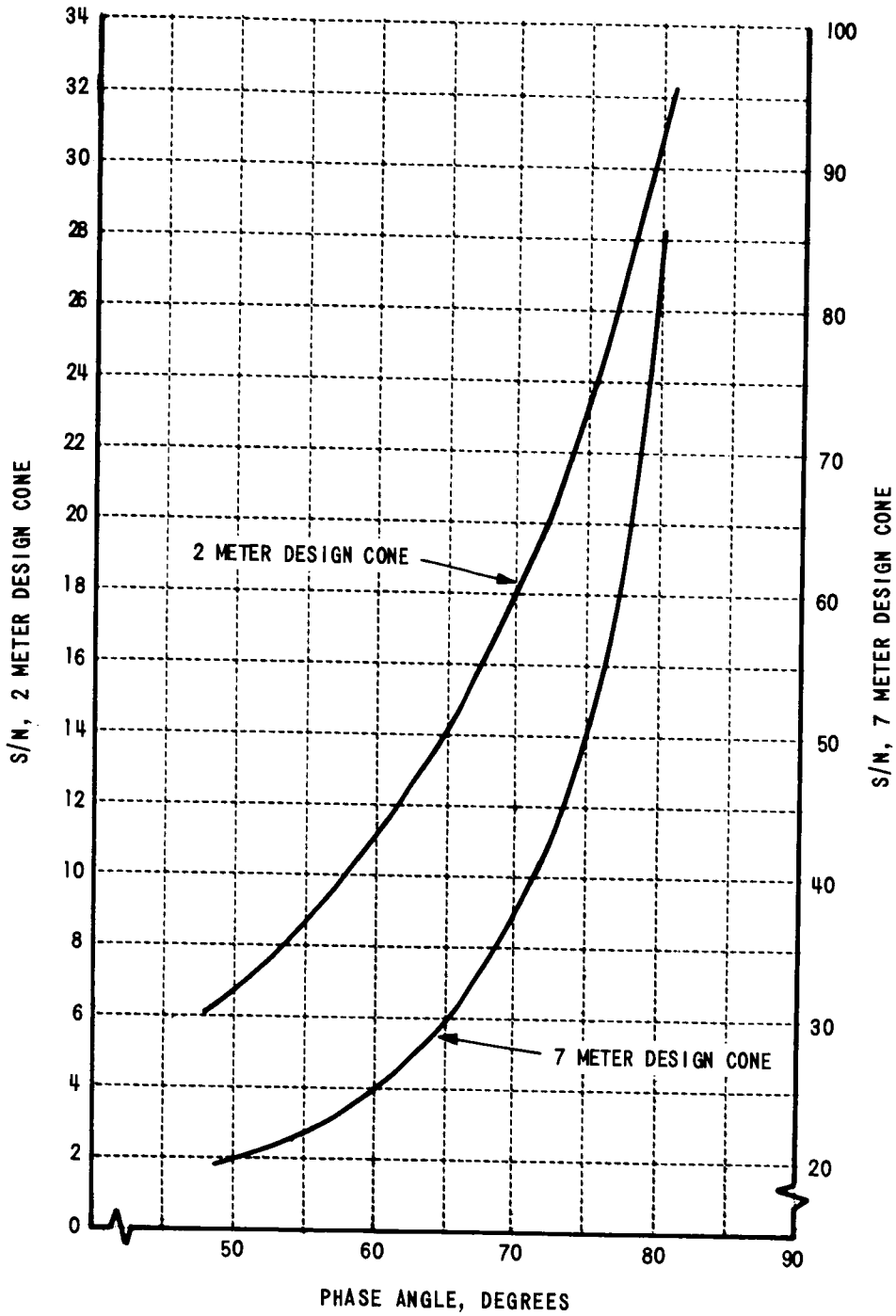

Figure 35 VARIATION OF SIGNAL TO NOISE RATIO WITH PHASE ANGLE

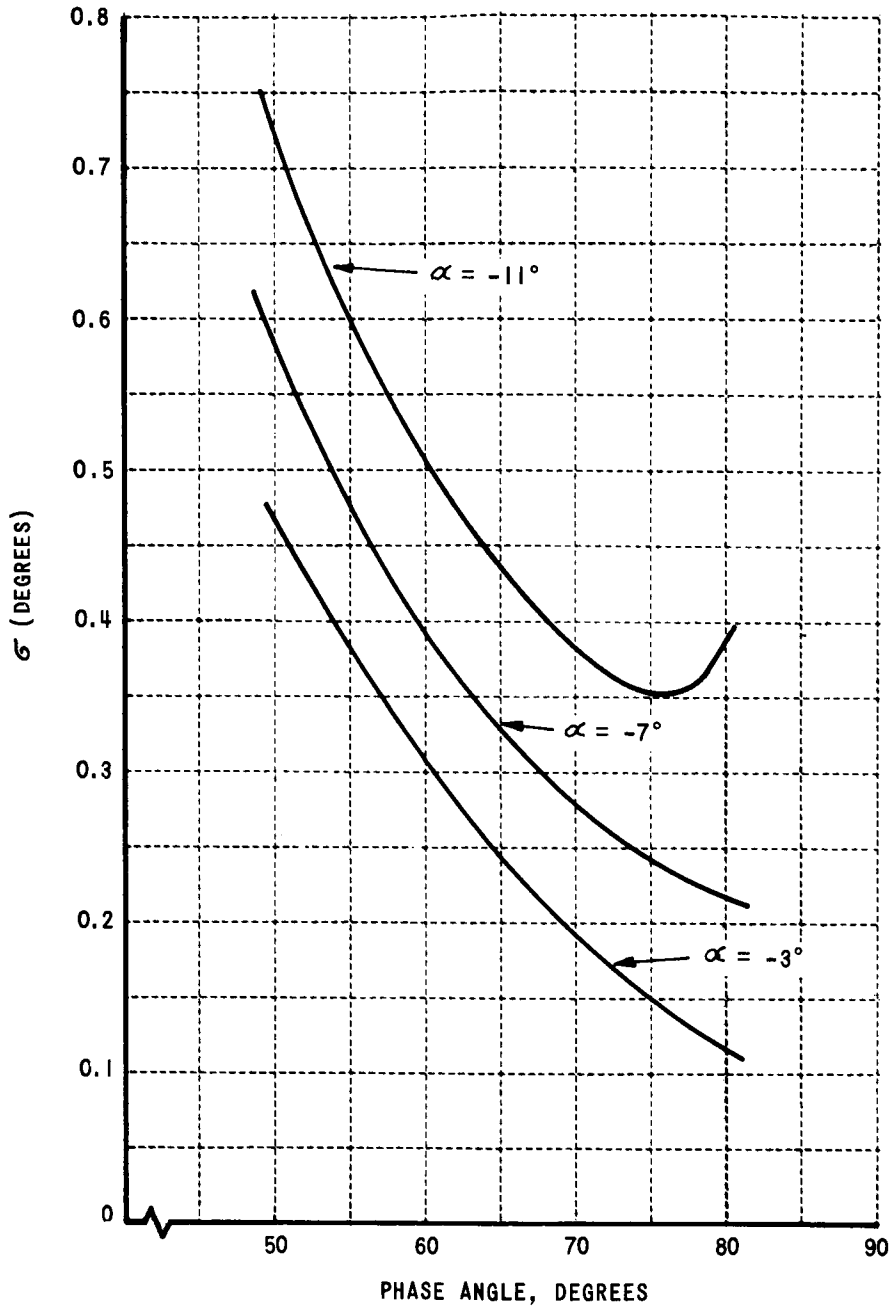

Figure 36 VARIATION OF ERROR IN SLOPE MEASUREMENT WITH PHASE ANGLE

Another factor which influences the contrast of the GRE image is the exposure level on the spacecraft film. The exposure may change due to local variations in normal albedo or due to changes in the exposure time. Changes in the exposure level correspond to selecting a different operating point on the Hurter-Driffield response curve for the bimat processed spacecraft film. This operating point or level is defined by the density produced on the spacecraft film by a flat surface near nadir in the photograph. Figs. 37 and 38 show the variation of S/N and σ with this density. The signal-to-noise ratio increases with increasing exposure level due to the increase in peak-to-peak density signal on the GRE film which occurs particularly when the cone casts a shadow. The decrease in the rate of change of S/N at higher exposures reflects the decreasing slope of the Hurter-Driffield response curve at the higher exposures. From the results which show that the signal-to-noise ratio increases with exposure level, one might expect that the error in estimating slope would decrease with increasing exposure level. In Fig. 38, the opposite effect is observed because σ depends upon the rate of change of contrast in the image whereas the signal-to-noise ratio depended directly upon the contrast. For the examples considered in this section, the contrast of the cone target is increasing while the rate of change in contrast for the inclined uniform area is decreasing. For other values of α, positive values (away from the sun), for example, σ would eventually become a decreasing function of exposure level.

The final factor investigated which influences the contrast of the signal on the GRE film is the effect of radiation exposure upon the performance criteria. During the mission, there is a possibility that the film in the spacecraft will receive some radiation exposure before development. The exposure due to the lunar scene is added to the radiation exposure to determine the density on the bimat processed spacecraft film. The variation of the criteria with fog density are presented in Figs. 39 and 40 and were evaluated assuming that the exposure time is held constant at its nominal value. As would be expected, any significant amount of

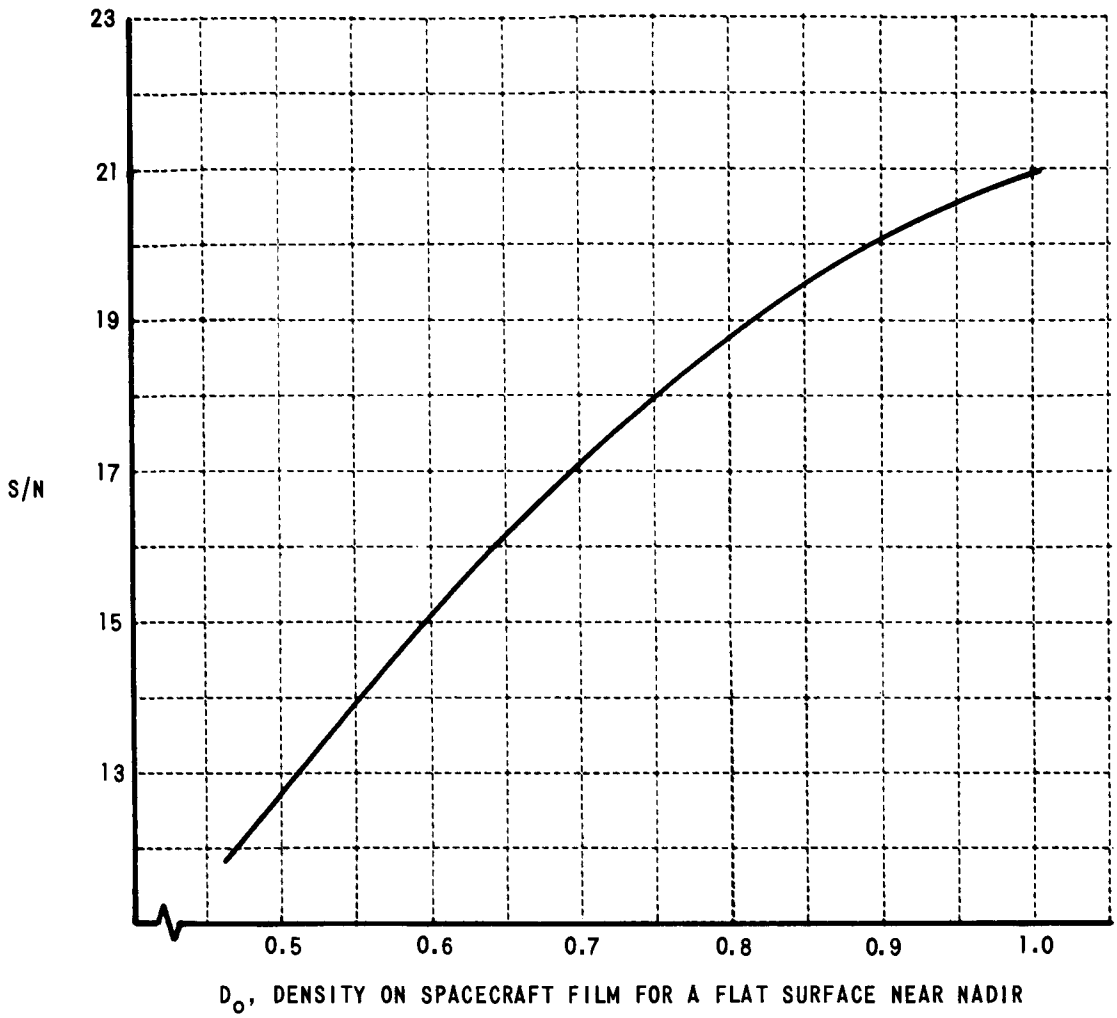

Figure 37 VARIATION OF SIGNAL-TO-NOISE RATIO WITH EXPOSURE LEVEL (2 METER DESIGN CONE, 70° PHASE ANGLE)

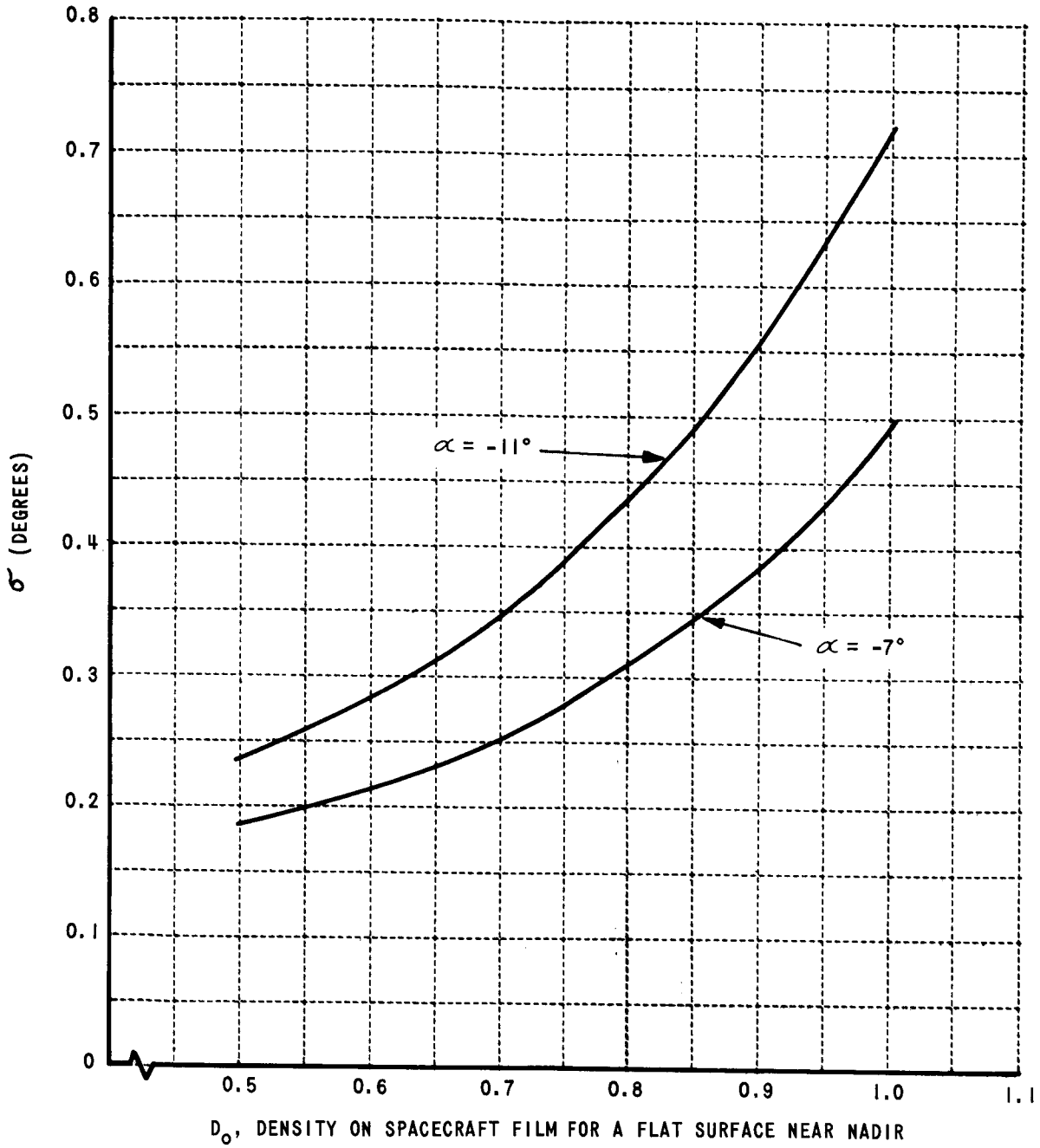

Figure 38 VARIATION OF ERROR IN SLOPE WITH EXPOSURE LEVEL (70° PHASE ANGLE)

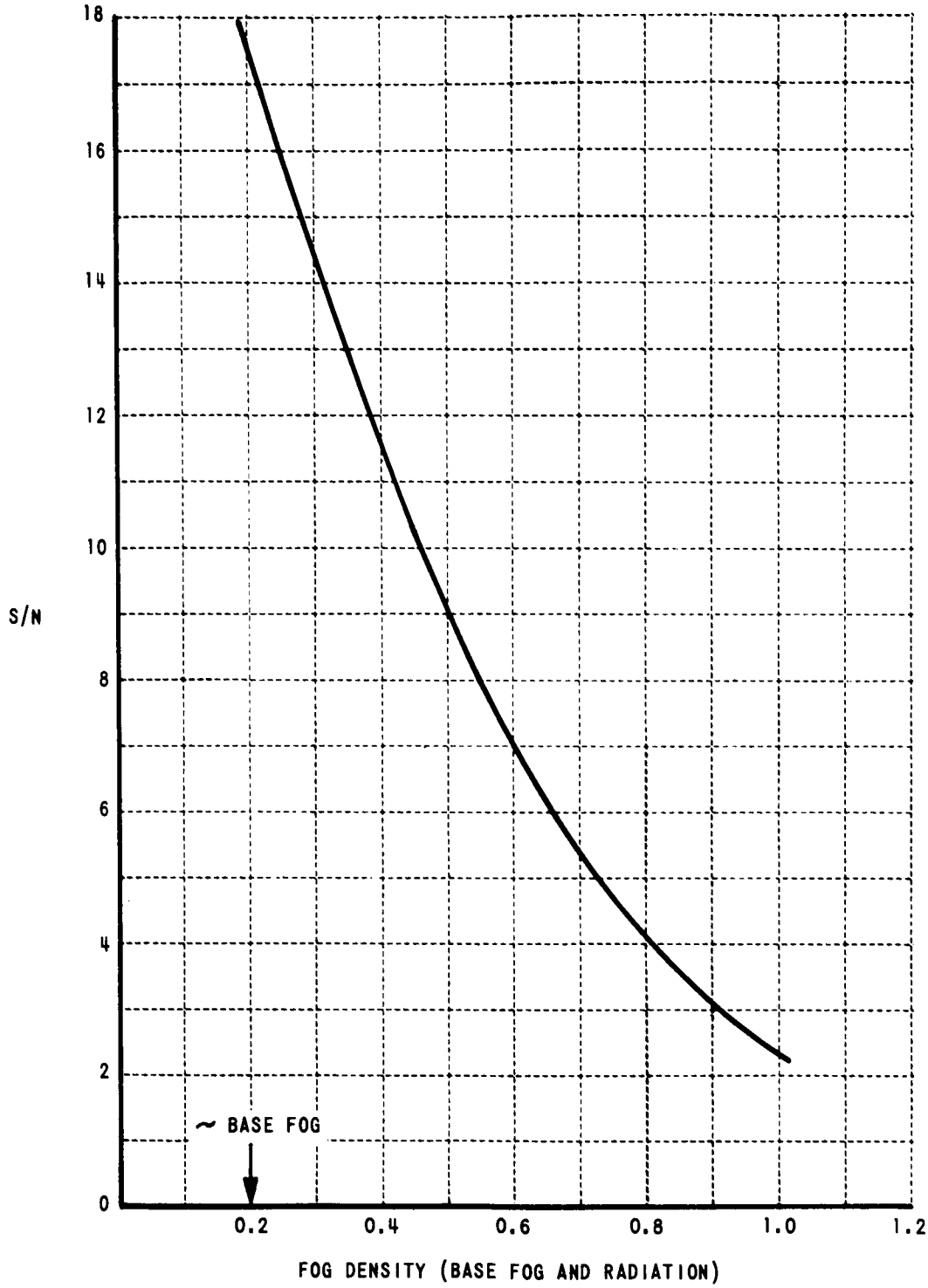

Figure 39 VARIATION OF SIGNAL-TO-NOISE RATIO WITH RADIATION EXPOSURE (2 METER DESIGN CONE, 70° PHASE ANGLE)

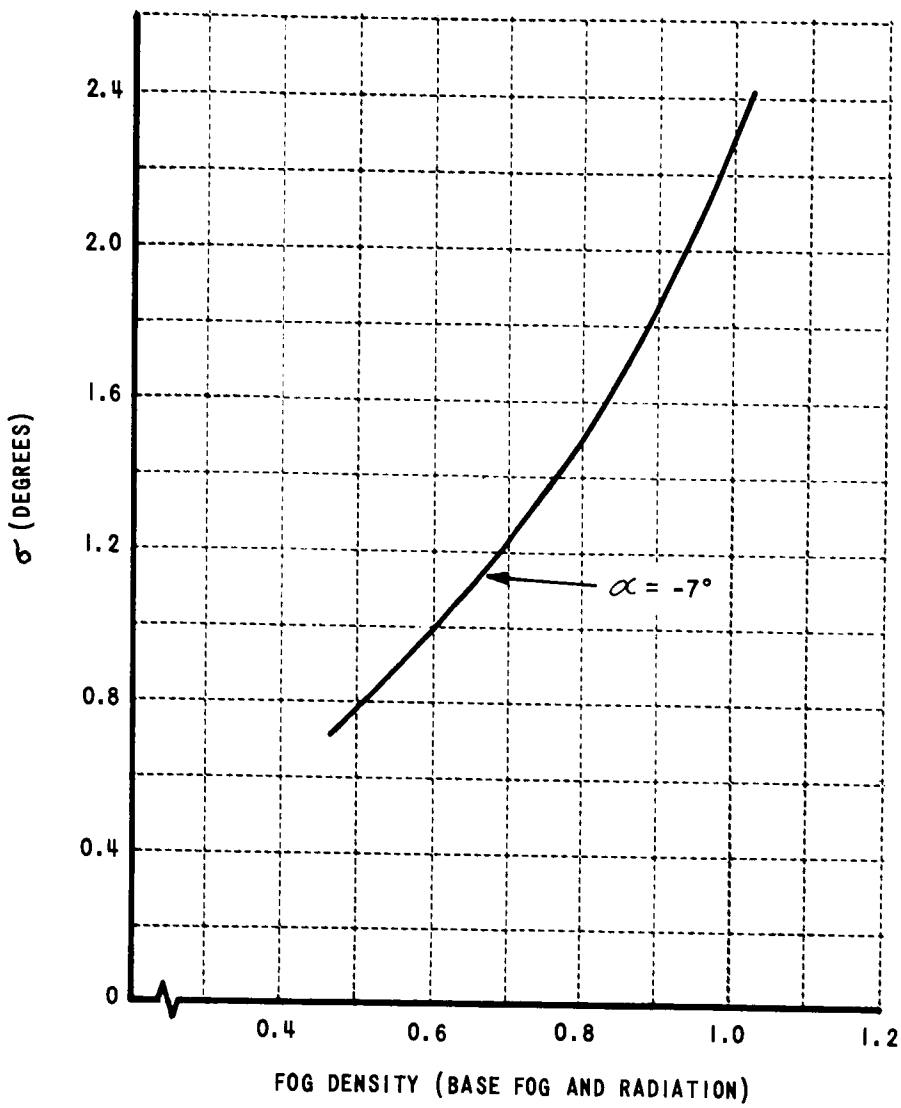

Figure 40 VARIATION OF ERROR IN SLOPE MEASUREMENT WITH RADIATION EXPOSURE (70° PHASE ANGLE)

radiation exposure will be detrimental to system performance. This is exhibited in the fact that the signal-to-noise ratio decreases with increased film fogging and the error in the measurement of α increases.

In addition to off-nominal operating conditions affecting the signal contrast, a possibility exists that operational degradations such as image motion, image vibration and defocus, will reduce the signal detail rendition capability of the photographic system. The effects of these three types of operational degradations upon the signal-to-noise ratio for a two-meter design cone and upon the error in measured slope for a uniform area 7 meters on a side and inclined 7° toward the sun were investigated. The results are shown in Figs. 41 and 42. In all cases, the signal-to-noise ratio decreases monotonically with the magnitude of the degradation and the error in slope measurement increases in accordance with the fact that the performance of the system is impaired by such operational degradations. It should be noted that the rate of change of the performance criteria is smallest for degradations whose magnitude is less than 1 meter.

This occurs because the point spread of the camera system whose inherent width is about 1 meter dominates the combined point spread when the magnitude of operational degradations are less than 1 meter. For operational degradations larger than 1 meter, the point spread of the degradations is more influential and the performance criteria change more rapidly. When the degradations exceed two meters, the signal-to-noise ratio as shown in Fig. 41, the rate of change begins to decrease again. In this case, the width of the combined point spread is greater than the geometric size of the test cone considered. The two meter design cone, however, is a relatively high contrast object and the signal-to-noise ratio remains appreciable even in the presence of severe degradations. Such degradations are not sufficient to submerge the signal into the noise in the GRE image.

As indicated previously, the geometrical size of the test target influences the values of the criteria. For example, increasing the height of a cone having a fixed diameter increases its contrast or peak-to-peak signal and, therefore, increases the signal-to-noise ratio. This is shown

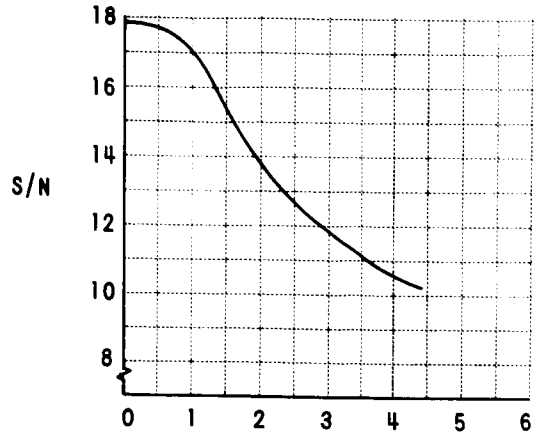

MAGNITUDE OF IMAGE MOTION (METERS ON LUNAR SURFACE)

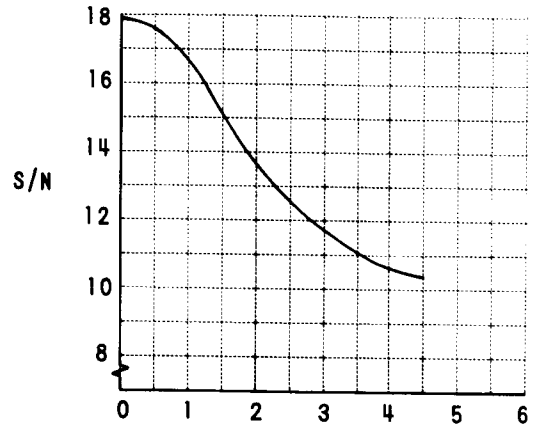

MAGNITUDE OF DEFOCUS (METERS ON LUNAR SURFACE)

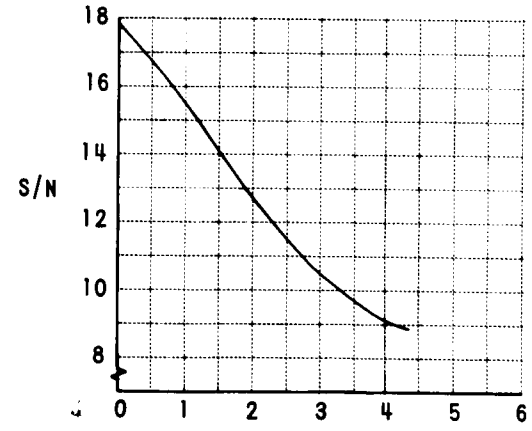

MAGNITUDE OF VIBRATION (METERS ON LUNAR SURFACE)

Figure 41 VARIATION OF SIGNAL-TO-NOISE RATIO WITH OPERATIONAL DEGRADATIONS (2 METER DESIGN CONE, 70° PHASE ANGLE)

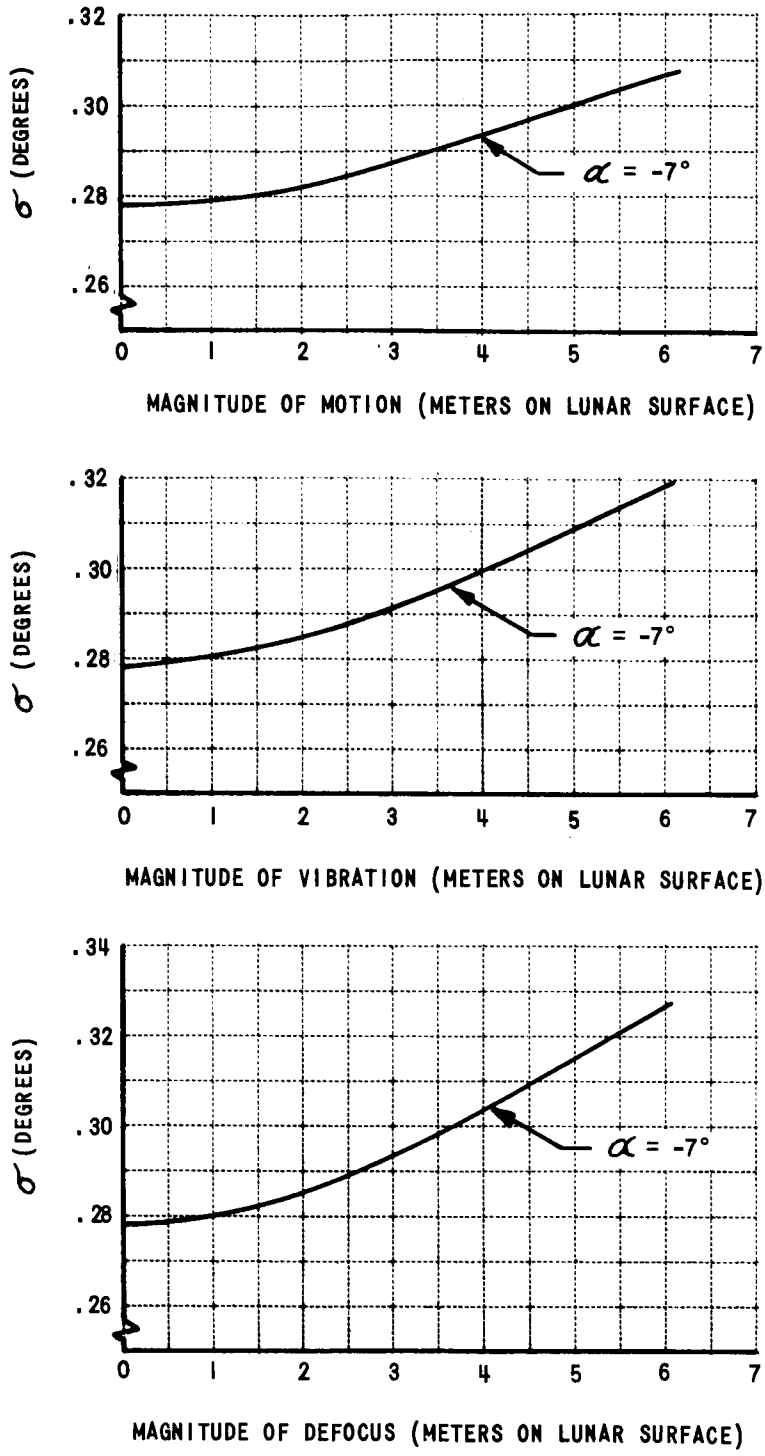

Figure 42 VARIATION OF ERROR IN SLOPE MEASUREMENT WITH OPERATIONAL DEGRATIONS (70° PHASE ANGLE)

in Fig. 43 where the solid curve represents the signal-to-noise ratio for a cone with a base-to-height ratio of 14 and a varying diameter. At a 2 meter diameter, this cone would have a height of 1/7 meters. Also shown by the "X" in the figure is the larger signal-to-noise ratio due to a cone with a two meter diameter and a 1/2 meter height (2 meter design cone).

In the computations of the error in the slope estimate, the target size was kept fixed at 7 meters. The value of the error, however, depends upon the target size, ℓ , and it would be reasonable to expect that the error in the estimate of slope would increase as the size of target becomes smaller. This behavior is shown in Fig. 44 for a slope angle of 7° toward the sun. Note that the increase in the error becomes more rapid as the size of the target approaches the resolution limit of the photographic system. In addition to the size of the target, the previous computations also were confined to an inclination toward the sun of 7°. The variation in the error at other angles was examined and is shown in Fig. 45. The fact that the error is observed to decrease as the surface inclines more away from the sun can be predicted from the previous results presented in Fig. 38 which show that the error decreases with the exposure level in the spacecraft film. In both cases, the error calculations were made assuming that the total noise power is constant. The noise power, in fact, decreases as the exposure increases in the spacecraft film and therefore the effects shown in Fig. 38 and Fig. 45 would be somewhat less pronounced if the variation of the total noise power with exposure level were taken into account.

4.3 Effect of the Accuracy of the Quality Parameters Measurements Upon the Performance Criteria. - As indicated in the previous section, the criteria are calculated from the measured values of the quality parameters which include the modulation transfer function of the photographic system, the dc response curve from GRE film density to aerial exposure, and the total noise power in the GRE image. The relationship between the accuracy of the computed criteria and the accuracy of the measured values of the quality parameters is developed in detail in Appendix C. The combined effect of the error in the measurement of each of the quality parameters

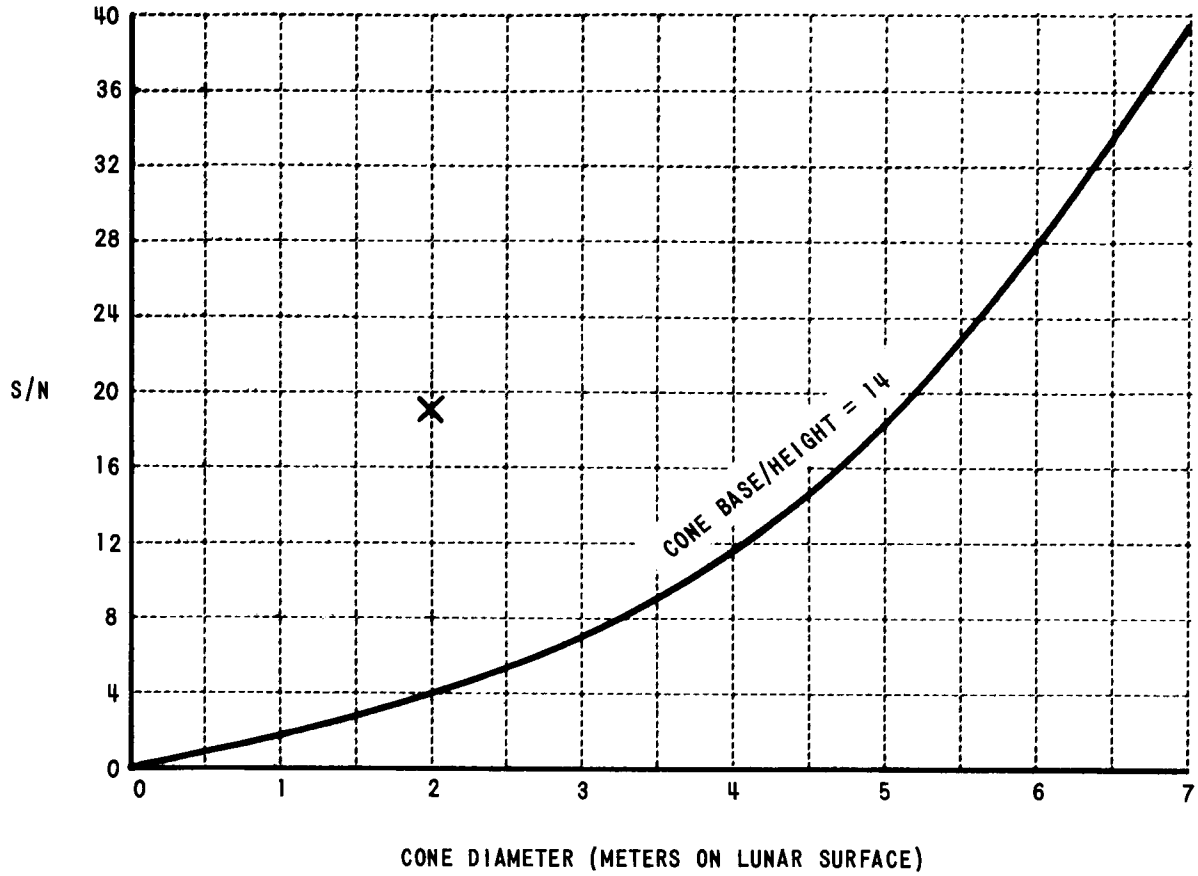

Figure 43 VARIATION OF SIGNAL-TO-NOISE RATIO WITH CONE SIZE (70° PHASE ANGLE)

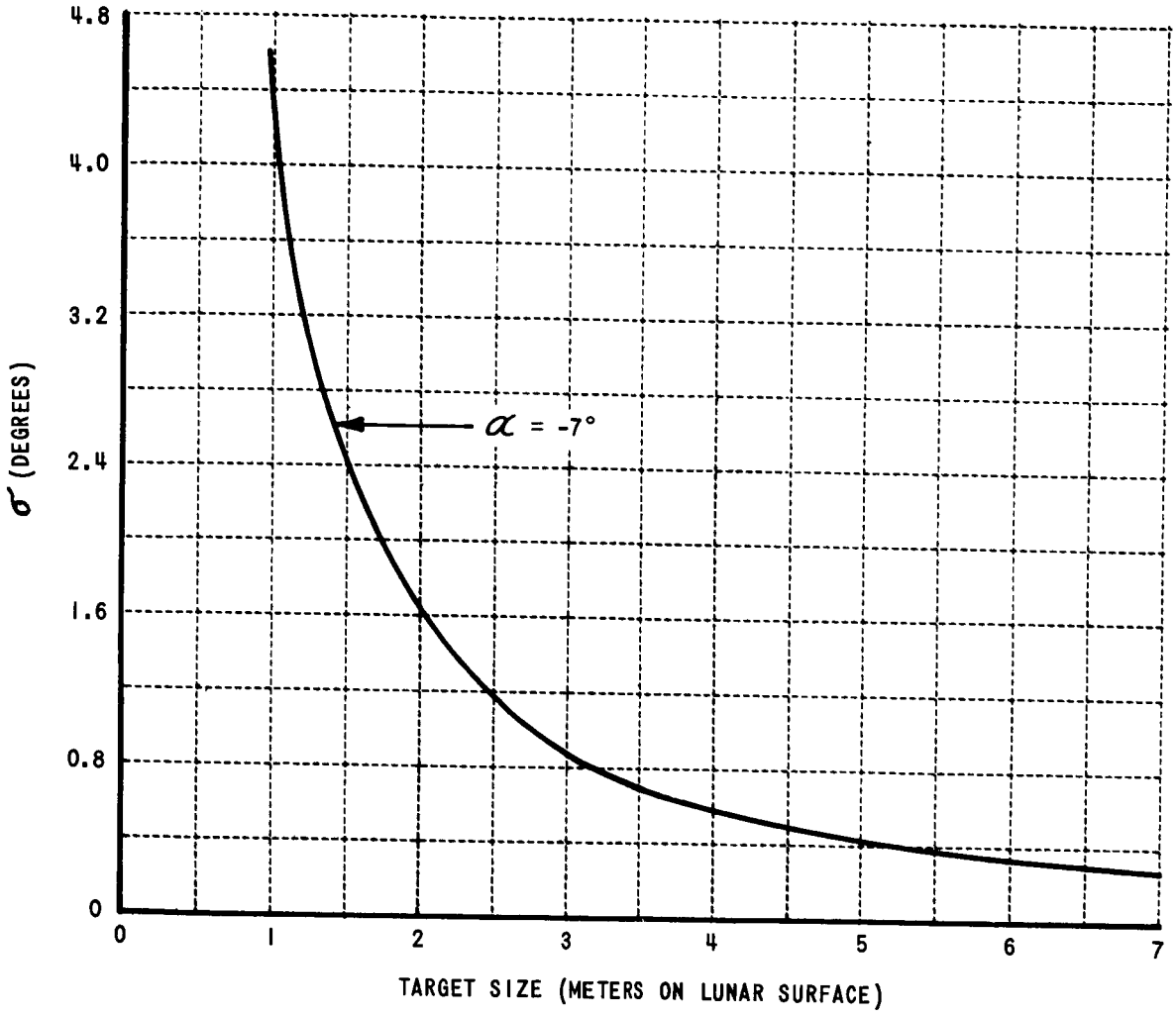

Figure 44 VARIATION OF ERROR IN SLOPE MEASUREMENT WITH TARGET SIZE (70° PHASE ANGLE)

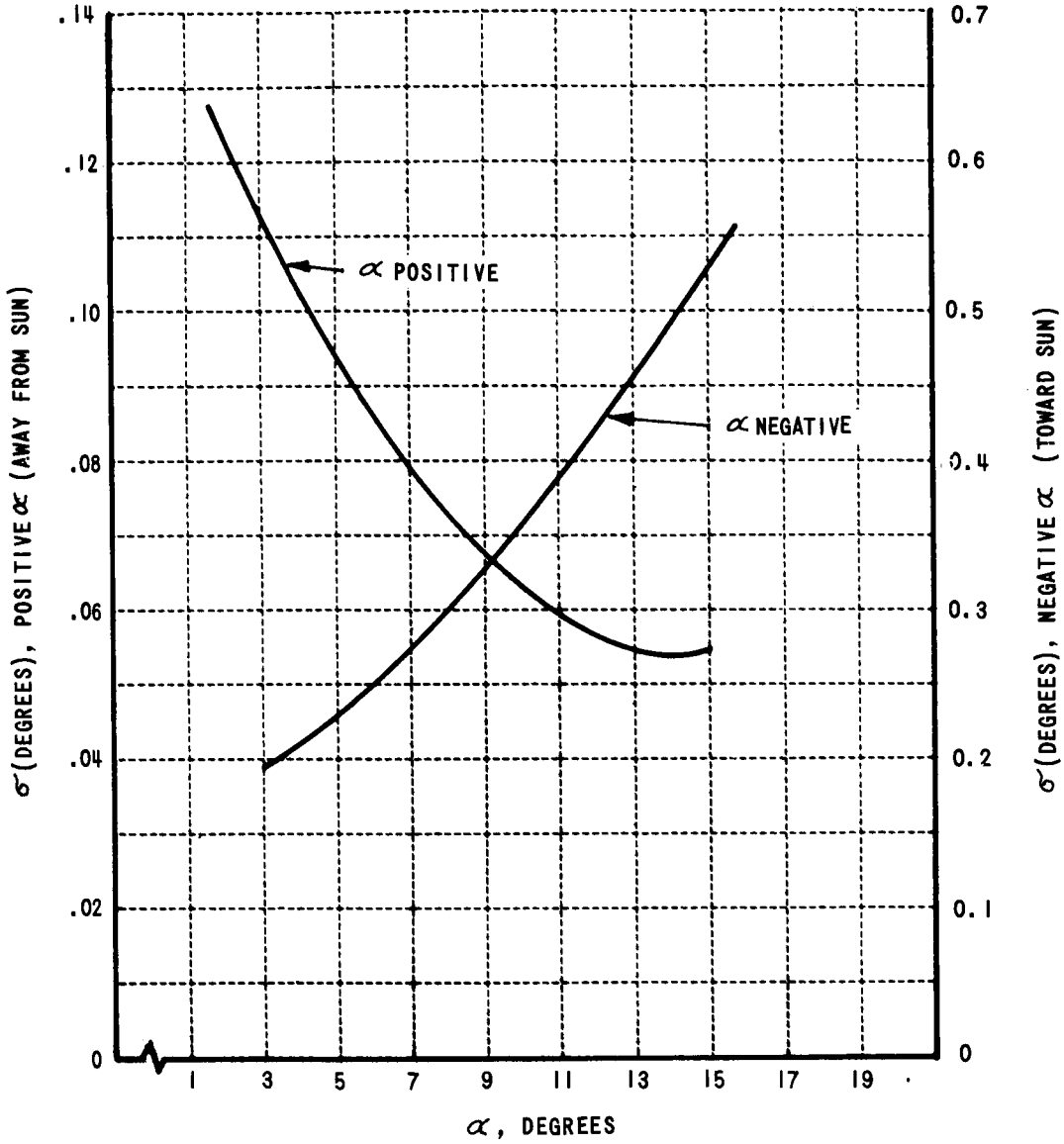

Figure 45 VARIATION OF ERROR IN SLOPE MEASUREMENT WITH α (70° PHASE ANGLE)

imposes a limit in the accuracy attainable in estimating system performance. The resulting fractional error or standard deviation in the calculated value of the signal-to-noise ratio is expressed in Appendix C as

$$\epsilon_{S/N} = \sqrt{\left(\frac{\Delta\tau}{\tau_0}\right)^2 + \frac{\epsilon_{TNP}^2}{4}} \tag{27}$$

where ϵ_{TNP} is the fractional error in the measured value of the total noise power within the signal bandwidth and the ratio $\Delta\tau/\tau_0$ is an upper bound in the fractional error of the measured value of the total system transfer function. From the error analysis presented earlier in this report, an upper bound for the fractional error in the measurement of the transfer function is approximately 4.5% whereas the error in the total noise power measurement may vary anywhere from 4% to 10%. Substituting these values into Eq. (27), it is concluded that the signal-to-noise ratio will be evaluated with an accuracy in the range of 6% to 11%.

The accuracy to which the error in slope measurement can be evaluated is similarly shown in Appendix C to be given by the expression

$$\epsilon_\sigma = \sqrt{\epsilon_\delta^2 + \left(\frac{\Delta\tau}{\tau_0}\right)^2 + \left(\frac{\epsilon_{TNP}}{4}\right)^2} \tag{28}$$

The additional term in this expression, namely, ϵ_δ represents the accuracy to which the rate of change of density on the GRE film can be predicted as a function of the slope angle or brightness longitude. From the data presented in Section 3.4.4 and, in particular, that of Table 7, it is estimated that the slope of the total response curve (i.e., GRE density vs exposure) can be evaluated to an accuracy of about 3% when 10 to 15 step tablets are employed in the evaluation. Substituting into expression (28), it is found that the error in slope measurement can be estimated with an accuracy in the range of 7% to 11%.

4.4 <u>Applicability of the Criteria to Operational Techniques for Extraction of Topographic Data.</u> - The criteria described in the previous sections as a measure of Lunar Orbiter photographic system performance are valid on the basis of their selection relative to the objectives of a Lunar

Orbiter Mission. However, if one wishes to extend their use beyond evaluating system performance to assess the accuracy attainable in extracting topographic data from the reconstructed photographs, the applicability of the criteria must be given additional examination. In this regard, the following points should be considered: (1) How appropriate are the specified topographic models in evaluating operational techniques? (2) How valid is the assumption of optimum performance for extraction?, and (3) Are there any additional errors in photometric calibration not included in the evaluation of the criteria?

The topographic models specified by NASA, that is, the test cones and the inclined square area, were used to design the Lunar Orbiter photographic system and therefore it is natural that they should be used in its evaluation. Small protuberances and depressions in the lunar surface whose magnitude and distribution would influence the suitability of an area for the Apollo program should be detectable in a high resolution photographic frame. The two-meter and seven-meter test design cones are the topographic features specified for evaluating this capability. In rating detectability, this does not appear to be an unreasonable choice for a model. One objection that could be raised to the model is the lack of complexity. In actual lunar photographs, obstructions can be expected to lie on sloped surfaces or in relatively cluttered areas with other obstructions in the near proximity. In contrast, the model assumes that the cone exists on a flat surface and is the only obstruction present in that area of the surface. The lack of complexity of this topographic model should not seriously impair the ability of the criterion of signal-to-noise ratio to describe the detectability of obstructions of equivalent geometrical size in the Lunar Orbiter photographs.

In addition to detecting obstructions, the photographic data is to provide information regarding surface slopes. In this case the voltage or density signal on the ground must be related to the inclination of the surface by use of the photometric function and the signal response of the complete photographic system*. The topographic model specified to evaluate the

* Attention is confined to obtaining topographic data (surface slopes) photometrically from monoscopic photographs as opposed to stereo techniques.

capability of measuring slopes is a uniform square area inclined at a constant angle from the surrounding horizontal area. Whereas the cone target appears to be consistent with the techniques employed in detecting obstructions, the uniform inclined area would not appear to be as representative of the operational techniques used to obtain topographic profiles from the Lunar Orbiter photography. The objection that the model lacks complexity which exists on the lunar surface is more serious in this case. For example, suppose that a square area seven meters on a side is examined in a high resolution photographic frame. It cannot be expected that such an area would have a uniform slope but, in fact, that a reasonable amount of clutter or random variations in slope perturb the average slope across the area. This is in contrast to the model, which assumes that the inclined area is uniform. The fluctuations about the average slope can be regarded to be equivalent to additional noise in the reconstructed image and would cause the estimates of the error in slope measurements to increase appreciably. In addition, most operational techniques for obtaining topographic profiles will not measure the slope over a square area as large as seven meters on a side. This topographic model, therefore, may not be appropriate when evaluating the accuracy to which topographic profiles will be made from the Lunar Orbiter photographs.

In addition to choosing models which are appropriate to the operational techniques used in extracting topographic information, consideration must be given to the extraction procedure. In deriving the performance criteria from the parameters selected to measure the quality of the Lunar Orbiter system, it was assumed that the information available in the photographic image was extracted in an optimum manner. In rating relative system performance, that is, performance according to design specifications, this assumption is reasonable. However, in practical circumstances it may not be possible to define or implement optimum extraction procedures. The fact that most extraction procedures are sub-optimum means that the criteria based upon optimum performance represent the limiting accuracy (possibly unattainable) in the extracted topographic data. For example, in their present form the criteria assume that the modulation transfer function of the photographic system is known and used to an advantage in

the data extraction. In other words, for a given object on the lunar surface the corresponding noiseless image in the GRE film can be predicted. Suppose that an observer looking at the reconstructed photograph is attempting to detect one of the design cones. To simulate the optimum extraction, the observer would have to know the image to be expected from such a target. By searching for an image expected with nominal performance in the system, whereas the true system included a degradation say of two meters of image motion (unknown to him), the signal-to-noise ratio would be less than that obtained with the optimum extraction procedures. In terms of "matched filter theory", the filter employed by the observer is not matched to the expected signal on the GRE film. Such a mismatch causes a deterioration in the output signal-to-noise ratio. In the operational techniques used to detect obstructions on the lunar surface, the observe in fact, will not have any preconceived notion about the expected shape of the obstruction and therefore the detection procedure would be sub-optimum. It should be pointed out that although operational information extraction techniques may be sub-optimum in nature, there should be a strong correlation between the criterion based upon optimum performance and the actual performance attained. For example, the signal-to-noise ratio for detection of the test cones should correlate with psychophysical data of the objects detectable in a Lunar Orbiter photograph.

The system performance criteria were developed assuming that the photometric function and the normal albedo are known quantities since they are not explicitly part of the Lunar Orbiter imaging system. These quantities will, however, play a major role in the extraction of topographic data from the Lunar Orbiter photographs. It is doubtful that the variation in lighting conditions produced by the changes in the photometric function or albedo will greatly influence the detectability of obstructions on the lunar surface as determined by the signal-to-noise ratio. However, an error in the photometric function would introduce additional errors into the slope measurement which are not included in the performance criteria. Similarly, the measurement of the total signal level response of the photographic system was made by averaging over several of the step tablets in the edge data.

Consequently, variations dependent upon position in the photographic format such as the signature of the scanner in the spacecraft and processing variations along the film are not included in the response. Such local variations will influence the topographic profile obtained from the photographs, however. Therefore, to evaluate the accuracy of obtaining topographic profiles from photometric measurements on the Lunar Orbiter imagery, additional system artifacts influencing the photometric calibration must be included in the analysis.

From the discussion presented above, it can be concluded that the values of the criteria will not adequately describe the accuracy of topographic data obtained from the Lunar Orbiter photographs using operational techniques, since it was not intended that the system performance criteria be used in this manner. Additional investigation is required if evaluation of the accuracy to which data can be extracted from the Lunar Orbiter photographs using operational techniques is to be made.

5. THE STUDY OF THE FEASIBILITY OF ADVANCED MEASUREMENT CONCEPTS

This section reports the results of several secondary studies undertaken during the Phase II effort. These studies were primarily concerned with demonstrating the feasibility of applying more sophisticated techniques to measure the quality parameters used in image evaluation. The basic procedure for the evaluation of the quality parameters is to select a target and measure the structure in its image. From the structure, information is extracted which allows the evaluation of the quality parameter. This procedure is complicated by the fact that the measured image structure is modified by random errors introduced by both the imaging system being evaluated and the measurement procedures. The values obtained when measuring the structure of the image at discrete points in the image plane represent space ordered observations of a random process. The problem in evaluating the image quality parameters is to extract the information from this discrete random process in such a way to establish the true value of the quality parameter.

Let us consider the particular problem of evaluation of the modulation transfer function from edge targets. We can imagine the edge trace to be the signal which is perturbed by the transmission channel or information bearing media by introducing a random process or noise (almost always assumed to be addition). A transformation of the observed edge trace is desired so that as much as possible of the undesired noise can be removed producing a better replica of the information bearing signal. This transformation or filter is nothing more than a realization of an estimator applied to the experimental data. Therefore, the process of evaluating the modulation transfer function is an example of the application of estimation theory. To evaluate the transfer function in a given direction, we select and edge perpendicular to that direction and measure the edge spread function. The modulation transfer function is then the Fourier transform of the derivative of the edge spread function. The problem, therefore, is to estimate the edge spread function from the observed edge trace data. This

process can be carried out either manually or automatically using appropriate computational procedures. An elementary situation exists when the frequency band containing the signal and the band containing the noise are mutually exclusive. In this case, simple numerical filtering techniques such as low pass filtering of the observed edge trace data can be used as an automatic estimation procedure. Unfortunately, simple numerical filtering techniques are not very useful in the case of the Lunar Orbiter imaging system because a large portion of the noise is contained in the same band as the signal. Low pass filtering to remove the noise degrades the signal or edge which adversely affects the measurement of the edge spread function and hence the modulation transfer function. The current procedure for evaluating the Lunar Orbiter imaging system uses the manual technique employing an "educated" observer to hand smooth the data. This technique, although reasonably accurate, is rather laborious and an automatic estimation technique is more desirable. In addition, the application of automatic techniques to the evaluation of the edge spread function has the advantage that the residual difference between the observed edge trace data and the estimated edge spread function can be used to provide information about the noise level quality parameter selected to represent the system.

In the process of estimation, one can employ either linear or nonlinear estimators. One technique has appeared in the literature[5] which uses a linear estimator to evaluate the modulation transfer function from the observed edge trace data. The procedure is to expand the transfer function as a Fourier series in which the coefficients of the series are parameters to be estimated. The corresponding edge spread function is also a linear combination of these Fourier series coefficients. In practice, the Fourier series must be truncated at a finite number of terms and by choosing more sampling points than unknowns, one can use the smoothing properties of least squares to estimate the Fourier coefficients from the observed data.

The studies conducted during the Phase II effort were concerned with the feasibility of employing several types of nonlinear estimation techniques to extracting the edge spread function from the observed data (micro-

densitometer edge trace). The techniques considered included the formal application of nonlinear parametric estimation theory and an intuitive approach toward the development of non-parametric filtering processes for extracting the edge spread function from the noisy data.

In the non-parametric approach, the goal is to develop filtering techniques which are similar to the hand smoothing. A brief study was made of several adaptive filtering techniques which are designed to take advantage of the shape of the signal. The knowledge which the observer obtains by first glance at an edge trace includes the approximate location of the edge and the maximum and minimum levels of the edge. A rough knowledge of these characteristics of an edge can be obtained from a very low pass filtered output of the observed data. The first of two variations of adaptive filtering investigated involves a space varying filter. The principles of this technique are illustrated in the sketch in Fig. 46. Using the knowledge about the location of the edge, the width of the filter is adjusted so that it averages over a large interval in the portion of the edge trace data which is generally constant while it follows the observed data more closely by averaging over much smaller intervals across the edge where the observed data contains large changes. The purpose of this "adaptation" is to remove the noise at the beginning and the end of the trace, while retaining the edge gradient (and unfortunately, the noise) near the edge. The primary problem in implementing this technique is the development of a method for appropriately controlling the width of the space varying filter. One possibility is to control the width of the space varying filter by employing the derivative of the low pass filtered trace. The interval employed in filtering the observed edge trace data would be small in the region where the derivative is large and large in the region where the derivative is small.

The second possibility investigated was based upon following the smooth or low passed trace as closely as possible, while not deviating from the observed data by more than the expected noise level. To implement this technique, the difference between the noisy data and the low passed filter trace is required as indicated In Fig. 46. In addition,

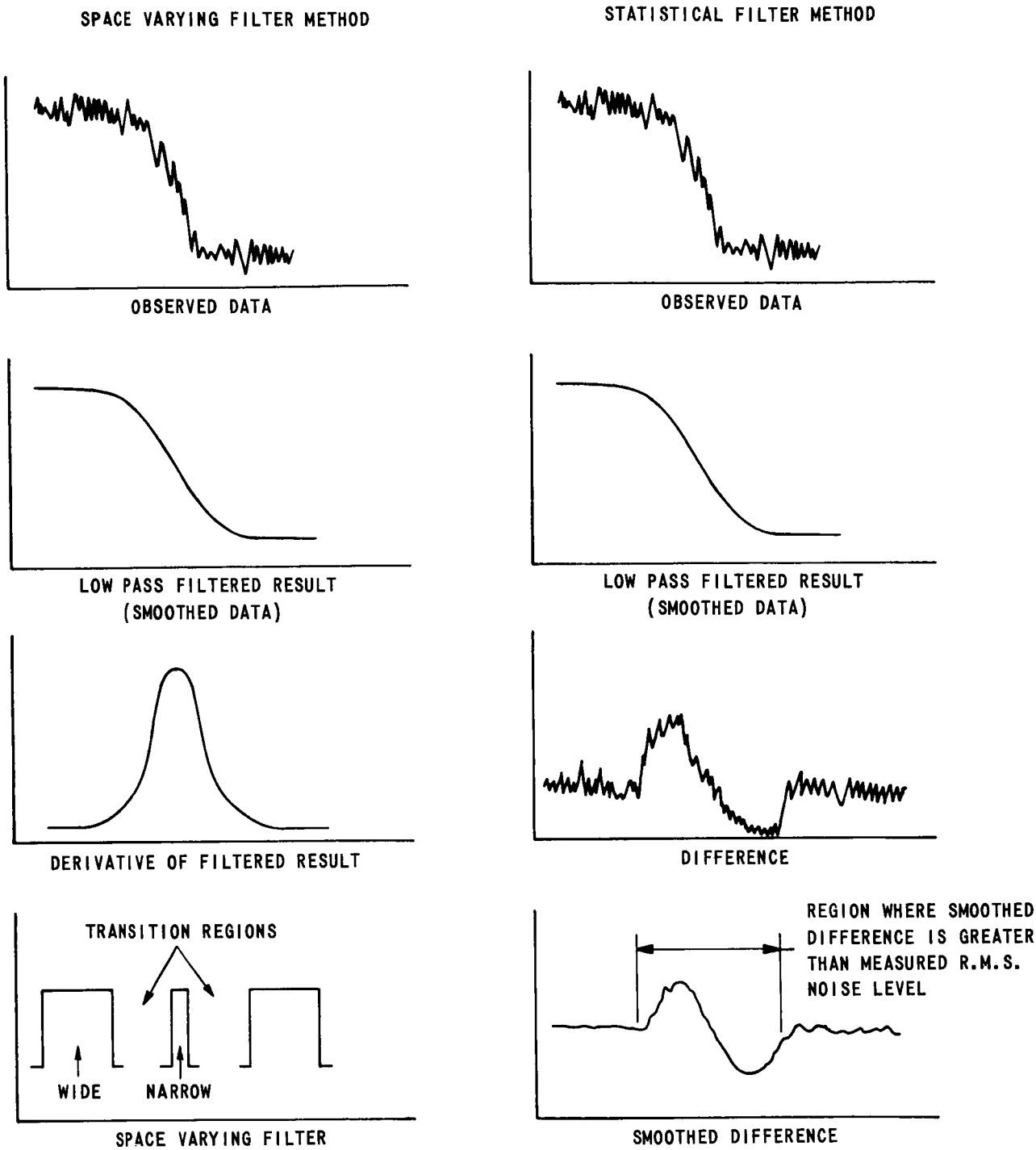

Figure 46 SKETCH ILLUSTRATING ADAPTIVE FILTERING TECHNIQUES

at one end of the trace the rms fluctuation is evaluated to estimate the noise level. The difference between the smooth trace and the original data is then compared to this value of the noise level, and where the difference is small, it is assumed that the difference is noise and the smooth trace is accepted as correct. On the other hand, where the difference becomes large compared to the rms value, the smooth function is assumed to be in error and the difference or some portion of the difference is added back in to yield a better estimate. The amount which is added back in depends upon the size of the difference compared to the measured rms value of the noise level. Because this procedure is somewhat statistical in nature*, this approach is called "the statistical filter method" in contrast to the space varying filter method described previously. The main problem in employing the statistical filter method is to establish a rule for the amount of the observed difference which is to be added back to the low passed filter trace to form the estimate of the edge spread function. Although other non-parametric, nonlinear filtering schemes can be envisioned, attention was confined to these two methods to demonstrate feasibility. Both of these methods were tested by employing simulated edge trace data and found to yield similar results. Fig. 47 shows one of the most promising results obtained by using the space varying filter on a simulated edge of a gray level in the edge data. This same simulated edge was employed previously to evaluate the accuracy of the modulation transfer function measurement techniques discussed in Section 3.4.2. The edge was simulated using nominal values for system performance and non-white noise. The spectrum of the noise added to the edge closely agrees with the one-dimensional analytical spectrum presented in Fig. 14(c) of the Phase I Final Report[1]. Fig. 47 shows the original noisy trace, the estimated edge spread function and the difference between the estimated edge spread function and the true edge spread function. Using this technique, the total noise power in the filtered trace (i.e., estimated edge

---

* By virtue of the fact that one compares the magnitude of the difference signal against the noise level.

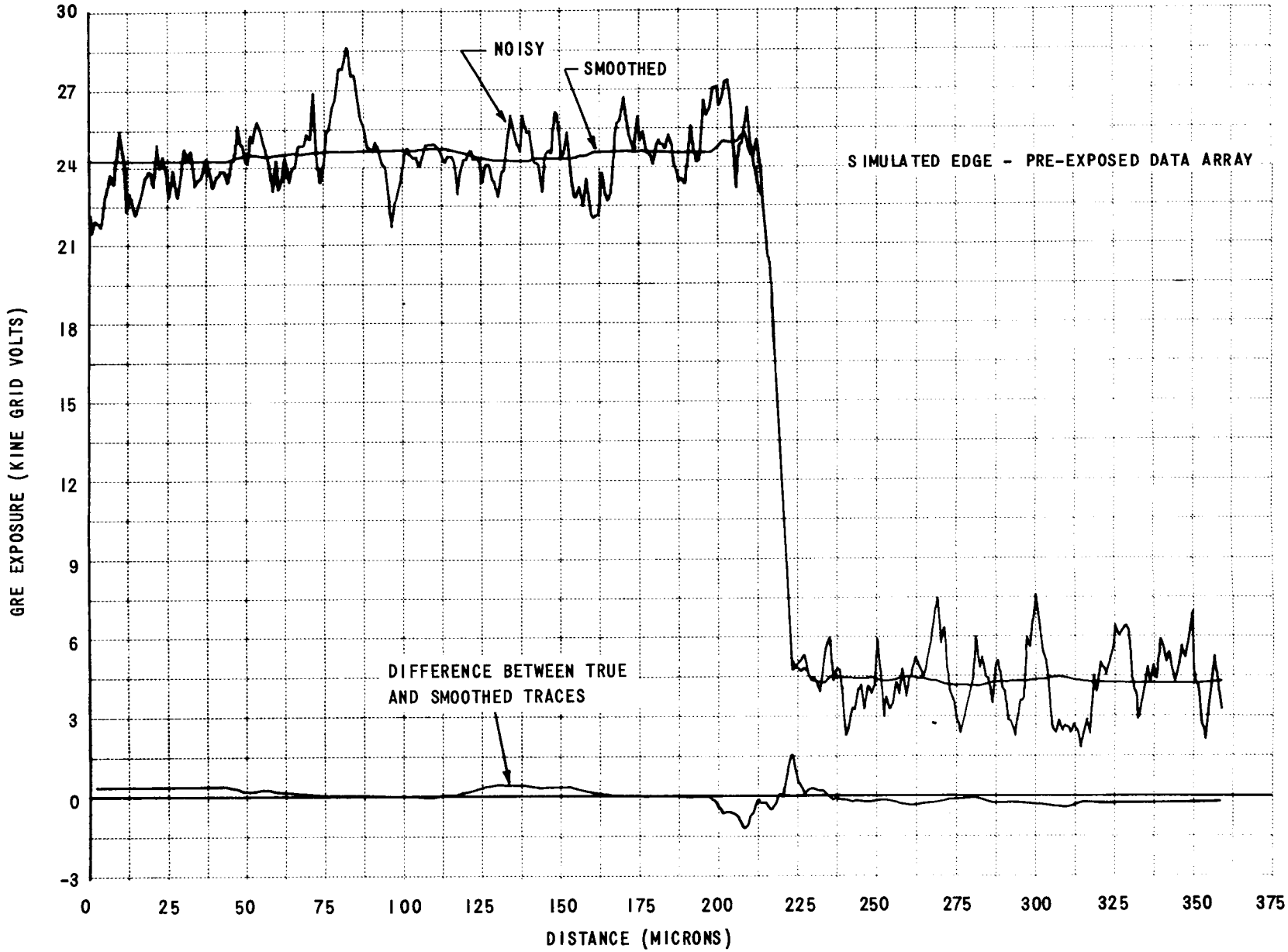

Figure 47 NOISE FILTERING EMPLOYING AN ADAPTIVE FILTER AND A SIMULATED EDGE

spread function) is reduced by a factor of 17 from the noisy data. If this estimated edge spread function is used to measure the scanner-communications-GRS modulation transfer function, the result shown in Fig. 48 is an improvement over the result obtained from manual smoothing by a single observer (also shown in the figure).

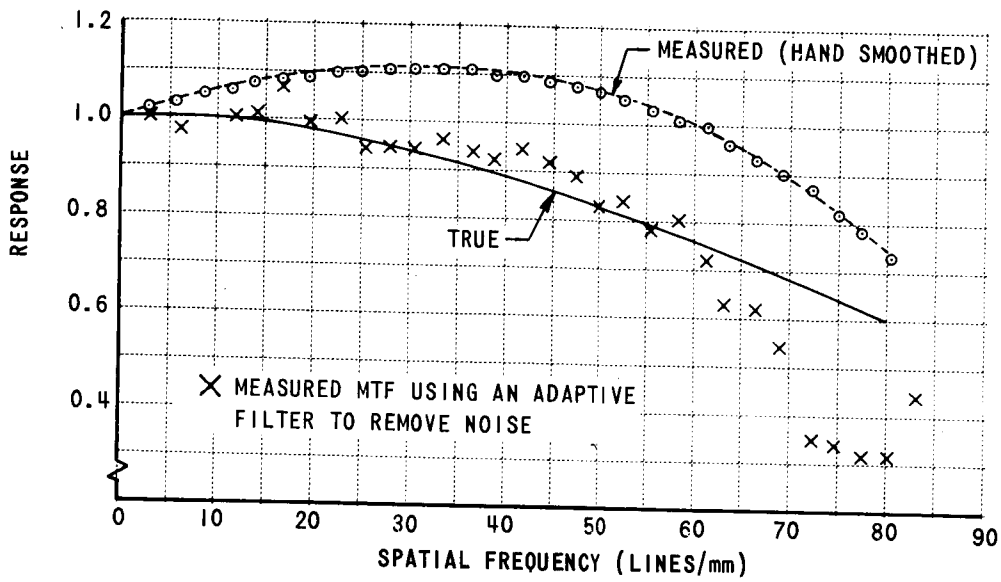

SCANNER-COMMUNICATIONS-GRS MTF

Figure 48 MODULATION TRANSFER FUNCTION MEASUREMENT FROM NOISY SIMULATED MICRODENSITOMETER TRACE USING SPACE VARYING FILTER

The feasibility study also included the formal application of nonlinear parametric estimation theory[4] to the evaluation of the modulation transfer function from edge trace data. Computers have had a considerable impact on the use of nonlinear parametric estimation. As noted in Reference 4, "nonlinear estimation problems, which heretofore had been diligently avoided, are now almost considered routine for numerical evaluation". In the feasibility study, several nonlinear parametric techniques were pro-

grammed for automatic computation. One technique was selected from the general class of gradient methods and another technique was selected from the general class of direct search methods. The former technique is a modified Gauss-Newton method[6]. Gradient techniques generally rely upon the use of a Taylor series expansion of the nonlinear expressions involving the parameters to be estimated. The usual approach is to linearize the mathematical expression by truncating the series after the first derivative assuming that the incremental change in any of the parameters is confined to the local neighborhood about an initial estimate. This procedure lends itself well to an iterative computational scheme in which each new set of parameters represents a better estimate of the true parameter set than the initial parameters employed in that step of iteration. The new parameters are employed as the initial parameters for the next step of the iteration and this process is repeated until a minimum of the loss function is obtained. The most common loss function is the residual sum of squares conventionally employed in the theory of least squares. One of the problems associated with solutions of nonlinear parametric estimation problems is the fact that the set of equations obtained by employing a truncated Taylor series expansion may be ill-conditioned. Such ill-conditioned equations are typified by extreme sensitivity to small changes or small errors in the parameters and frequently this situation produces a lack of convergency of the iterative solution. Several methods exist for reducing the ill-conditioning of the linearized equations and consequently improving the convergence of an interated solution. The modified Gauss-Newton method employed here limits the correction that can be applied at each stage of the iteration process. In this procedure, the magnitude of the correction to the initial set of parameters is regulated in such a way to yield the smallest value of the loss function (the residual sum of squares). Another method for avoiding ill-conditioned equations is to retain higher order terms in the Taylor series expansions at the expense of increased complexity.

The second nonlinear parametric estimation technique whose feasibility was examined employs a direct search method. In contrast to the gradient methods, these techniques do not compute the first or higher order derivatives in order to obtain improved estimates of the parameters. Instead, the parameters are changed by controlled amounts and a new value of the residual sum of squares computed. If the residual sum of squares decreases, the new value is assumed to be a better estimate. The method investigated during this study did not involve any diagonal stepping, that is, all of the parameters except one are held fixed in each iteration and this parameter altered until a minimum sum of squares is found.

In practice, the two major problems in employing these nonlinear parametric estimation procedures are the selection of the appropriate parametric forms and the determination of a set of parameter estimates to use in the initial iteration. It is best to select functions that have the desired flexibility and a minimum number of parameters. As the number of parameters increases, the response surface (that is, the residual sum of squares plotted as a function of the parameters) becomes more complex and usually proliferated with numerous local minima. In this case, it is likely that the iterated solution will correspond to one of these local minima and yield a value for the fitted function (a transfer function in our case) which is not representative of the true value. In order to obtain the solution corresponding to the absolute minimum, the number of local minima must be suppressed or the initial values selected for the parameters must be chosen sufficiently close to the absolute minimum so that the local minima are avoided in the subsequent iterative solution. Therefore, the selection of the initial set of parameters is an important part of the parametric estimation procedure. One method for obtaining initial estimates of the parameters is to employ those equivalent to the nominal or design values for the system being evaluated. Another method is to select a reduced data set equal to the number of parameters from the experimental data and to solve the analytical expressions for the parameters using this reduced data set. The solutions for the parameters are then used as the initial estimates.

Although it is customary to search for an absolute minimum of the loss function, in isolated cases, the values of the parameters corresponding to an absolute minimum of the loss function may not equal the true values of the parameters. This occurred in the analysis which yielded the results presented in Fig. 49. Both of the nonlinear parametric techniques were employed to estimate the scanner-communications-GRS modulation transfer function from the noisy edge trace (Fig. 47). In both techniques, the parametric fit had a tendency to follow the noise in the data and reduce the residual sum of squares to a value below that which would be expected from the known total noise power employed in simulating the edge trace. It should be pointed out that the parametric estimation procedures assumed that the noise was uncorrelated from point to point (equivalent to a white noise spectrum) whereas the noise actually added during simulation did have some correlation between points in order to simulate the spectral shape expected from the Lunar Orbiter system. The "complete" knowledge about the "random process" is not being used in the estimation procedures and may account for these results. In practice, however, this is likely to be the case. The spectrum of the random process would not be known unless extensive measurements are made.

The results shown in Fig. 49 compare favorably to the results presented in the previous figure for the non-parametric, nonlinear estimation techniques.

On the basis of these results, it is felt that additional study of the application of nonlinear estimation techniques to the measurement of the modulation transfer function from edge trace data is certainly warranted. A study should be made to determine the accuracy required in the initial guesses to insure convergence to the true values of the parameters and hence, the true modulation transfer function and to assess the effect of the signal-to-noise ratio (that is, the peak-to-peak signal to the RMS noise) upon the precision of the estimation techniques.

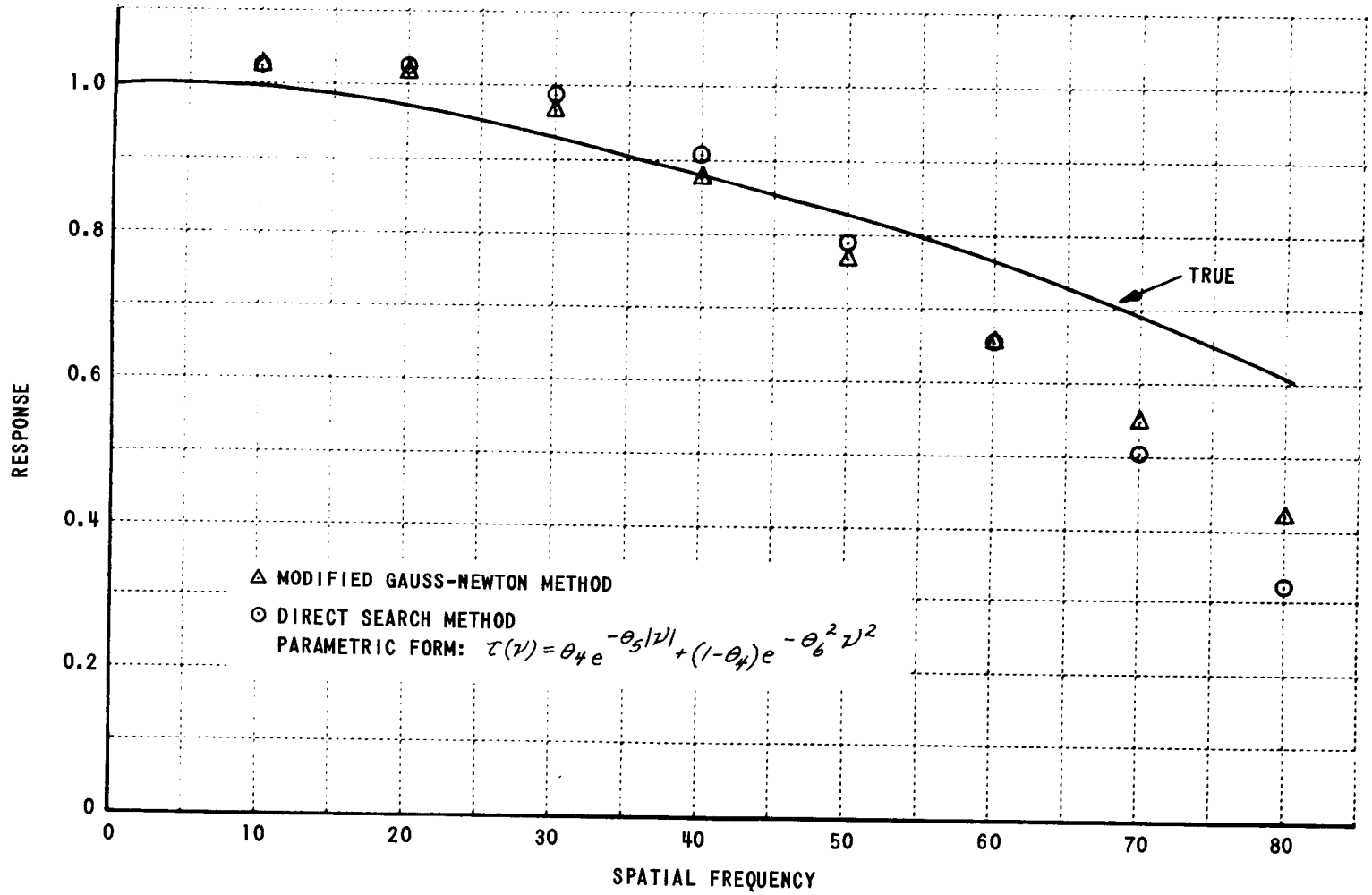

Figure 49 MEASURED MODULATION TRANSFER FUNCTION FROM NOISY SIMULATED MICRODENSITOMETER TRACE USING PARAMETRIC ESTIMATION TECHNIQUES

6. CONCLUSIONS

The implementation and accuracy of a method developed to make quantitiative measurements of those factors which define the quality of the monoscopic photographs to be received from the Lunar Orbiter spacecraft was investigated. These factors, which include the frequency response or modulation transfer function for the complete imaging system, the noise level in the image, and the dc transfer characteristic or system gain, have been related to two system performance criteria which describe the ability of the system to detect and measure topographic features, obstacles and slopes.

The following procedure illustrated in Fig. 50 was established:

(1) Microdensitometer scans are made over selected crater shadow edge images and edges in the pre-exposed data array to evaluate the detail rendition properties of the Lunar Orbiter imaging system. About 25 edges should be selected in each case.

(2) To measure the noise level in the reconstructed image a microdensitometer scan using a small circular aperture 2.5 microns in diameter is made over one of the gray levels in the step tablet of the pre-exposed data array. Since the noise level is signal dependent, the scan is made across the gray level closest to the average density for the photographic frame under analysis. About 7 samples should be employed.

(3) To measure the signal level or the dc transfer characteristics, microdensitometer scans are made over the entire series of controlled gray levels in the pre-exposed data array. Such scans are made in approximately 15 framelets for each frame being analyzed.

(4) From these data, the two-system performance criteria, namely, the error in slope angle or brightness longitude measurement and the signal-to-noise ratio for detection of obstacles are evaluated for the lighting conditions of the particular photograph frame under analysis.

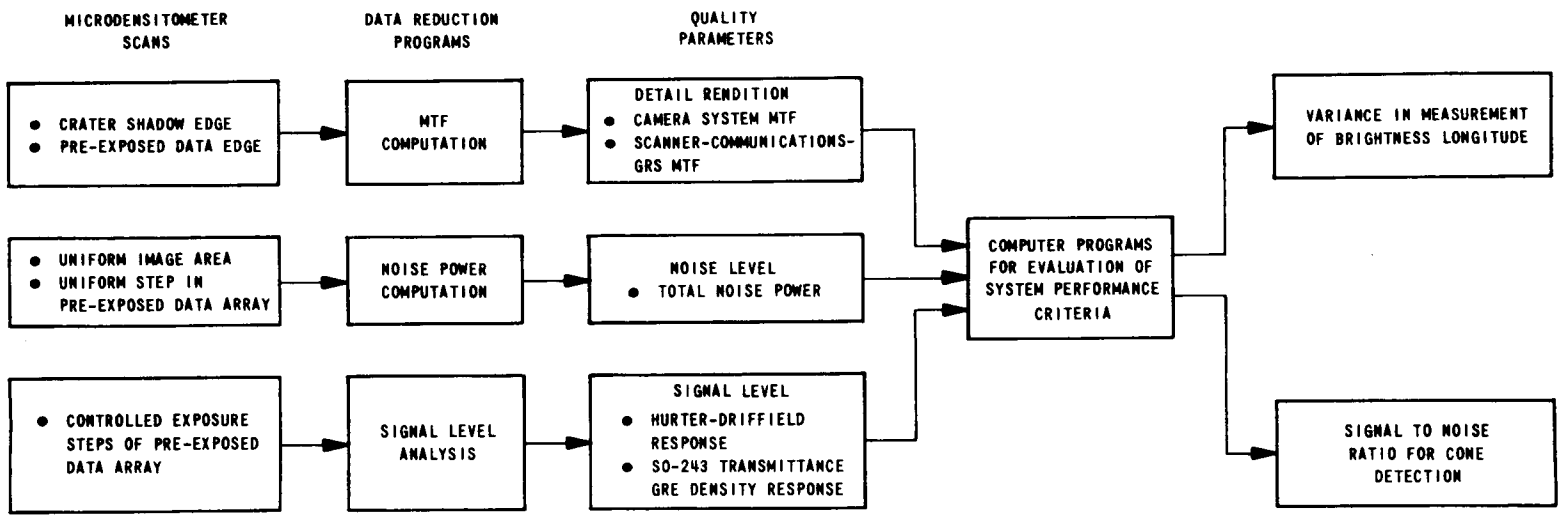

Figure 50 LUNAR ORBITER PHOTOGRAPHIC QUALITY EVALUATION FLOW DIAGRAM

As a result of the study of the accuracy of the established measurement techniques, it was found that the technique for measuring the noise level quality parameter was the least accurate and, consequently was the limiting factor in establishing system performance. Using the established techniques both of the system performance criteria will be evaluated with an accuracy in the range of 6 to 11%, depending upon the noise level in the reconstructed image. The larger the noise level the more accurately the performance criteria can be evaluated.

The feasibility study for employing nonlinear estimation techniques to measure the transfer function from microdensitometer traces across initially sharp edges in the object scene provided encouraging results and indicate that this study should be pursued further to advance the state of the art of edge trace analysis techniques for evaluating the spatial frequency response of imaging systems.

APPENDIX A

STUDY OF THE EFFECTS OF THE COMBINED GRE NONLINEARITIES

Two nonlinear response relationships are employed in the Ground Reconstruction System. The kinescope spot brightness is a nonlinear function of the received or "input" voltage signal and the Hurter-Driffield response curve of the reconstruction film (exposure or brightness versus density) is nonlinear. The voltage-to-brightness relationship is so chosen that the combined effect of the nonlinearities (which process the signal in tandem) yields a linear relationship between the input voltage and the reconstructed density for a dc input signal. Because of the spread of the reconstructing spot, the exposure is integrated from two different signals in the region where adjacent scan lines overlap. The average of the density signal recorded on the GRE film is not equivalent to the density that would arise if the system were linear. The extent to which this lack of linearity produced by the spread of the scan spot affects the results of the established data analysis techniques was investigated and is reported in this appendix.

The study was made by simulating the density signal on the GRE film normal to the scan lines. The scan line structure was included in the simulation by assuming that the GRE kinescope spot was gaussian in shape, namely

$$E(x) = \begin{cases} E_0 \, e^{-8(x/\omega)^2} & |x| < 3d/2 \\ 0 & \text{otherwise} \end{cases} \qquad \text{(A-1)}$$

where x is the distance relative to the spacecraft film, ω is the "width" of the scan spot, d is the scan line separation, and E_0 is the maximum exposure at the peak of the scan spot. Several widths between 3.7 μ and 6.6 μ at the spacecraft film scale were chosen for the study and the spacing between scan lines was fixed at 3.3 μ so that the larger widths correspond to greater overlap of scan line structure. For these values the truncation of the gaussian spot indicated in Eq. (A-1) occurs at a point where the response is less than 1% of the peak response.

An array of exposure values equal to the peak response at successive scan lines was used as the input to a special purpose computer program written to synthesize density signals on the reconstructed film in the direction orthogonal to the scan line structure. For each input object two output signals or density traces are determined. One trace represents the actual output generated by the GRE. In this case, the exposure is integrated at each point of the trace and converted to density by employing the nominal Hurter-Driffield response curve for the reconstructing film. The second trace generated by the program represents the output of a linear system. The individual exposures at a point in the trace are converted to density and added to yield the density trace. Compensation of the dc level is made to account for the base fog of the reconstructing film. This simulation program was used to evaluate the effects of the combined nonlinearities upon the signal level and detail rendition quality parameter measurement techniques. The input test object for the latter evaluation was an edge whose derivative in exposure was gaussian in shape. The simulated traces from two of the five cases are presented in Figs. A-1 and A-2. Unfortunately, the energy contained in the scan spot given by Eq. (A-1) is not constant, so the larger spot widths have a greater amount of energy producing slightly greater density values in the simulated output. The scan line structure is removed from each trace by using the digital filtering techniques described in the main text (Section 3. 3. 1). The corresponding "smoothed" traces are also shown in the figures. The smooth traces are differentiated and Fourier transformed to determine the modulation transfer function in a manner identical to that which yielded the scanner-communications-GRS modulation transfer function. The results for the smoothed traces shown previously are given in Figs. A-3 and A-4. Although the combined nonlinearities tend to produce sharper edge images, this difference between the actual GRE system performance and a truly linear system can be seen to be small. The results are summarized by showing the difference in response as a function of spatial frequency for all the spot sizes studied in Fig. A-5. In the evaluation of the scanner-communications-GRS modulation transfer function such differences would be further magnified by the correction for the

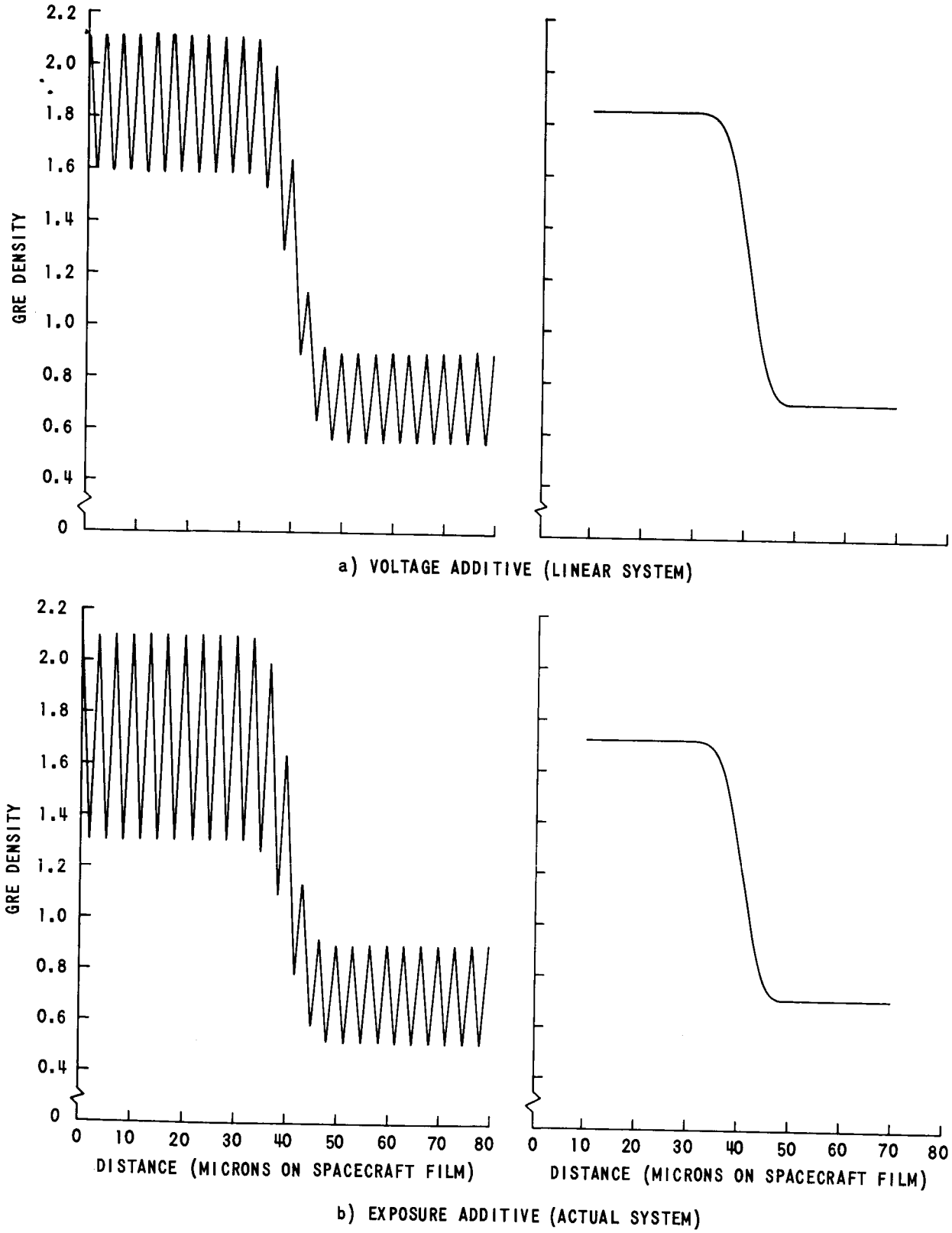

Figure A-1 SIMULATED DENSITY TRACES WITH AND WITHOUT SCAN LINES FOR A 3.7 MICRON GRE SCAN SPOT

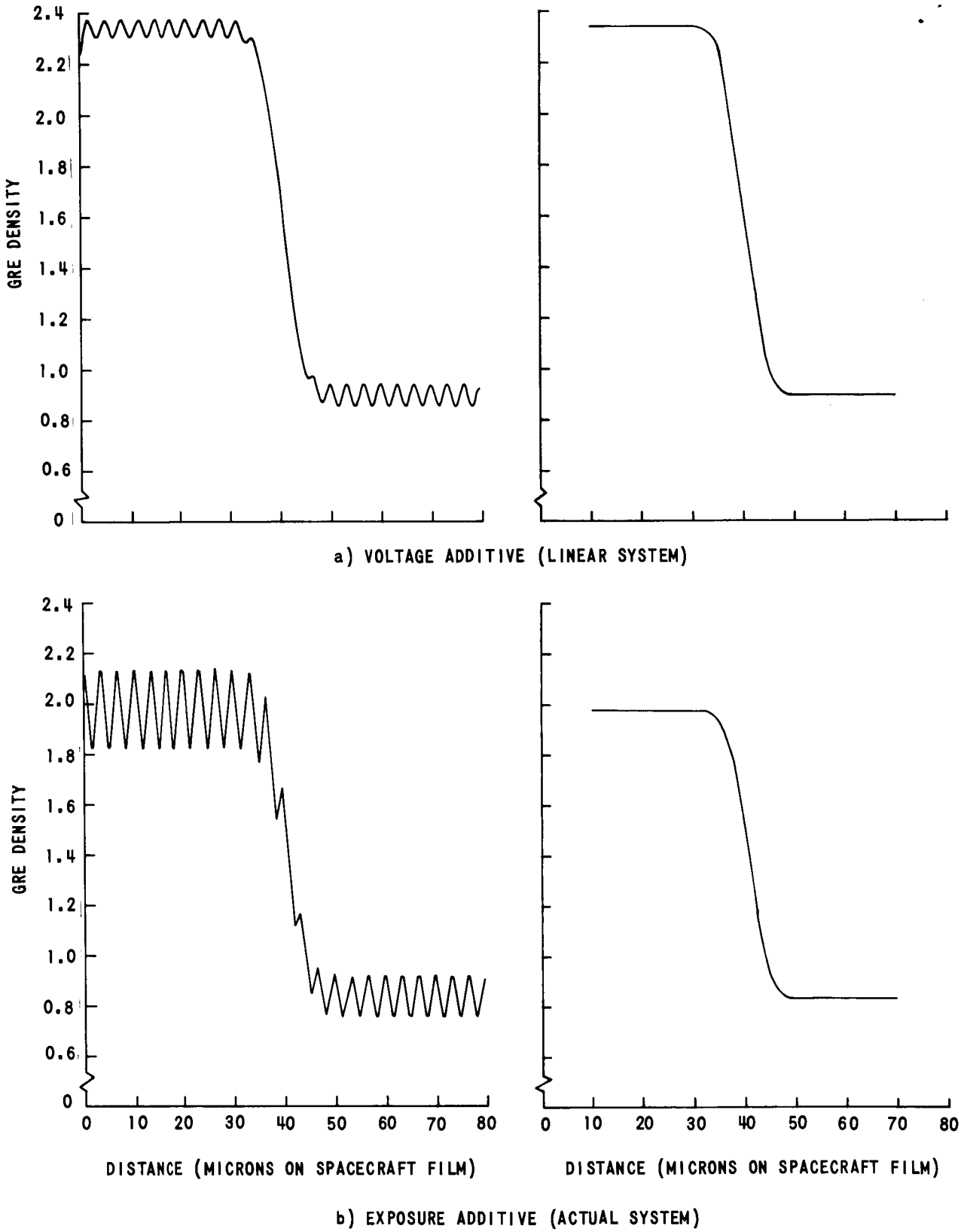

Figure A-2 SIMULATED DENSITY TRACES WITH AND WITHOUT SCAN LINES FOR A 4.7 MICRON GRE SCAN SPOT

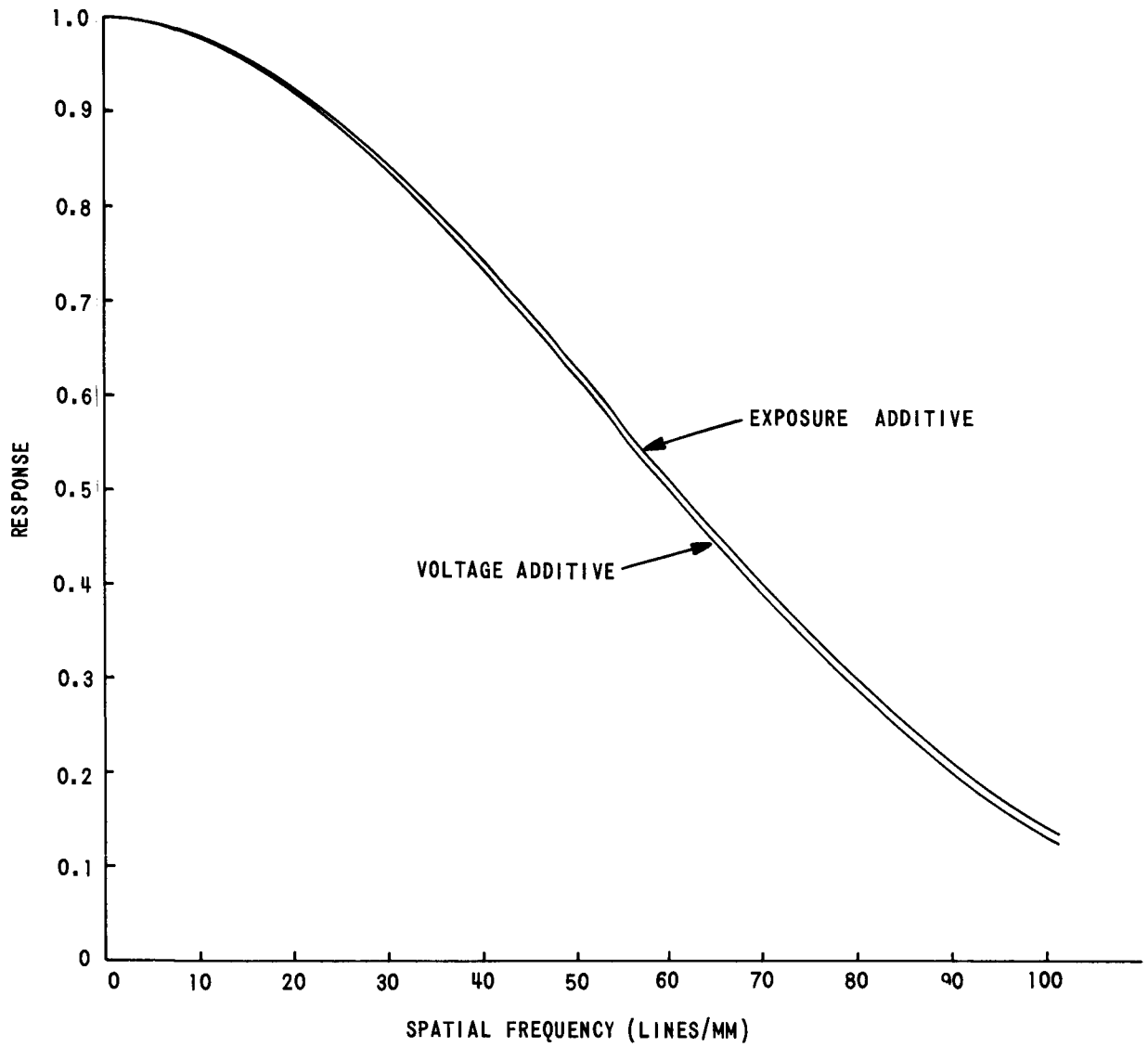

Figure A-3 RESULTING MTF FROM DENSITY TRACES OBTAINED USING A 3.7 MICRON GRE SCAN SPOT

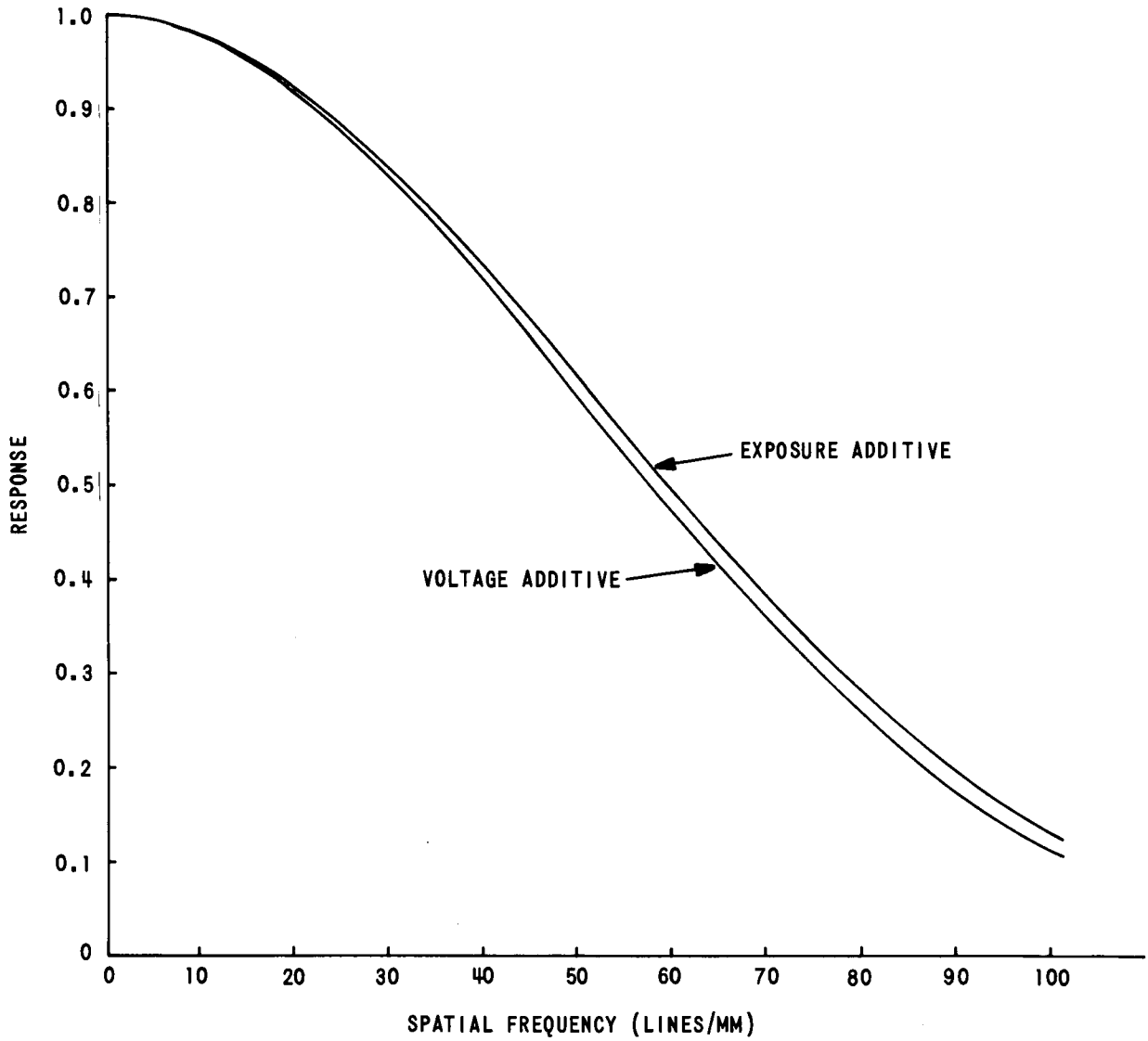

Figure A-4 RESULTING MTF FROM DENSITY TRACES OBTAINED USING A 4.7 MICRON GRE SCAN SPOT

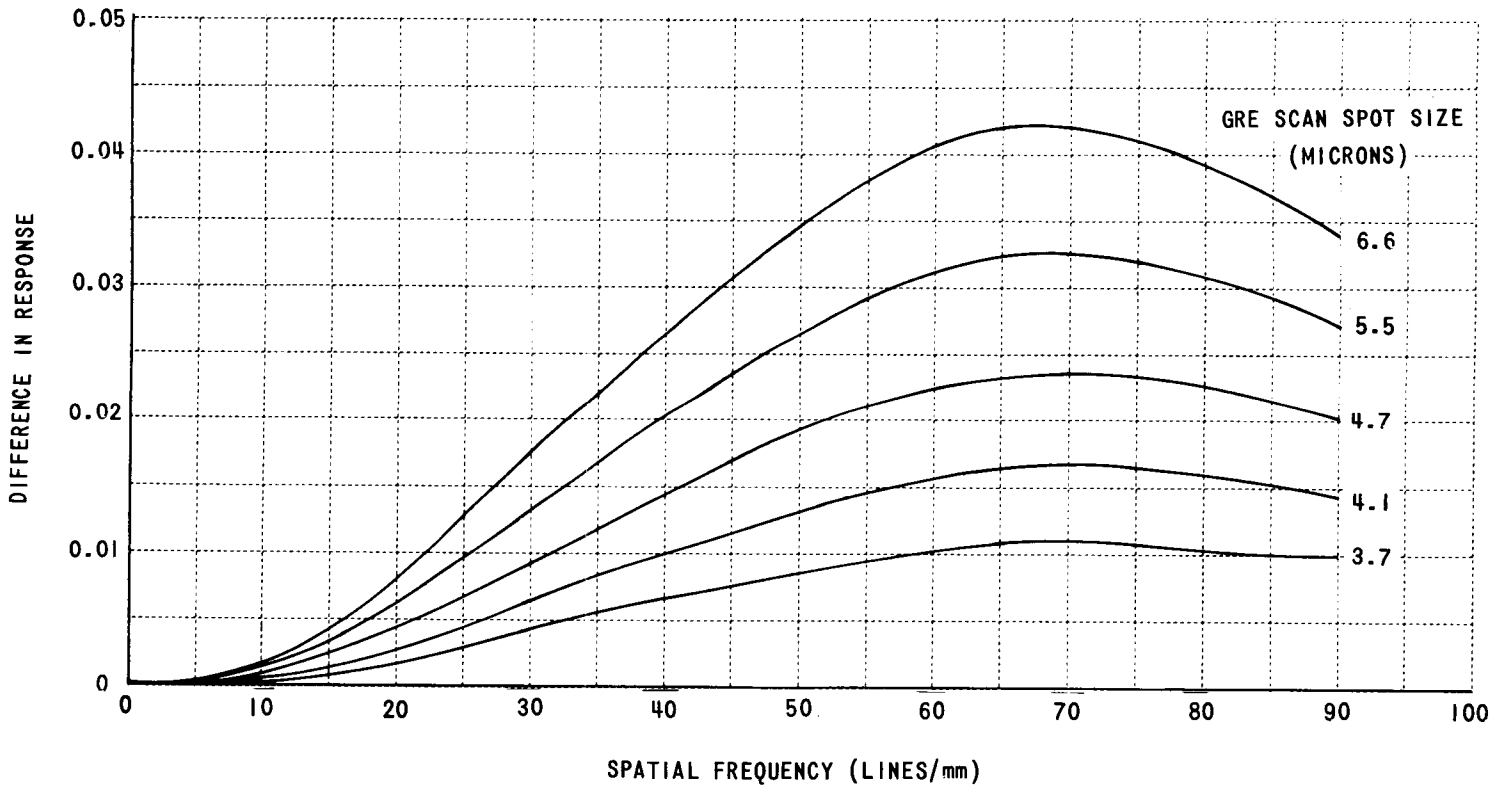

Figure A-5 DIFFERENCE BETWEEN THE ACTUAL (MEASURED) MTF AND THE MTF FOR A LINEAR SYSTEM

finite sharpness of the original edge. Nevertheless, these differences would still be small compared to the accuracy of the measurement techniques and it is concluded that the combined effect of the nonlinearities may be ignored.

To investigate the influence of the nonlinearities upon the signal level measurements, an input test object containing several different exposure levels was employed. The densities of each level for the actual system were plotted against the corresponding values for the linear system and are shown in Fig. A-6. Although the individual responses of the nonlinearities are matched, the integration of exposure by the reconstructing film will introduce a slight deviation which increases with density and scan spot size. At densities below 2.0, the region expected for the reconstructed Lunar Orbiter imagery, the effects are small.

On the basis of this study, it is concluded that the nonlinear effects in the GRE will introduce small perturbations in the observed data which may be neglected and that for purposes of evaluating the performance of the complete Lunar Orbiter imaging system, the reconstruction system may be considered to be a linear element.

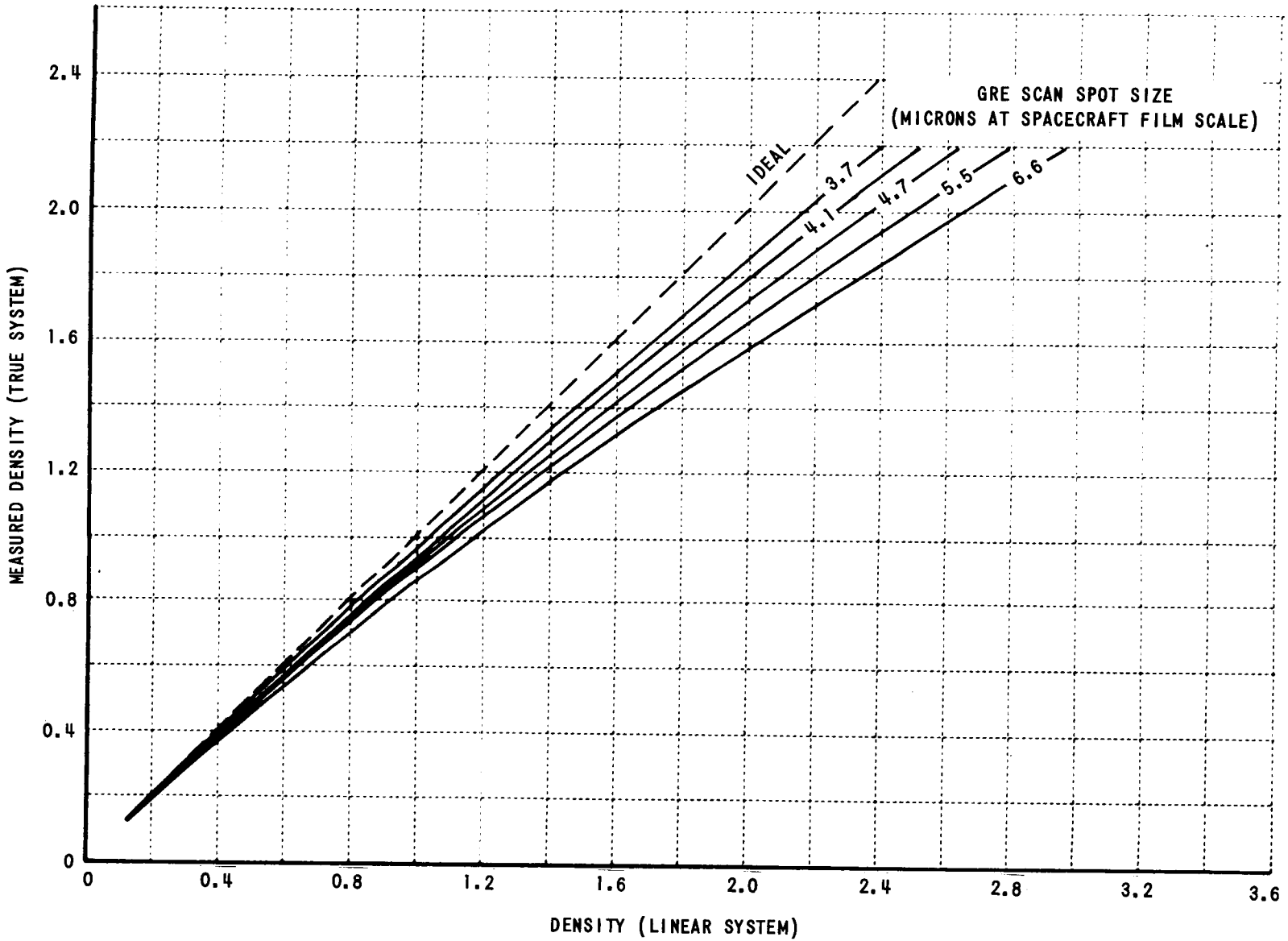

Figure A-6 EFFECT OF GRE NONLINEARITY UPON MEASURED DENSITIES OF UNIFORM GRAY LEVELS

APPENDIX B

MATHEMATICAL MODEL OF THE EXPECTED INTENSITY FUNCTION INSIDE A CRATER LOCATED AT AN OFF-NADIR POSITION

This appendix contains the development of the mathematical formulas to evaluate the intensity distribution inside a spherical crater. In an appendix of a previous report[1] the mathematical model of the expected intensity function was derived for a crater located at or near the nadir. These expressions are generalized here to a crater located some distance away from the nadir in the reconstructed image. This will be accomplished if the brightness longitude is expressed in terms of the relative positions of the sun, the surface normal and the spacecraft. To this end we take the model of the crater to be a sphere of radius, a , surrounded by a level plane which cuts out a sector of the sphere that has a diameter, D , and a depth d . In the local coordinate system (see Figure B-1) with the origin

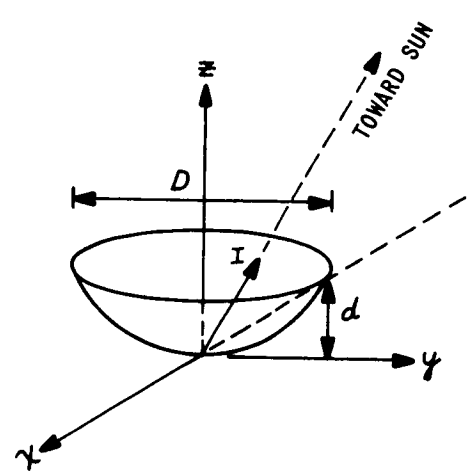

Figure B-1 MODEL AND COORDINATE GEOMETRY

at the center of the crater it is assumed that the sunlight is incident in the xz plane with the $+z$ axis being the local zenith. Three vectors are defined:

$\hat{I}$ a unit vector toward the sun,

$\hat{E}$ a unit vector in the emission direction; that is along the line connecting the origin and the spacecraft, and

$\hat{N}$ the normal to the crater surface.

If we define the following angles relative to the local coordinate system*,

γ - zenith angle of surface normal,

ϕ - azimuth angle of surface normal,

γ_s - zenith angle of sun,

γ_c - zenith angle of camera, and

ϕ_c - azimuth angle of camera,

the vectors $\hat{I}$, $\hat{E}$ and $\hat{N}$ can be written as

$$\hat{I} = -\sin\gamma_s\,\hat{i} + \cos\gamma_s\,\hat{k}$$

$$\hat{E} = \cos\phi_c \sin\gamma_c\,\hat{i} + \sin\phi_c \sin\gamma_c\,\hat{j} + \cos\gamma_c\,\hat{k} \quad \text{and} \qquad \text{(B-1)}$$

$$\hat{N} = \cos\phi \sin\gamma\,\hat{i} + \sin\phi \sin\gamma\,\hat{j} + \cos\gamma\,\hat{k}$$

To determine α, the brightness longitude, it is convenient to define a coordinate system in which $\hat{E}$ and the normals to sun-spacecraft plane constitute axes. Consequently, we define a new local coordinate system $x'y'z'$ in which the z' axis is in the direction of the emission vector $\hat{E}$ and the $x'z'$ plane is the phase plane, that is, contains the vectors $\hat{E}$ and $\hat{I}$. The unit vectors defining the new coordinate system in terms of the original coordinate system are

---

* The various zenith and azimuthal angles are defined in the standard fashion of a spherical coordinate system with respect to an xyz coordinate system.

$$\hat{Z}' = \hat{E} = \lambda_3 \hat{i} + \mu_3 \hat{j} + \nu_3 \hat{k}$$

$$\hat{Y}' = \hat{I} \times \hat{E} / \sin g = \lambda_2 \hat{i} + \mu_2 \hat{j} + \nu_2 \hat{k} \quad \text{and}$$

$$\hat{X}' = \hat{Y}' \times \hat{Z}' = \lambda_1 \hat{i} + \mu_1 \hat{j} + \nu_1 \hat{k} \qquad \text{(B-2)}$$

where g is the phase angle (angle between $\hat{I}$ and $\hat{E}$) and (λ_i, μ_i, ν_i) are direction cosines which can be obtained by employing the expressions in (B-1). The components of the normal vector in the new coordinate system are found by taking the dot product of $\hat{N}$ with $\hat{X}'$, $\hat{Y}'$ and $\hat{Z}'$; namely

$$\begin{aligned} \hat{N}_{X'} &= \hat{N} \cdot \hat{X}' \\ \hat{N}_{Y'} &= \hat{N} \cdot \hat{Y}' \\ \hat{N}_{Z'} &= \hat{N} \cdot \hat{Z}' \end{aligned} \qquad \text{(B-3)}$$

We denote the projection of the normal into the phase plane ($x'z'$ plane) by $\vec{N}_p$ (see Figure B-2), and the angle between $\hat{Z}'$ and this vector is α , the brightness longitude, which appears in the photometric function.

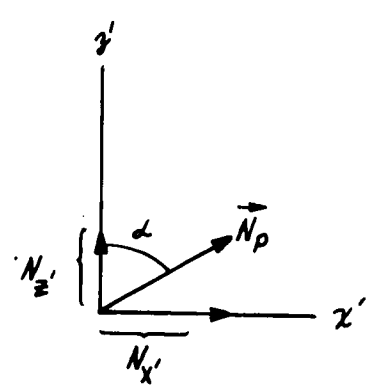

Figure B-2 GEOMETRY FOR THE LOCAL NORMAL PROJECT INTO PHASE PLANE

From the figure it is easily seen that

$$\alpha = \tan^{-1} \frac{N_{x'}}{N_{z'}} = \tan^{-1} \left\{ \frac{\hat{N} \cdot \hat{x}'}{\hat{N} \cdot \hat{z}'} \right\} \tag{B-4}$$

From Eq. (B-2) we may write

$$\alpha = \tan^{-1} \left\{ \frac{\lambda_1 \cos\phi \sin\gamma + \mu_1 \sin\phi \sin\gamma + \nu_1 \cos\gamma}{\lambda_3 \cos\phi \sin\gamma + \mu_3 \sin\phi \sin\gamma + \nu_3 \cos\gamma} \right\} \tag{B-5}$$

As a simple example assume that the camera is overhead so that the center of the crater is at nadir. The camera zenith angle, γ_c , is zero. In addition, if the surface normal is in the sun plane and toward the sun, so that

$$\phi = \pi$$

then the value of the brightness longitude should be negative if the formulation is correct. With these assumptions the direction cosines $(\lambda_i , \mu_i , \nu_i)$ become:

$$\lambda_1 = \sin\gamma_s / \sin g , \quad \mu_1 = 0 , \quad \nu_1 = 0$$

$$\lambda_2 = 0 , \quad \mu_2 = \sin\gamma_s / \sin g , \quad \nu_2 = 0$$

$$\lambda_3 = 0 , \quad \mu_3 = 0 , \quad \nu_3 = 1$$

Substituting these values into Eq. (B-5) yields

$$\alpha = \tan^{-1} \left\{ \frac{\sin\gamma_s \cos\phi \tan\gamma}{\sin g} \right\}$$

Since both zenith angles γ and γ_s are in the interval $[0, \pi/2]$ and the phase angle g for this case is in the interval $[0, \pi/2]$ all the terms are non-negative except for $\cos\phi$ which has a value of -1 since $\phi = \pi$. Therefore the tangent of α is negative and α is negative as desired.

To determine the brightness longitude at a particular point inside a crater the five angles γ , ϕ , γ_s , γ_c and ϕ_c must be evaluated. They are determined as follows:

(1) γ_s , γ_c and ϕ_c are assumed constant within the crater. This is reasonable. In particular, we can determine ϕ_c with sufficient accuracy by direct measurement on the reconstructed photo frame. It is the angle between a vector in the sun plane from the shadow toward the sunlight portion of the crater and the line from the crater to the nadir measured positive counterclockwise. In addition, if the distance between the nadir (point N in Fig. B-3) and the crater (point C), denoted by d_N , is measured from the reconstructed photograph the value of the camera zenith angle determined from the geometry shown in Fig. B-3 is

$$\gamma_c = \theta_1 + \theta_2 = \frac{d_N}{R_s - h} + \tan^{-1} \frac{d_n}{h} \qquad \text{(B-6)}$$

The values of R_s , the radius of the spacecraft and h , the altitude, are provided as part of the "Photographic Support Data" for the mission. This source also provides the value of γ_s the solar zenith angle directly under the heading "sun angle at nadir".

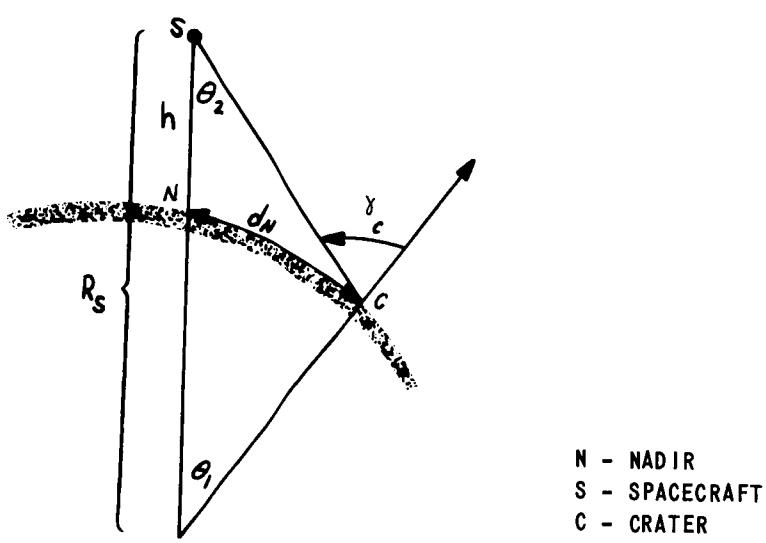

Figure B-3 GEOMETRY FOR EVALUATING THE CAMERA ZENITH ANGLE

(2) ϕ is usually taken to be 0 or π since, in most cases, traces will be obtained in the sun plane (that is along the x axis in Fig. B-1).

(3) γ is determined from the crater geometry. It is easily shown that the zenith angle of the normal is given by

$$\gamma(x, y) = \tan^{-1}\left\{\sqrt{\frac{x^2+y^2}{a^2-x^2-y^2}}\right\} \tag{B-7}$$

where a is the radius of curvature of the crater. We have shown previously (Appendix B of reference 1) that the radius of curvature can be calculated by knowing γ_s, the shadow length and the crater diameter. The latter two quantities are easily measured on the reconstructed imagery.

This determines α, the brightness longitude, as desired. There are additional quantities which can be easily obtained and are of value, such as, the phase angle, the angle between the sun plane and the phase plane, and the brightness longitude for a flat surface at the crater position. The phase angle, g, is defined to be the angle between the incident and emission direction, namely

$$\cos g = \hat{I} \cdot \hat{E} \quad .$$

Employing Eq. (B-1) we find that the phase angle can be expressed in terms of γ_s, γ_c and ϕ_c as

$$\cos g = \cos\gamma_s \cos\gamma_c - \sin\gamma_s \sin\gamma_c \cos\phi_c \tag{B-8}$$

The angle between the phase plane and the sun plane as projected on the lunar surface is of interest because the edge traces are made in the sun plane and analyzed assuming a constant phase angle. This is a reasonable assumption if the angle between the intersection of the planes on the lunar surface is small. Denoting this angle by β we may evaluate the $\cos\beta$ by taking the dot product between the projection of the unit normal to the phase plane, $\hat{\gamma}'$, into the xy plane (lunar surface) and the normal to the sun plane. If $\hat{\gamma}'_p$ is the projection of $\hat{\gamma}'$ onto the xy plane

we have

$$\vec{Y}_p' \cdot \hat{j} = |\vec{Y}_p'| \cos\beta \quad .$$

Now from Eq. (B-2) we find that

$$\vec{Y}_p' = \lambda_z \hat{i} + \mu_z \hat{j}$$

and substituting that

$$\cos\beta = \frac{\mu_z}{\sqrt{\lambda_z^2 + \mu_z^2}}$$

It is more convenient to compute $\tan\beta$ which can be expressed as

$$\tan\beta = \frac{\lambda_z}{\mu_z} = \frac{-\sin\phi_c \sin\gamma_c \cos\gamma_s}{\cos\gamma_c \sin\gamma_s + \cos\phi_c \sin\gamma_c \cos\gamma_s} \qquad \text{(B-9)}$$

The brightness longitude, α_o , for a flat surface located near the crater or equivalently at the center of the crater is determined by letting $\gamma = 0$ in Eq. (B-5). This process yields

$$\alpha_o = \tan^{-1}\frac{\gamma_1}{\gamma_3} = \tan^{-1}\left\{-\frac{\tan\gamma_c}{\sin g}\left[\sin\gamma_c \cos\gamma_s + \cos\gamma_c \sin\gamma_s \cos\phi_c\right]\right\} \qquad \text{(B-10)}$$

To summarize, the following quantities must be measured from the reconstructed photograph for each crater traced in order to reduce the edge trace data: (1) shadow length, (2) crater diameter, (3) distance between the crater and the nadir, and (4) the azimuth angle between the sun plane through center of the crater and the nadir. Additional data such as the spacecraft radius, spacecraft altitude, and the solar zenith angle are obtained from the "Photographic Support Data". All of this information is used as input to the camera modulation transfer function evaluation program.

APPENDIX C

DERIVATION OF SYSTEM PERFORMANCE CRITERIA

A set of indices which specify how well the imaging system performed with respect to Lunar Orbiter objectives, referred to as system performance criteria, are derived in this appendix. The criteria are based upon the objective of establishing the general roughness of the lunar surface in support of the Apollo Program. Two criteria specified by NASA to assess how well this objective is met are: (1) a signal-to-noise ratio for the detection of a right circular cone, with a vertical axis, and protruding from or recessed into a horizontal surface; and (2) the variance in the estimate of the slope of a uniform area 7 meters square inclined toward or away from the sun (see Fig. 33 of the main text). A similar set of criteria were described in the Phase I Report[1] and part of the analysis presented in this appendix is an extension of the analysis presented there. The discussion of each of the criteria is divided into two topics. The first topic considered is the relationship between the criterion and the measured quality parameters. This is followed by an analysis of the effect of the accuracy of the measurements of the quality parameters upon the computed values of the criterion.

Signal-to-Noise Ratio for Cone Detection

The test object chosen for detection is a conical obstruction of height, h and radius r. In this analysis the phase angles are not restricted, as previously done in the Phase I report to the range where no shadow is cast by the obstacle. It is still assumed that the object is low contrast so that the photographic system may be approximated by a linear system. In practice, however, the test cones may have a sufficiently large height-to-radius ratio compared to the phase angle so that the irradiance distribution produced by the cone is high contrast in nature. This is particularly true when a shadow is cast by the cone. In these circumstances

the approximation of a linear system is inaccurate* but not unreasonably so and is therefore retained on the basis of expediency.

The detection process is represented by a filter "matched" to the expected density signal recorded on the GRE film. This filter is used to make a decision in the optimum manner as to whether an obstacle or only a noisy background is present. The relationship between the performance of this "matched" filter in terms of the signal-to-noise ratio and the quality parameters is derived below assuming that the noise in the GRE image is approximately white.

The one-dimensional matched filter of communication theory is "optimum" for deciding which one of two possible signals $s_1(t)$ or $s_2(t)$ occurs in the presence of additive gaussian noise. The filter is optimum in that it yields the maximum signal-to-noise ratio which in the case of white noise is

$$\rho = \frac{1}{N_0} \int_0^\infty \left[s_1(t) - s_2(t) \right]^2 dt \tag{C-1}$$

where N_0 is the two-sided noise power density. The integral in (C-1) is called the "quadratic content" and denoted by Q. Thus we may write

$$\rho = \frac{Q}{N_0} \tag{C-2}$$

This result is extended to two dimensions by taking Q to be

$$Q = \iint \left[D_1(x, y) - D_2(x, y) \right]^2 dx\, dy \tag{C-3}$$

and N_0 to be the noise power density of the "all-sided" spectrum. In Eq. (C-3), $D_1(x, y)$ denotes the noise-free density signal on the GRE film due to the presence of a conical target and $D_2(x, y)$ denotes the corresponding uniform density signal for a level surface. It should be noted the signal-to-noise ratio defined by Eq. (C-2) is a measure of the

* The error made tends to yield slightly higher signal-to-noise ratios than those representative of system performance.

ratio of the signal power to the noise power. If the signal-to-noise ratio is to measure the peak-to-peak signal with respect to the rms noise as is required for the current analysis the amplitude signal-to-noise ratio for the matched filter must be employed. This is given by

$$\frac{S}{N} = \sqrt{Q/N_o} \tag{C-4}$$

The computational expression for Q, developed in Appendix F of the Phase I Final Report, is

$$Q = \iint \phi_\Delta(\xi,\eta)\, \phi_W(\xi,\eta)\, d\xi\, d\eta \tag{C-5}$$

where $\phi_\Delta(\xi,\eta)$ is the autocorrelation of the difference between the two GRE density signals if no degradation were introduced by the imaging system and $\phi_W(\xi,\eta)$ is the autocorrelation function of the effective point spread of the Lunar Orbiter photographic system. The computational program, developed during Phase I can be employed, with minor modifications, to evaluate the amplitude signal-to-noise ratio for various cone targets and values of the quality parameters. The results of such evaluations for nominal and off-nominal conditions are presented in Section 4.2 of the main text. Increased signal-to-noise ratios correspond to a greater percentage of detections or a lower percentage of "false alarms". In evaluating lunar surface roughness, a "false alarm" is in essence deciding that the surface is rough when, in fact, it is smooth. It is desirable, therefore, to have a signal-to-noise ratio for detecting cones which allows a high percentage of detections and a reasonable percentage of "false alarms".

Using the expressions above the signal-to-noise ratio is calculated from the measured values of the quality parameters which include the modulation transfer function of the Lunar Orbiter System*, the total response curve from GRE film density to aerial exposure, and the total noise power in the GRE image. The relationship between the accuracy of

---

* The system modulation transfer function is the product of the modulation transfer functions measured for the camera system and the scanner-communication-GRE system.

the computed signal-to-noise ratio and the accuracy of the measured values of the quality parameters is discussed below. The accuracy attainable in the quality parameter measurements is considered in the main text.

The value of Q in expression (C-4) includes the measured values of two of the quality parameters; the modulation transfer function and the response curve, whereas N_o is directly proportional to the measured total noise power. Since Q and N_o are determined from independently measured quality parameters, we may consider the accuracy of their computed values to be independent and employ a rule for propagation of errors based upon a Taylor series expansion, namely[3]

$$\epsilon_f = \sqrt{\sum_i \left[\frac{\partial f(x_1, x_2, \ldots)}{\partial x_i}\right]^2 \epsilon_{x_i}^2} \qquad \text{(C-6)}$$

where the x_i are statistically independent variables having standard deviations or fractional errors ϵ_{x_i} and ϵ_f is the resulting standard deviation or fractional error in the value of f which is a function of the variables, x_i. From this expression we can show that the fractional error in the calculated signal-to-noise ratio is one-half the rms value of the fractional error in Q and the fractional error in the measurement of the total noise power. To estimate the fractional error in Q recall from Eq. (C-3) that

$$Q = \iint \left[D_1(x,y) - D_2(x,y)\right]^2 dx\, dy$$

where $D_1(x,y)$ and $D_2(x,y)$ are density signals on the GRE film. An equivalent expression for Q may be written in terms of spatial frequency by employing Parseval's theorem. This expression is given by[7]

$$Q = \iint \left|\tau(\nu_x, \nu_y)\right|^2 \left|S_D(\nu_x, \nu_y)\right|^2 d\nu_x\, d\nu_y \qquad \text{(C-7)}$$

where $\tau(\nu_x, \nu_y)$ is the modulation transfer function of the Lunar Orbiter system* and $S_D(\nu_x, \nu_y)$ is the spectrum of the difference between the

* For convenience we assume that $\tau(\nu_x, \nu_y)$ is the magnitude of the transfer function in the subsequent analysis.

density signals obtained from a perfect imaging system. Let $\tau_m(\nu_x, \nu_y)$ be the measured modulation transfer function and assume that its accuracy is given by

$$\left|\tau_m(\nu_x, \nu_y) - \tau(\nu_x, \nu_y)\right| < \Delta_\tau << 1 \tag{C-8}$$

over the frequency range of interest. The measured quadratic content becomes

$$Q_m = \iint \left|\tau_m(\nu_x, \nu_y)\right|^2 \left|S_D(\nu_x, \nu_y)\right|^2 d\nu_x \, d\nu_y \tag{C-9}$$

From Eq. (C-8) it follows that

$$\left|\tau_m^2(\nu_x, \nu_y) - \tau^2(\nu_x, \nu_y)\right| < 2\Delta_\tau \, \tau(\nu_x, \nu_y) \tag{C-10}$$

where the second order term of Δ_τ^2 has been neglected. Substituting (C-10) into (C-9) and employing (C-7), it follows that

$$\left|Q_m - Q\right| < 2\Delta_\tau \int \tau(\nu_x, \nu_y) \left|S_D(\nu_x, \nu_y)\right|^2 d\nu_x \, d\nu_y \tag{C-11}$$

Now one can choose a value τ_0 such that

$$\tau_0 < \tau(\nu_x, \nu_y)$$

over the frequency range of interest. This range is determined by the rate at which $S_D(\nu_x, \nu_y)$ decreases with ν_x, ν_y. Therefore

$$\tau_0 \int \tau(\nu_x, \nu_y) \left|S_D(\nu_x, \nu_y)\right|^2 d\nu_x \, d\nu_y < Q \tag{C-12}$$

Substituting this into Eq. (C-11) yields

$$\frac{\left|Q_m - Q\right|}{Q} < \frac{2\Delta_\tau}{\tau_0} \tag{C-13}$$

for the fractional error in Q if it is assumed that the error in the measurement of the response curve, relating GRE film density to aerial exposure, would introduce negligible errors into the spectrum of the difference signal.

The resulting fractional error or standard deviation in the calculated value of signal-to-noise ratio is given by

$$\epsilon_{S/N} = \sqrt{\left(\frac{\Delta\tau}{\tau_o}\right)^2 + \frac{\epsilon_{TNP}^2}{4}} \tag{C-14}$$

where ϵ_{TNP} is fractional error in the measurement of the total noise power in the GRE image.

Variance of Slope Angle Measurement

The terrain model chosen for determining the variance in slope measurement is a uniform square area inclined toward or away from the sun at an angle α. If such a test object did exist on the lunar surface the accuracy to which α could be measured from the reconstructed image on the GRE film can be determined by employing maximum likelihood techniques of statistical communication theory[8]. This is done below to relate the measured quality parameters to the variance in the estimate of α and establish the second system performance criterion. This variance corresponds to the minimum variance to be expected from an unbiased estimate and is therefore indicative of limiting performance which may not be achieved in actual data reduction. The resulting mathematical expressions for the variance are similar in structure to those for the signal-to-noise ratio discussed previously. In fact, if the "signal" is defined as the derivative, with respect to α, of the density distribution on the GRE film, then the variance is seen to be the reciprocal of the signal-to-noise ratio of a filter matched to this signal. Given an object which is a square area of length ℓ on a side inclined at an angle α from a horizontal surface, the density signal which would be recorded on the GRE film in the absence of any system degradation (perfect image) is given by

$$D(x, y; \alpha, \ell) = D_o + \Delta D(\alpha)\, rect(x/\ell)\, rect(y/\ell) \tag{C-15}$$

where D_o is the GRE film density corresponding to a flat surface and $\Delta D(\alpha)$ is the difference in GRE film density between the flat surface and the inclined surface. For α positive (away from the sun) $\Delta D(\alpha)$

is positive and for α negative (towards the sun) $\Delta D(\alpha)$ is negative. Both D_o and $\Delta D(\alpha)$ include, in a direct manner, the response curve from GRE film density to aerial exposure which is one of the measured quality parameters. The "rect" functions in Eq. (C-15) simply define the boundaries of the uniform square area relative to the scale of the GRE film. Following the techniques outlined in Appendix E of the Phase I Report, the variance in the maximum likelihood estimate of α can be derived as

$$\sigma^2 = \frac{N_o}{\iint \left[\iint P(x-x', y-y') D(x', y'; \alpha, \ell) dx' dy' \right]^2 dx dy} \qquad \text{(C-16)}$$

where N_o is the noise power density of the "all-sided" spectrum and $P(x,y)$ is the point spread function for the Lunar Orbiter system. It is possible to substitute Eq. (C-15) into (C-16) and develop an expression for σ^2. However, for purposes of interpretation and computation, a more convenient representation can be obtained. An analogous expression for σ^2 can be written in terms of spatial frequency[8], namely

$$\sigma^2 = \frac{1}{\iint \frac{|\tau(\nu_x, \nu_y)|^2}{G(\nu_x, \nu_y)} \left| \frac{\partial S_D(\nu_x, \nu_y; \alpha, \ell)}{\partial \alpha} \right|^2 d\nu_x d\nu_y} \qquad \text{(C-17a)}$$

where $\tau(\nu_x, \nu_y)$ is the modulation transfer function of the Lunar Orbiter System, $G(\nu_x, \nu_y)$ is the spectrum of the noise in the GRE image and $S_D(\nu_x, \nu_y; \alpha, \ell)$ is the spectrum of the "perfect image" on the GRE film described by expression (C-15). Under the present approximation of a white noise spectrum $G(\nu_x, \nu_y)$ is set equal to N_o and, therefore

$$\sigma^2 = \frac{N_o}{\iint |\tau(\nu_x, \nu_y)|^2 \left| \frac{\partial S_D(\nu_x, \nu_y; \alpha, \ell)}{\partial \alpha} \right|^2 d\nu_x d\nu_y} \qquad \text{(C-17b)}$$

The similarity between the signal-to-noise ratio for a matched filter and the variance in the maximum likelihood estimate of α mentioned previously can be seen by comparing the integral in Eq. (C-17b) to the quadratic content given by Eq. (C-7).

From Eq. (C-15) it is easily shown that

$$\frac{\partial S_D(\nu_x, \nu_y; \alpha, \ell)}{\partial \alpha} = \frac{\partial \Delta D(\alpha)}{\partial \alpha} \ell^2 \, sinc(\pi \ell \nu_x) \, sinc(\pi \ell \nu_y) \qquad \text{(C-18)}$$

where $sinc(x) = \frac{\sin(x)}{x}$. Substituting into Eq. (C-17b) becomes

$$\sigma^2 = \frac{N_0}{\left[\frac{\partial \Delta D(\alpha)}{\partial \alpha}\right]^2 \ell^4 \iint \left|\tau(\nu_x, \nu_y)\right|^2 sinc^2(\pi \ell \nu_x) \, sinc^2(\pi \ell \nu_y) \, d\nu_x \, d\nu_y} \qquad \text{(C-19)}$$

In this expression, two of the quality parameters, N_0 and $\tau(\nu_x, \nu_y)$ appear directly. The third quality parameter, namely the response from the GRE film density to aerial exposure, is included in $\partial \Delta D(x)/\partial \alpha$, the rate of change of the density level on the GRE film with respect to α . The influence of the system modulation transfer function, $\tau(\nu_x, \nu_y)$ upon σ^2 is seen to depend upon ℓ the size of the test object through the terms $sinc^2(\pi \ell \nu_x)$ and $sinc^2(\pi \ell \nu_y)$. For large ℓ both of these functions decrease rapidly with ν_x and ν_y and only the value of transfer function at low frequencies $(\nu_x, \nu_y \leq 1/\ell)$ contributes in the integral to alter the magnitude of the variance. As ℓ becomes smaller, the transfer function at correspondingly higher frequencies becomes more important, as would be expected.

The error in the slope measurement is calculated for the measured values of the three quality parameters. Since these factors cannot be measured without error, there is a limit in the accuracy attainable in the computed value of σ . The analysis of this limit, presented below, closely follows the analysis previously made in this appendix for the signal-to-noise ratio because of the similarity between these two performance criteria.

To evaluate the accuracy attainable in σ , let

$$L = \ell^4 \iint \left|\tau(\nu_x, \nu_y)\right|^2 sinc^2(\pi \ell \nu_x) \, sinc^2(\pi \ell \nu_y) \, d\nu_x \, d\nu_y ,$$

$$\delta = \left| \frac{\partial \Delta D(\alpha)}{\partial \alpha} \right|$$

and rewrite Eq. (C-19), taking the square root, as

$$\sigma = \frac{1}{\delta}\sqrt{N_o/L} \tag{C-20}$$

Applying the rule for the propagation of errors, given previously in Eq. (C-6), to Eq. (C-20), the error in σ , ϵ_σ , becomes

$$\epsilon_\sigma = \sqrt{\epsilon_\delta^2 + \frac{\epsilon_{TNP}^2}{4} + \frac{\epsilon_L^2}{4}} \tag{C-21}$$

Because of the correspondence between L and the quadratic content Q defined by Eq. (C-7), the previous analysis may be used directly to write that

$$\frac{\epsilon_L^2}{4} < \left(\frac{\Delta\tau}{\tau_o}\right)^2 \tag{C-22}$$

where $\Delta\tau$ is the maximum deviation between the measured and true modulation transfer function and τ_o is the lower bound on the true modulation function. The error in σ becomes

$$\epsilon_\sigma = \sqrt{\left(\frac{\Delta\tau}{\tau_o}\right)^2 + \frac{\epsilon_{TNP}^2}{4} + \epsilon_\delta^2} \tag{C-23}$$

where the terms, ϵ_δ , represents the accuracy to which the rate of change of density on the GRE film can be predicted as a function of the slope angle or brightness longitude.

APPENDIX D

SUPPORTING ANALYSIS FOR NOISE MEASUREMENT TECHNIQUES

This appendix contains a supporting analysis for the techniques used to evaluate the noise level quality parameter. This parameter is the effective white noise power density in the spatial frequency band containing the signal (within 20 lines/mm at the GRE film scale). The primary objective of the noise measurement procedure is to evaluate the total noise power in this band. As a result of the combined effects of the spacecraft scanning spot, the sampling process and the frequency response of the communications system, the maximum spatial frequency in the noise input at the GRE is below 20 lines/mm. In fact, most of the noise power is confined to the signal band below 15 lines/mm. The two additional noise sources; namely, the reconstructing film grain and the kinescope phosphor noise, in the ground reconstruction system, will contribute noise power at spatial frequencies beyond the 20 line/mm limit imposed on the noise in the input signal. The total noise power in the reconstructed image can easily be measured by scanning a uniform area with a small aperture and computing the variance of the resulting trace. The problem, therefore, is to adjust this value of the noise power to represent that portion which occurs only within the signal band. Two approaches which can be employed to adjust the noise power include numerical techniques based upon digital filtering and associated computational formulas or a combination of analog and digital techniques in which the filtering effect of the microdensitometer aperture is used to the best advantage. The former method was implemented in this study and will be described below. An analysis of the reliability of this technique, presented in the main body of this report, revealed that the accuracy of the selected approach is the limiting factor in the accuracy to which the system performance can be measured. It is probable that the method employing the combination of the numerical and analog techniques would yield more accurate estimates of the noise level quality parameter and therefore would be more desirable. The details of the alternate techniques are also discussed at the end of this appendix.

To evaluate the noise level quality parameter, a uniform area in the reconstructed image is scanned in the mechanical scan direction with a circular aperture 2.5 microns in diameter on the GRE film. This aperture is sufficiently small so that the two-dimensional noise spectrum of the reconstructed image is essentially unaffected by the frequency response of the scanning aperture. As illustrated in Fig. D-1, the effect of the data acquisition procedure is primarily to integrate the noise spectrum in the electrical scan direction collapsing it into a one-dimensional spectrum corresponding to the output signal spectrum of the microdensitometer. Since the scan line spacing in the reconstructing image is approximately 24 microns and the sampling interval of the digitized microdensitometer output is 2 microns, the scan line structure is adequately reproduced in the output signal. Because of this structure, the power spectrum of the output signal will have a central order of approximately a 40 line/mm bandwidth and various higher orders located at multiples of the scan line frequency about equal to 40 lines/mm and there will be essentially no overlap between orders. The next process in the data reduction is to remove the scan line structure by employing the numerical filtering technique described in Section 3.3.1. This operation eliminates the noise power outside the central order in the power spectrum. This filtered noise trace is resampled at approximately 20 micron intervals corresponding to a folding frequency of 25 lines/mm which is greater than the cutoff of the scan line removal filter (See Fig. 6 in the main text). The resampling procedure will not affect the spectrum to an appreciable extent. The variance of the resampled trace is therefore the total noise power of the original two-dimensional power spectrum in a band from -20 lines/mm to +20 lines/mm in the mechanical scan direction and, because of the integration performed by the microdensitometer scanning operation, the region is large in the electrical scan direction, limited only by effective aperture dimensions. We desire to further limit the noise power to a band from -20 to + 20 lines/mm in both the mechanical and electrical scan directions. This is done by assuming that the total noise power in the bands from 15 to 20 lines/mm is primarily due to the grain of the reconstructing film. If the filtered noise trace is then filtered again by a series of 5 high pass filters whose frequency response was shown previously in Fig. 12 of the main text.

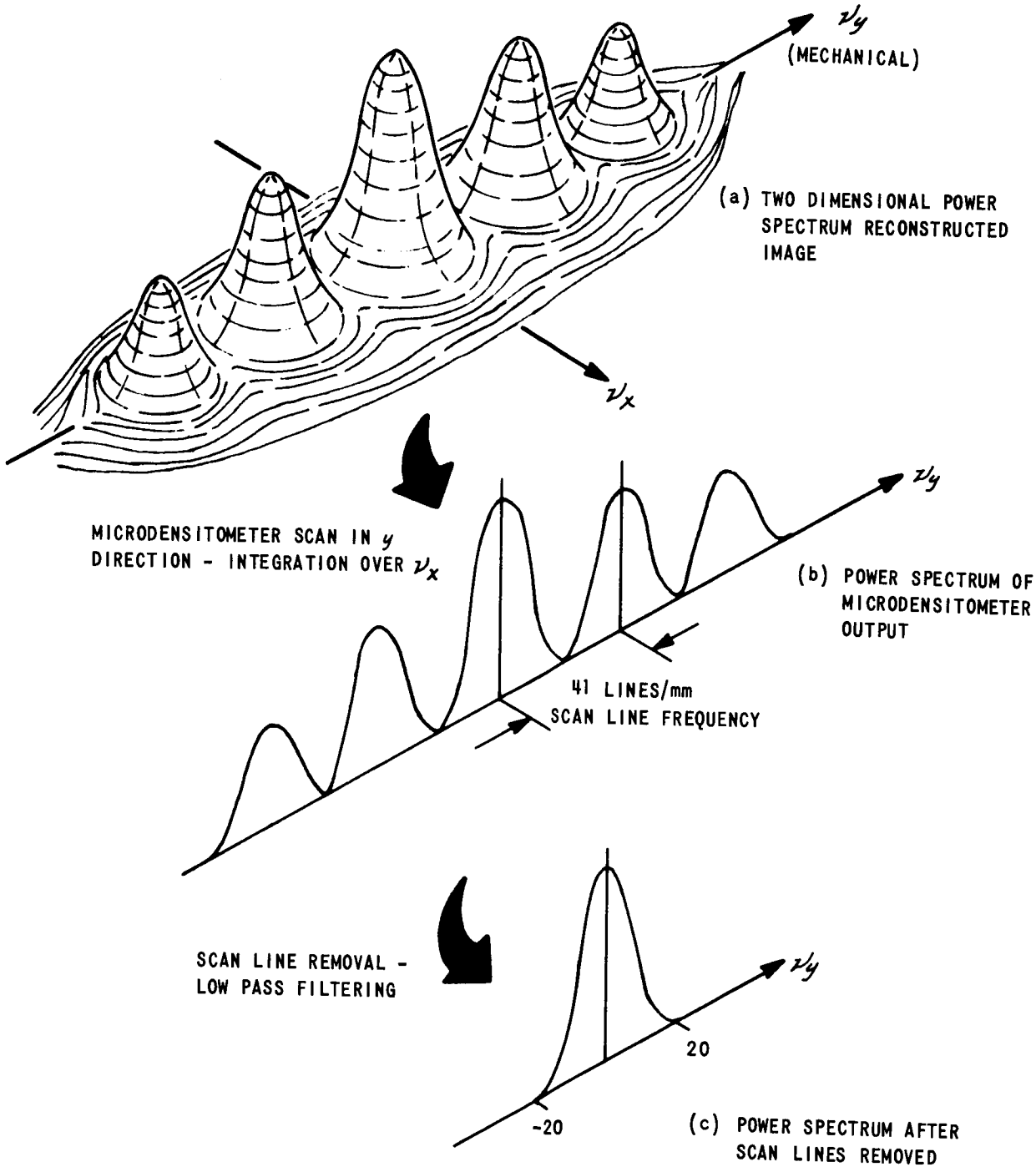

Figure D-1 SKETCH OF EFFECTS OF SEVERAL ANALYSIS PROCEDURES UPON THE POWER SPECTRUM

The noise power passed by filters no. 4 and 5 lies principally in the bandwidth between 15 and 20 lines/mm and therefore should consist primarily of noise due to the grain of the reconstructing film. By assuming that the grain of the reconstructing film has a white spectrum, the equivalent total noise power in the entire band can be estimated from the measured power of the filter traces. In order to compute the total noise power due to the reconstructing film grain over the entire bandwidth, we need the ratio of the filtered power to the total noise power when a white noise source is analyzed by the numerical filtering procedures described above. The analysis presented below assumes that a white noise field is scanned by circular aperture and subsequently undergoes two numerical filtering processes. The first process is a low pass filtering by the filter which is used to remove the scan line structure and the second process is the filtering by one of the five high pass filters. The successive numerical filtering by the low pass scan line removal filter and one of the high pass analysis filters is equivalent to a single filtering operation with a bandpass filter. In previous work performed at CAL[9] it has been shown that the one-dimensional spectrum, $\phi(\omega)$, obtained by scanning a white noise field with a circular aperture of radius, r_0, is

$$\phi(\omega) = \frac{k^2 N_0 r_0}{2\pi} \frac{H_1(2 r_0 \omega)}{(r_0 \omega)^2} , \tag{D-1}$$

where ω is the angular frequency in radians per millimeter, N_0 is the constant spectral density of the two-dimensional noise field, k is some gain factor and $H_1(z)$ is a Struve's function of order one. Employing an integral representation of the Struve function[10], namely

$$H_1(z) = \frac{2z}{\pi} \int_0^{\pi/2} \sin(z \cos\phi) \sin^2\phi \, d\phi \tag{D-2}$$

and substituting into Eq. (D-1) yields

$$\phi(\omega) = \frac{4k^2 N_0 r_0}{\pi^2} \int_0^{\pi/2} \frac{\sin(z\cos\phi)\sin^2\phi}{z} \, d\phi \tag{D-3}$$

where we have let $z = 2r_0\omega$. The numerical filtering process may be mathematically represented by

$$D_n' = \sum_{k=-m}^{m} W_k D_{n-k}$$

where W_k is the kth weighting coefficient, D_{n-k} is the density recorded at the (n-k)th data point and D_n' is the output of the filter at the nth data point. It is assumed that the numerical filter has 2m + 1 weights. If we assume that the filter is an even function it can be shown that its frequency response, $F(\omega)$, has the form

$$F(\omega) = W_0 + 2\sum_{k=1}^{m} W_k \cos(k\omega\Delta) \tag{D-4}$$

where Δ is the interval between data points. When the noise trace is filtered, the noise power, σ_f^2, in the filtered signal is given by

$$\sigma_f^2 = \int_{-\infty}^{\infty} \phi(\omega)\left|F(\omega)\right|^2 d\omega \tag{D-5}$$

The total noise power in the unfiltered trace, σ_T^2, is obtained from Eq. (D-5) by setting $\left|F(\omega)\right|^2 = 1$. The ratio of the filtered power to the total power, $(\sigma_f/\sigma_T)^2$, is therefore

$$\left(\frac{\sigma_f}{\sigma_T}\right)^2 = \frac{\int_0^{\infty} \phi(\omega)\left|F(\omega)\right|^2 d\omega}{\int_0^{\infty} \phi(\omega)\, d\omega} \tag{D-6}$$

where the fact that $\phi(\omega)$ and $F(\omega)$ are both even functions have been used to reduce the ranges of integration. Substituting Eqs. (D-3) and (D-4) into (D-6), we find that the ratio is given by

$$\left(\frac{\sigma_f}{\sigma_T}\right)^2 = W_0^2 + 4W_0 \sum_{k=1}^{m} W_k \frac{\int_0^\infty \phi(\omega)\cos(k\omega\Delta)\,d\omega}{\int_0^\infty \phi(\omega)\,d\omega}$$

$$+ 2\sum_{k=1}^{m}\sum_{l=1}^{m} W_k W_l \frac{\int_0^\infty \phi(\omega)\left[\cos\{(k-l)\omega\Delta\} + \cos\{(k+l)\omega\Delta\}\right]d\omega}{\int_0^\infty \phi(\omega)\,d\omega} \tag{D-7}$$

All of the integrals in Eq. (D-7) are of the form

$$I(k') = \frac{\int_0^\infty \phi(\omega)\cos(k'\omega\Delta)\,d\omega}{\int_0^\infty \phi(\omega)\,d\omega} \tag{D-8}$$

Letting d equal the diameter of the scanning aperture (i. e., $2r_0$) and substituting (D-3) into (D-8) yields

$$I(k') = \frac{\int_0^\infty \cos\left(\frac{k'z\Delta}{d}\right)\int_0^{\pi/2} \frac{\sin(z\cos\phi)\sin^2\phi}{z}\,d\phi\,dz}{\int_0^\infty\int_0^{\pi/2} \frac{\sin(z\cos\phi)\sin^2\phi}{z}\,d\phi\,dz} \tag{D-9}$$

because $\phi(\omega)$ is analytic for all values of $z = \omega d$. We can invert the order of integration and noting that in the range of integration for the angle ϕ , $\cos\phi$ is non-negative, so that the integral in the denominator of Eq. (D-9) reduced to $\frac{\pi}{2}\int_0^{\pi/2} \sin^2\phi\,d\phi = \pi^2/8$, and Eq. (D-9) becomes

$$I(k') = \frac{8}{\pi^2}\int_0^{\pi/2} \sin^2\phi \int_0^\infty \frac{\sin(z\cos\phi)}{z}\cos\left(\frac{k'\Delta z}{d}\right)dz\,d\phi\,. \tag{D-10}$$

Now, the integral

$$\int_0^\infty \frac{\sin bz\cos az}{z}\,dz = \begin{cases} \pi/2 & \left|\frac{a}{b}\right| < 1 \\ 0 & \left|\frac{a}{b}\right| > 1 \end{cases}$$

which substituted into (D-10) and integrated yields

$$I(k') = \begin{cases} \frac{4}{\pi}\left\{\frac{\hat{\phi}}{2} - \frac{\sin 2\hat{\phi}}{4}\right\} & 0 < \left|\frac{k'\Delta}{d}\right| < 1 \\ 0 & \left|\frac{k'\Delta}{d}\right| > 1 \end{cases} \tag{D-11}$$

where $\hat{\phi} = \cos^{-1}\left(\left|\frac{k'\Delta}{d}\right|\right)$.

It should be noted that $I(k') = 0$ if $\Delta > d$, that is, if the sampling interval is greater than the diameter of the scanning aperture. We arrive at the desired result by employing (D-11) to reduce the various integrals in (D-7) and find that

$$\left(\frac{\sigma_f}{\sigma_T}\right)^2 = W_0^2 + 2\sum_{k=1}^{m} W_k^2 + 2\sum_{k=1}^{m} W_k^2 I(2k) + 4\sum_{k=1}^{m-1}\sum_{l>k}^{m} W_k W_l\left[I(l-k) + I(l+k)\right] + 4W_0\sum_{k=1}^{m} W_k I(k) \tag{D-12}$$

It can be seen that as the ratio of the sample length to the aperture diameter becomes unity, the samples become independent of each other and the last three terms in (D-12) vanish leaving the result that

$$\left(\frac{\sigma_f}{\sigma_T}\right)^2 = W_0 + 2\sum_{k=1}^{m} W_k^2 \tag{D-13}$$

Since the diameter of the circular scanning aperture is 2.5 microns and samples are taken every 2 microns, the ratio of the sampling interval to the scanning diameter is approximately equal to 1 and (D-13) adequately represents the ratio of the filtered noise power to the total noise power. The weights corresponding to the combined effect of the low pass scan line removal filter and the analysis filters were evaluated and used to compute the ratio of the filtered noise power to the total noise power presented in Table D-1. These results were verified by simulating the noise trace in a digital computer employing a gaussian random number generator. Assuming that the noise trace is obtained by scanning with an aperture diameter which is less than the sampling interval which is a valid approximation in the analysis procedures, successive noise samples are independent of each other and can be simulated by uncorrelated gaussian

Table D-1

RATIO OF FILTERED-TO-TOTAL NOISE POWER

FILTER NO.	ANALYTICAL VALUE	EMPIRICAL RESULTS		
		RATIO	STANDARD DEVIATION	EQUIVALENT %
1	0.503	0.500	±0.030	6
2	0.386	0.376	±0.027	7
3	0.242	0.235	±0.023	10
4	0.127	0.128	±0.020	16
5	0.0635	0.066	±0.015	23

random variables. In the empirical evaluation, four independent simulated traces were employed with each containing 2800 to 2900 points. Each of the simulated noise traces were processed in the noise level evaluation program described previously in Section 3. 3. 3. The average value of the ratio of the filtered noise power to the total noise power is presented for each of the five filters in Table D-1. Good agreement was obtained between the analytical and empirical values as seen from the table. Also included is the percentage deviation between the four empirical values used to obtain the average.

To compute the total noise power density we simply divide the measured noise power from the filtered trace by the corresponding factor presented in the table. Therefore, in the noise analysis if we take the noise power passed by filter no. 5 and divide it by 0. 0635 we have an estimate of the total noise power due to the grain of the reconstructing film in the filtered noise trace. To obtain an estimate of the total noise power in the signal band we subtract, from the measured total noise power, this estimate of the total noise power due to the reconstructing film grain which yields an estimate of the total noise power in the signal band from all the noise sources except the grain of the reconstructing film. The next step is to compute the amount of power in the signal band due to the reconstructing

grain. Since we have an estimate of the total noise power due to the grain, it is convenient to compute the ratio of the power in the signal band to the total power. If we let $\tau_m(\nu_x, \nu_y)$ represent the frequency response of the microdensitometer and $\tau_f(\nu_x)$ the one-dimensional response of the scan line removal filter, the desired ratio is given by

$$R = \frac{\iint_{-20\,\text{lines/mm}}^{+20\,\text{lines/mm}} |\tau_f(\nu_x)|^2 \, |\tau_m(\nu_x, \nu_y)|^2 \, d\nu_x \, d\nu_y}{\iint_{-\infty}^{\infty} |\tau_f(\nu_x)|^2 \, |\tau_m(\nu_x, \nu_y)|^2 \, d\nu_x \, d\nu_y} \tag{D-14}$$

Note that $\tau_m(\nu_x, \nu_y)$ is the product of two frequency response functions. The first, representing the response of the scanning aperture is[11]

$$\tau(\nu) = \frac{2J_1(2\pi\nu R)}{2\pi\nu R}, \qquad \nu = (\nu_x^2 + \nu_y^2)^{1/2}$$

where $2R = 2.5\,\mu$. The second function describes the frequency response of the microdensitometer optics, namely a 10X objective having a 0.25 numerical aperture. If we assume the optics are diffraction limited then this function is given by[11]

$$\tau(\nu) = \begin{cases} \frac{2}{\pi}\left[\cos^{-1}(\nu/\nu_0) - (\nu/\nu_0)\sqrt{1-(\nu/\nu_0)^2}\,\right] & \nu \le \nu_0 \\ 0 & \nu \ge \nu_0 \end{cases}$$

where $\nu_0 \simeq$ 2X numerical aperture/λ. Combining these functions, we determine that $\tau_m(\nu_x, \nu_y)$ is

$$\tau_m(\nu_x, \nu_y) = \begin{cases} \frac{2J_1(2\pi\nu R)}{\pi^2 \nu R}\left[\cos^{-1}(\nu/\nu_0) - (\nu/\nu_0)\sqrt{1-(\nu/\nu_0)^2}\right] & \nu \le \nu_0 \\ 0 & \text{otherwise} \end{cases} \tag{D-15}$$

where $\nu = (\nu_x^2 + \nu_y^2)^{1/2}$. Fig. D-2 is a graphic representation of Eq. (D-15). Note that above 220 lines/mm the value of $|\tau_m(\nu_x, \nu_y)|^2$ which is also shown in the figure, is negligible. If we evaluate Eq. (D-14) using the value of $|\tau_m(\nu_x, \nu_y)|^2$ shown in the figure, we find that

$$R = 0.20 \tag{D-16}$$

that is about 20% of the estimated total noise power due to the reconstructing grain is within the signal band. Since the microdensitometer optics are not diffraction limited as was assumed in arriving at Eq. (D-15), the actual value of $|\tau_m(\nu_x, \nu_y)|^2$ will be less than that shown in Fig. D-2, especially in the region above 100 lines/mm. Consequently, it can be expected that the value of R will be greater than 20% derived above. (The decrease in $|\tau_m(\nu_x, \nu_y)|^2$ will cause the integral in the denominator of Eq. (D-14) to decrease while the numerator remains unchanged.) In lieu of measuring $\tau_m(\nu_x, \nu_y)$ which would be difficult, it is reasonable to assume the 25% of the measured grain noise is in the signal band. Therefore in arriving at the noise level quality parameter we subtract from the measured total noise power 3/4 of the estimated power of reconstructing film grain obtained from the noise power passed by filter no. 5. Mathematically, this may be written as

$$P_{ADJ} = P_T - \frac{3}{4}\,\frac{P_5}{0.0635} \qquad \text{or}$$

$$P_{ADJ} = P_T - 11.8\,P_5 \tag{D-17}$$

By dividing the adjusted total noise power, P_{ADJ}, by the signal bandwidth, one determines the equivalent white noise power density which is the "noise level quality parameter".

Using Eq. (D-17) and the data presented in Table D-1 an error analysis is presented in Section 3.4.3 indicating that an error of about 18% could be expected in a single estimate of the noise level quality parameter. This is somewhat higher than initially expected and is a direct result of the accuracy of estimating the contribution to the total noise power from the grain of the reconstructing film and the subsequent correction required to limit the adjusted power to the signal band. In retrospect, we see a potentially more accurate method of achieving the

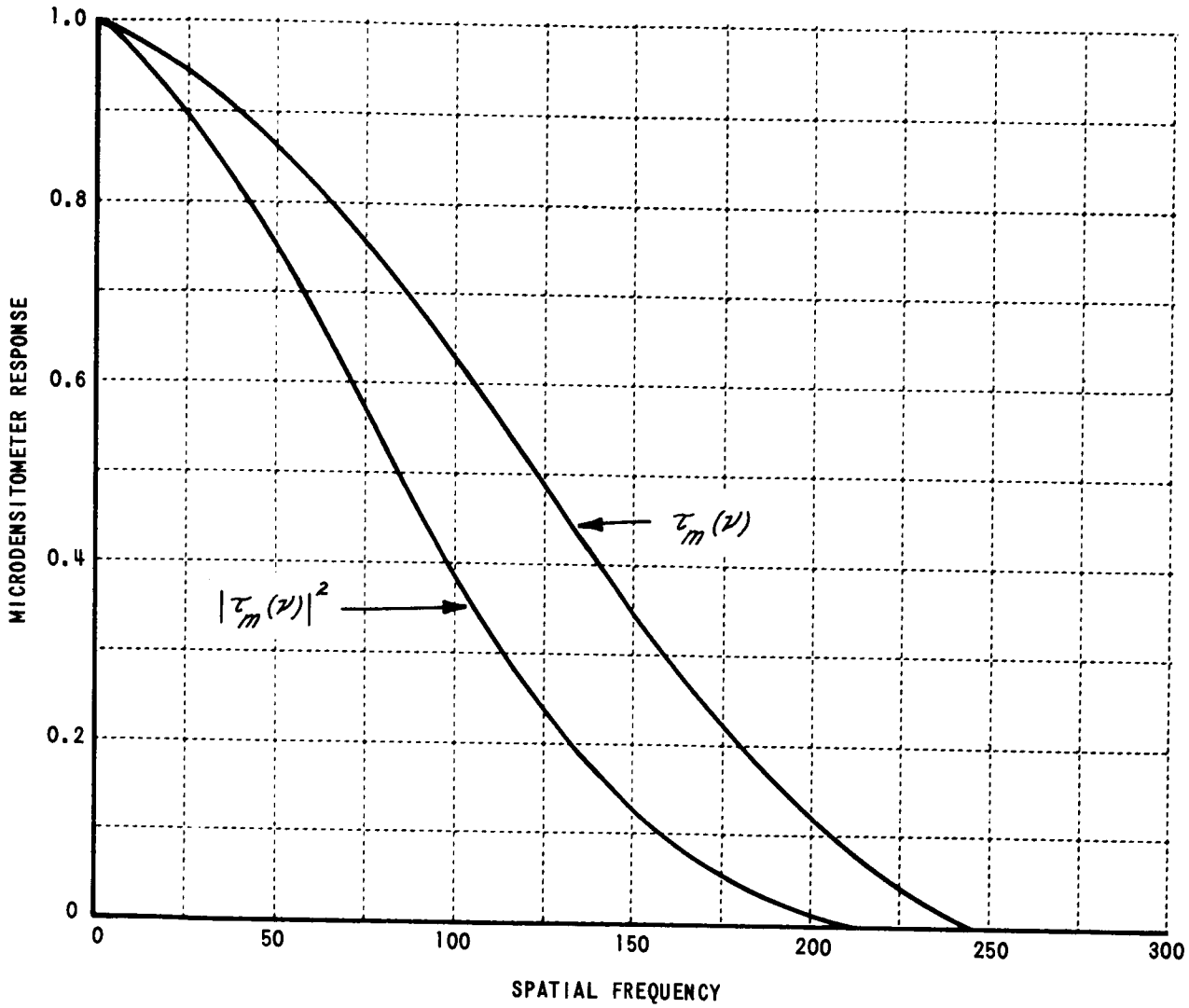

Figure D-2 FREQUENCY RESPONSE OF MICRODENSITOMETER (10 X OBJECTIVE, 2.5μ DIAMETER APERTURE SCAN SPOT)

same result by obtaining the noise trace using other than a circular microdensitometer aperture. The size of the aperture must remain small compared to the scan line spacing in the direction of scan, i. e., across the scan line structure. However, the length of the scanning aperture controls the region of integration in the orthogonal direction. If a rectangular aperture 2 microns wide and approximately 50 microns long is selected the integration performed by the scanning process will be limited primarily to the band from -20 lines/mm to +20 lines/mm in the direction. The required correction to the measured total noise power would be reduced in magnitude and therefore the accuracy in estimating the adjusted total noise power substantially improved.

REFERENCES

1. Kinzly, R. E. ; Roetling, P. G. ; and Holladay, T. M. : Project SLOPE - Study of Lunar Orbiter Photographic Evaluation. Phase I Final Report. NASA CR-66158, CAL Report No. VS-2182-D-2, 20 May 1966.

2. Lanczos, C. : Applied Analysis. Prentice Hall, Inc., 1956.

3. Beers, Y. : Theory of Error. Addison-Wesley, 1953.

4. Deutsch, R. : Estimation Theory. Prentice Hall, Inc., 1965.

5. Barakat, R. : Transfer Function from Edge Spread Function. J. Opt. Soc. Am., Vol. 55, No. 10, October 1965, pp. 1217.

6. Hartley, H. O. : The Modified Gauss-Newton Method for Fitting of Non-Linear Regression Functions by Least Squares. Technometrics, Vol. 3, No. 2, May 1961, pp. 269.

7. Harris, J. L. : Resolving Power and Decision Theory. J. Opt. Soc. Am., Vol. 54, No. 5, May 1965, p. 606.

8. Swerling, P. : Parameter Estimation Accuracy Formulas. IEEE Transactions on Information Theory, Vol. IT-10, No. 4, 1964, p. 302.

9. Trabka, E. A. : Wiener Spectrum of Scans Obtained from an Isotropic Two-Dimensional Random Field. J. Opt. Soc. Am., Vol. 55, No. 2, February 1965, pp. 203.

10. Jahnke, E. ; and Emde, F. : Tables of Functions. Dover Publications, 1945.

11. O'Neill, E. : Introduction to Statistical Optics. Addison-Wesley, 1963.